JSCSEN 79(4)389–516(2014)

ISSN 1820-7421(Online)

Journal of the Serbian Chemical Society

Electronic version

VOLUME 79

No 4

BELGRADE 2014

Available on line at

www.shd.org.rs/JSCS/

Journal of the Serbian Chemical Society
JSCS-info@shd.org.rs • www.shd.org.rs/JSCS

J. Serb. Chem. Soc. Vol. 79, No. 4 (2014)

CONTENTS

Published by the Serbian Chemical Society
Karnegijeva 4/III, P. O. Box 36, 11120 Belgrade 35, Serbia
Printed by the Faculty of Technology and Metallurgy
Karnegijeva 4, P. O. Box 35-03, 11120 Belgrade, Serbia

Journal of the Serbian Chemical Society
JSCS-info@shd.org.rs • www.shd.org.rs/JSCS
J. Serb. Chem. Soc. 79 (4) 389–400 (2014)
JSCS–4593
UDC 547.857.4.004.12+542.913+546.172–31:615.9:615.276
Original scientific paper

The synthesis, characterization and biological evaluation of a new nitric oxide donor agent

LENUTA PROFIRE[1]*, MARIA APOTROSOAEI[1], ANCA OPREA[2], MIHAI BREBU[2], FLORENTINA LUPASCU[1], CATALINA ELENA LUPUSORU[3] and CORNELIA VASILE[2]

[1]*Department of Pharmaceutical Chemistry, Faculty of Pharmacy, "Grigore T. Popa" University of Medicine and Pharmacy, 16 University Str., 700115, Iasi, Romania,* [2]*Department of Physical Chemistry of Polymers, "P. Poni" Institute of Macromolecular Chemistry, Romanian Academy, 41A Grigore Ghica Voda Alley, 700487, Iasi, Romania and* [3]*Department of Pharmacology, Faculty of Medicine, "Grigore T. Popa" University of Medicine and Pharmacy, 16 University Str., 700115, Iasi, Romania*

(Received 24 January, revised 1 July 2013)

Abstract: The synthesis of a new xanthine nitric oxide donor (TSP-81) is discussed. The designed compound included two structural moieties, *i.e.*, theophylline (1,3-dimethylxanthine) and acetaminophen (4-hydroxyacetanilide), linked by the nitric oxide donor alkyl chain as a spacer. The compound was characterized by microanalysis (CHN), ^{1}H-NMR, ^{13}C-NMR, FT-IR and UV–Vis spectroscopy and thermogravimetric analysis. The thermal behaviour showed that TSP-81 melts with decomposition in four steps, the most important ones being the 2nd one (the registered weight loss being 17.6 %) and the 3rd one (with a registered weight loss of 30.4 %). The toxicity degree, the anti-inflammatory effect and the ability of releasing nitric oxide of TSP-81 was also evaluated. The biological assays established that TSP-81 exhibits enhanced biological properties, such as lower toxicity and higher anti-inflammatory effect, compared to theophylline and acetaminophen, the drugs used as the parent molecules. Thus, TSP-81 is approximately 2 times more active than theophylline and 4 times more active than acetaminophen in reducing cotton pellet granuloma formation. Furthermore, the release of nitric oxide (NO) appears to play an important role in enhancing the anti-inflammatory effect.

Keywords: xanthine; acethaminophen; toxicity; anti-inflammatory.

INTRODUCTION

In the last few years many research groups have focused their efforts on the discovery and development of "molecular hybrids" characterized by a nitric oxide (NO) releasing moiety, in order to enhance the pharmacological profile of

* Corresponding author. E-mail: nprofire@yahoo.com
doi: 10.2298/JSC130124131P

the parent drug.[1] NO is an important endogenous mediator generated by nitric oxide synthase (NOS) enzymes.[2] NO, biosynthesised by endothelial cells, is mainly considered to be a fundamental modulator of cardiovascular function, where it acts as a powerful vasodilator, inhibits platelets activation/aggregation and is involved in ischemic preconditioning, thus ensuring important cardioprotective effects.[3] In 1998, R. Furchgott, L. Ignarro and F. Murad were awarded the Nobel Prize in Physiology and Medicine for their discoveries concerning NO as a signalling molecule in the cardiovascular system. Increasing data suggest a considerable "modulating" effect of nitric oxide as a pleiotropic agent, acting on several body parts.[4–6] There is important evidence that NO is involved in several inflammatory disorders. Indeed, every cell and many immunological parameters are virtually modulated by NO.[7] It has been shown that NO can be pro-inflammatory (immunostimulatory, anti-apoptotic) or anti-inflammatory (immunosuppressive, pro-apoptotic), host-protective or host-damaging during infections.[8] For these reasons, NO has been described as a "double edge sword mediator" and this phenomenon is often referred to as the NO paradox. It is interesting to note that NO–NSAIDs exert analgesic and anti-inflammatory effects more potently than their parent NSAIDs (non-steroidal anti-inflammatory drugs), while they produce comparable suppression of prostaglandin (PG) synthesis.[7] The most suitable explanation for this is that the nitric oxide released by NO–NSAIDSs contributes to their analgesic and anti-inflammatory effects. The evidence to support this statement comes from the studies of an NO-releasing derivative of acetaminophen. It is known that acetaminophen is not a cyclooxygenase (COX) inhibitor, and exerts little if any anti-inflammatory effects.[9,10] However, an NO-releasing derivative of acetaminophen (NCX-701) was found to reduce carrageenan-induced paw oedema.[10]

Xanthines have been recognized for a long time for their use in the treatment of airways diseases, largely from the standpoint of the ability of these drugs to elicit bronchodilatation.[11] Theophylline has been used in the treatment of obstructive lung diseases, such as asthma and chronic obstructive pulmonary disease (COPD), for more than 75 years.[12] The molecular mechanism of bronchodilatation is likely explained by inhibition of phosphodiesterase (PDE) isoenzymes (III, IV and V). Recently, it has become clear that a number of inflammatory cells specifically possess the PDE isoenzyme IV, thus enhancing the chances that modulation of this enzyme would lead to anti-inflammatory effects. In support of this hypothesis, it has become increasingly apparent that xanthines, such as theophylline, and more selective PDE inhibitors, possess anti-inflammatory and immunomodulatory actions that may contribute to their clinical effects.[12]

In previous papers, the syntheses of new theophylline derivatives[13–15] and nitric oxide donors[16] were reported. In continuation of these studies, herein the synthesis, characterization and biological evaluation of a new xanthine nitric

oxide donor (TSP-81), as a potential drug useful in the treatment of asthma and chronic obstructive pulmonary disease, are presented.

EXPERIMENTAL

All chemicals were purchased from commercial sources (Sigma–Aldrich, Fluka) and were used without further purification. Solvents were purified and dried by standard methods. Melting points were determined by the open capillary method using the Buchi M 565 instrument. The progress of the reaction was monitored by thin-layer chromatography (TLC). The analysis of the CHN contents was realized on a Perkin Elmer 2400 II elemental analyzer. The UV–Vis spectra were recorded in an ethanol: water mixture (9:1) using an HP 8450A UV–Vis spectrophotometer. The FT-IR spectra were taken using the KBr pellet technique on a Bruker VERTEX 70 (USA) instrument, over the 500–4000 cm^{-1} wavenumber range, at a resolution of 4 cm^{-1}. The ^{1}H-NMR and ^{13}C-NMR spectra were recorded employing a Bruker Avance DRX-400 spectrometer using tetramethylsilane as an internal standard and DMSO-d_6 as solvent. Mass spectra were recorded using Agilent 6410 triple quadrupole mass spectrometer. The TG/DTG curves were recorded on a Paulik–Paulik–Erdey derivatograph under the following operational conditions: heating rate of 10 °C min^{-1}, temperature range of 25–600 °C, sample weight of ≈20 mg, platinum crucible and an air flow rate of 100 cm^3 min^{-1}. For each TG stage, the following thermal characteristics were determined: onset temperature (T_i), temperature corresponding to the maximum weight loss rate (T_m), and the temperature corresponding to the end of stage (T_f) (the errors in the temperature determinations were ±2 °C), the weight loss errors were ±1 % and the errors in the activation energy determinations were from ±15 to ±20 kJ mol^{-1}.

*Synthesis of 7-[3-(4-(acetylamino)phenoxy)-2-hydroxypropyl]-1,3-dimethyl-8-(morpholin-4-yl)-xanthine (**5**)*

7-[3-(4-(Acetylamino)phenoxy)-2-hydroxypropyl]-1,3-dimethyl-8-(morpholin-4-yl)xanthine (**5**) was prepared according to a literature procedure by reaction of 8-(morpholin-4-yl)--1,3-dimethylxanthine (**3**) with 4-(2,3-epoxypropoxy)acetanilide (**4**).[13] Yield: 68.6 %.

*Synthesis of 7-[-3-(4-(acetylamino)phenoxy)-2-((2-chloroacetyl)oxy)propyl]-1,3-dimethyl-8-(morpholin-4-yl)xanthine (**6**)*

7-[3-(4-(Acetylamino)phenoxy)-2-hydroxypropyl]-1,3-dimethyl-8-(morpholin-4-yl)xanthine (**5**, D6) (6.14 g, 13 mmol) in tetrahydrofuran (THF) (150 mL) was reacted with chloroacetyl chloride (1.12 mL, 14 mmol) and then triethylamine (TEA, 3.9 mL, 28 mmol) was added. The mixture of reaction was stirred for 10 h, at room temperature and then the solvent was distilled off under reduced pressure. Subsequently, the solid was washed with water, filtered and dried under vacuum. The product was recrystallized from absolute ethanol. Yield: 74.6 %.

*Synthesis of 7-[-3-(4-(acetylamino)phenoxy)-2-((2-(nitrooxy)acetyl)oxy)propyl]-1,3-dimethyl--8-(morpholin-4-yl)xanthine (**7**, TSP-81)*

To a solution of 7-[-3-(4-(acetylamino)phenoxy)-2-((2-chloroacetyl)oxy)propyl]-1,3--dimethyl-8-(morpholin-4-yl)xanthine (**6**) (5.49 g, 10 mmol) in dimethylformamide (DMFA, 150 mL) was added silver nitrate (1.87 g, 11 mmol) in DMFA (50 mL). The reaction mixture was stirred at room temperature for 24 h, in the dark and then filtered under vacuum. Afterwards, the liquid was distilled off under reduced pressure and the solid was washed with cold diethyl ether. Finally, the precipitate was filtered and dried under vacuum. The product was recrystallized from absolute ethanol. Yield: 63.5 %.

Acute toxicity assay

The acute toxicity was evaluated with the lethal dose test involving the administration of the compounds at increasing doses in order to determine the dose that would kill 50 % of the mice (LD_{50}) within a set time-frame.[17,18] The Swiss albino mice of either sex, aged 6 to 8 weeks weighing 20 to 25 g, were obtained from the Central Animal House, University of Medicine and Pharmacy "Grigore T. Popa", Iasi, Romania. The animals were kept in polyethylene boxes, in a controlled environment – constant temperature (24±2 °C) with a 12 h light–dark cycle and relative humidity of 40–70 %. They were kept without food for 24 h before the experiment and water was *ad libitum*. Groups of six mice were used and the studies were performed in accordance with the current guidelines for the veterinary care of laboratory animals,[19] and under the consent of the Ethics Committee for Animal Research of "Grigore T. Popa" University of Medicine and Pharmacy, Iasi, Romania. Each group was treated intraperitoneally with different concentrations of compounds in 0.5 % sodium carboxymethylcellulose (25, 50 and 75 mg mL^{-1}). A group of animals treated with 0.5 % carboxymethylcellulose was used as control group. The symptoms of toxicity and mortality were observed after 24, 48 and 72 h after administration and the LD_{50} of the compounds was estimated.

Cotton pellet-induced granulation inflammation

Tissue granulation was induced by surgical subcutaneous implantation of two cotton pellets in the dorsal region of the rats according to a published procedure[20] with a few modifications. Male Wistar rats, weighing 200–250 g, were divided into five groups of six animals each. Cotton pellets (60±2 mg each) were sterilized by dry heat at 160 °C for 2 h and aseptically implanted in the interscapular distance under the skin of the previously shaved back of the rats, which were anesthetized with thiopental sodium (25 mg kg^{-1}, *i.p.*). The compounds were administered orally at a concentration of 1/5 of the LD_{50} as a suspension in 0.5 % sodium carboxymethylcellulose (40 mg mL^{-1}) once a day for a period of six days. The animals of the control group received only the vehicle. On the seventh day, the rats were sacrificed and the pellets covered with the granulation tissue were extracted and dried in a hot air oven at 60 °C overnight. The difference between the final and initial weight of the pellets was regarded as the granuloma tissue production. A comparison was made between the granulation weight of the treated and control groups.

Detection of nitrite

Different volumes (0.05, 0.1 and 0.2 mL) of the compound (TSP-81) in dimethyl sulfoxide (DMSO) were added to 2 mL of a mixture of 50 mM phosphate buffer (pH 7.4) with methanol solution containing 5×10^{-4} M cysteine (1:1, *V*/*V*). After 1 h at 37 °C, 1 mL of the reaction mixture was treated with 1 mL of Griess reagent (sulphanilamide (4 g), *N*-(1--naphthyl)-ethylenediamine dihydrochloride (0.2 g), 85 % phosphoric acid (10 mL) in distilled water (final volume 100 mL)).[21] After 10 min at room temperature, the absorbance was measured at 540 nm. Sodium nitrite standard solutions (10–80 nmol) were used for the calibration curve. The results are expressed as the percentage of the NO release (n = 3) to a theoretical maximum release of 1 mol NO mol^{-1} of the test compound.

Statistical analysis

The statistical significance of the results was analyzed by the student's *t*-test. The results are expressed as the mean ± standard error of mean (*SEM*). Values of $P \leq 0.05$ were considered statistically significant.

RESULTS AND DISCUSSION

As shown in Scheme 1, 7-[-3-(4-(acetylamino)phenoxy)-2-((2-(nitrooxy)-acetyl)oxy)propyl]-1,3-dimethyl-8-(morpholin-4-yl)xanthine (TSP-81) was synthesized in several steps. In the first step, theophylline (1,3-dimethylxanthine) (**1**) by reaction with bromine in glacial acetic acid afforded 8-bromotheophylline (**2**), which was then treated with morpholine in ethanol solution, when 1,3-dimethyl--8-(morpholin-4-yl)xanthine (**3**) was obtained. In the next step, the intermediary **3** on reaction with 4-(2,3-epoxypropoxy)acetanilide (**4**) led to 7-[3-(4-(acetylamino)phenoxy)-2-hydroxypropyl]-1,3-dimethyl-8-(morpholin-4-yl)xanthine (**5** = = D6).[13] Subsequently, **5** was reacted with chloracetyl chloride in tetrahydrofuran in the presence of triethylamine as acceptor of protons to give the chloroacetyl derivative (**6**) was obtained. Finally, **6** on reaction with silver nitrate in dimethylformamide afforded 7-[-3-(4-(acetylamino)phenoxy)-2-((2-(nitrooxy)-acetyl)oxy)propyl]-1,3-dimethyl-8-(morpholin-4-yl)xanthine (**7** = TSP-81).

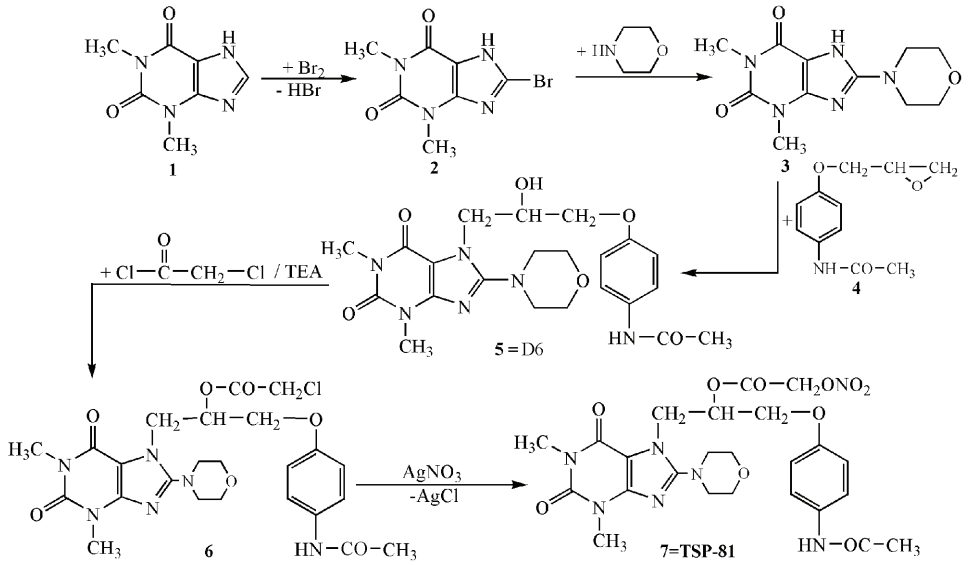

Scheme 1. Synthesis of TSP-81.

The structures of the new derivatives were proved by elemental analyses, UV–Vis, IR, ^{1}H-NMR, ^{13}C-NMR and mass spectroscopy.

The physical, analyticcal and spectral data of **5**–**7** are given in the Supplementary material to this paper.

The IR spectra of the compounds showed peaks for xanthine, acetaminophen and the alkyl chain, which confirm the structure of the compounds. The strong absorption bands at 1740 and 1755 cm^{-1} are due to the ester CO stretching vibration of the chloroacetyl intermediary (**6**) and TSP-81, respectively. The alkyl

halide bond (**6**) appeared at 690 cm^{-1} as a strong band that was absent from the spectrum of TSP-81. In the spectrum of TSP-81, a strong band at 1314 cm^{-1} due to the stretching vibration of the $–ONO_2$ group was observed.

The ^{1}H-NMR spectra (DMSO-d_6) indicated the presence of protons from the alkyl chain that linked the xanthine structure with the acetaminophen residue. The protons of the three methylene groups of TSP-81 appeared as two doublets at 3.91 (CH_2–C) and 4.12 (CH_2–O) and as singlet at 4.41 ppm (CH_2–CO). The proton of the methine group (CH) appears as a singlet at 4.52 ppm. In the ^{13}C-NMR spectra of the compounds **6** and TSP-81, the signals of the alkyl chain carbons appeared at 41.23, 74.49, 75.34 and 172.47 (**6**) and at 40.84, 74.75, 75.21, 169.52 (TSP-81). In the pectrum of the chloroacetyl derivative, the signal for the carbon that linked halide was identified at 50.57, while the carbon that linked the nitrate ester group (TSP-81) appeared at 68.81.

The results of the elemental analysis and mass spectroscopy were found to be in agreement with the values that were theoretically calculated.

Thermogravimetic analysis (TG/DTG) was used to describe the thermal behaviour of the derivatives. The thermogravimetic analysis of TSP-81 showed its four-step decomposition. The first step was insignificant as it showed a mass loss of only 4 %, probably resulting from traces of solvent or water remaining in the compound. The next two overlapping steps were the main steps of the decomposition process that started at a temperature of 167 °C. These two steps accounted for 17.6 and 30.4 % of the mass loss, respectively. The maximum rate of mass loss corresponding to these two steps occurred at 295 and 345 °C, respectively. The last thermogravimetric step started at 462 °C and ended at 725 °C with the maximum rate of mass loss occurring at 615 °C. This step corresponded to the decomposition of an intermediary compound (D6), which left a residue of 16 %. The thermogravimetric characteristics (T_i, T_m, T_f and mass loss) are summarized in Table I.

TABLE I. Characteristic data of thermogravimetric steps; T_i – the onset temperature; T_m – the temperature corresponding to the maximum rate of mass loss; T_f – the temperature corresponding to the end of a decomposition stage

Compound	Step	T_i / °C	T_m / °C	T_f / °C	Mass loss, %
TSP-81	1	60	112	167	4.0
	2	167	295	313	17.6
	3	313	345	462	30.4
	4	462	615	725	32.0
D6	2 and 3	244	300	473	5.4
			337		45.7
			389		57.8

The kinetic parameters of the thermal decomposition (activation energy, E_a, and reaction order, n), were evaluated using both integral and differential methods

employing a versatile commercial programme that gives the overall kinetic parameters by means of various methods. Four methods, *i.e.*, the Coats–Redfern, the Flynn–Wall, the van Krevelen and the Urbanovici–Segal methods, were used to evaluate the overall kinetic parameters.[22,23] The global kinetic parameters for each thermogravimetric step are given in Table II, the results obtained using the different methods being equivalent.

TABLE II. The global values of the kinetic parameters for thermal decomposition of the TSP-81

Kinetic parameter	Step 2	Step 3	Step 4	Kinetic parameter	Step 2	Step 3	Step 4
Coats–Redfern				Flynn–Wall			
E_a / kJ mol^{-1}	37.2	195.6	103.7	E_a / kJ mol^{-1}	43.4	196.3	112.1
n	0.0	2.9	1.2	n	0.0	2.9	1.2
van Krevelen				Urbanovici–Segal			
E_a / kJ mol^{-1}	47.5	232.8	137.4	E_a / kJ mol^{-1}	39.7	200.8	107.1
n	1.4	3.0	1.4	n	0.0	3.0	1.2

As expected, the global activation energy (E_a) increased with the temperature of the decomposition. The first step occurred by a zero reaction order mechanism, being diffusion controlled. For the other two steps, the reaction order increased, showing that the mechanism of decomposition was very complex. The decrease of the activation energy for the four steps could be due to the formation of an unstable intermediary at higher temperatures.

Comparing all the thermo-oxidative characteristics, it appears that the NO--donor compound (TSP-81) is less thermally stable than the intermediary D6 xanthine derivative. It could be supposed that the nitrooxyacetyl chain that links theophylline to acetaminophen destabilizes the molecule because of the increasing oxygen content that allows for an easier oxidation.

Acute toxicity assay

The LD_{50} (the dose causing the death of 50 % of the tested animals) is usually the initial step in the assessment and evaluation of the toxic characteristic of compounds. To establish the LD_{50}, the Karber arithmetic method was used that is based on the formula:[18]

$$LD_{50} = LD_{100} - \frac{\Sigma(a \times b)}{n} \quad (1)$$

where a is the difference between two successive doses of the tested compound; b is the arithmetic average of the animals from two successive series that died; n is the number of animals per group and LD_{100} is the 100 % lethal dose. The values of LD_{50} for TSP-81, the xanthine intermediary D6, theophylline and acetaminophen are given in Table III.

TABLE III. LD_{50} values for TSP-81, its intermediary (D6) and the parent compounds (theophylline and acetaminophen)

Compound	LD_{50} / mg kg^{-1}			
	24 h	48 h	72 h	Average
TSP-81	456	456	420	444
D6	439	439	390	423
Theophylline	205	205	190	200
Acetaminophen	351	351	312	338

The LD_{50} of TSP-81 that combines theophylline with acetaminophen using nitrate ester alkyl chain as a spacer was 444 mg kg^{-1}, which means that it was slightly less toxic than its intermediary, D6 (LD_{50} 423 mg kg^{-1}) but it is much less toxic than its parent compounds. TSP-81 is 2.2 times less toxic than theophylline and 1.3 less toxic than acetaminophen. These results are important because it is known that both theophylline and acetaminophen are associated with several side effects, especially when they are used in chronic treatment.

Cotton pellet-induced granulation inflammation

The cotton pellet-induced granuloma is widely used to assess the transudative and proliferative components of chronic inflammation.[24] The implanted material induces a host inflammatory response and modulates the release of inflammatory mediators that finally leads to tissue proliferation and granular formation.[25] The weight of the wet cotton pellets is correlated with transude material and the weight of the dry pellets is correlated with the granuloma tissue formation. A decreasing of granuloma tissue formation is an indicator of the antiproliferative effect of an anti-inflammatory drug. The effect of the tested compounds (TSP-81, D6, theophylline and acetaminophen) in reference with the control group (that received only 0.5 % carboxymethylcellulose), on the cotton pellet-induced granuloma in rats are given in Table IV. After six days, the dry weight of the granuloma tissue surrounding the cotton pellets was significantly lower ($P < 0.05$) for the group treated with TSP-81, compared to the control group, but also compared with its intermediary (D6) and parent compounds. TSP-81 exhibited a value of 15.32±1.09 related to 63.46±1.16 (control), 31.68±1.23

TABLE IV. The effects of the tested compounds on granuloma tissue formation (data represent average ± *SEM*, $n = 6$. *$P < 0.05$ *vs.* control)

Compound	Dose mg kg^{-1}	Weight of the dry cotton pellet, mg	Weight of the granuloma tissue, mg	Inhibition level %
TSP-81	90	76.82±1.14*	15.32±1.09*	75.85
D6	85	91.38±1.18*	31.68±1.23*	50.07
Theophylline	40	100.25±1.12*	38.77±1.20*	38.90
Acetaminophen	70	121.36±1.10*	60.28±1.22*	5.01
Control	Vehicle	124.46±1.15	63.46±1.16	–

(D6), 38.77±1.20 (theophylline) and 60.28±1.22 (acetaminophen). These results support the conclusion that TSP-81 is approximately 2 times more active than theophylline and 4 times more active than acetaminophen as an anti-inflammatory drug.

Detection of nitrite

The nitric oxide releasing property of TSP-81 was assessed in phosphate buffer, pH 7.4, in the presence of L-cysteine, as a source of SH groups, and it was calculated based on the nitric oxide released from standard sodium nitrite solution.

It is known that nitric oxide donors release NO through enzymatic and non-enzymatic pathways. The non-enzymatic pathway involves chemical reaction with acid, alkali, metals and compounds with SH groups.[26] The nucleophilic attack of L-cysteine on the nitrate group of TSP-81 resulted in the formation of a thionitrate as an intermediate to the formation of cysteine and nitrite during the next step (Scheme 2).

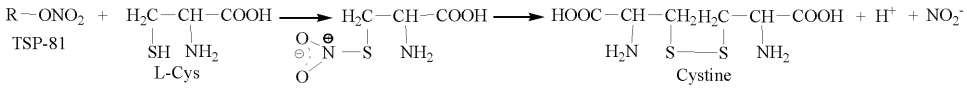

Scheme 2. The mechanism of the NO release from TSP-81.

The released nitrite was detected using the Griess reagent system that uses sulphanilamide and *N*-(1-napthyl)ethylenediamine dihydrochloride (NED) under acidic conditions. The red–pink azo compound was detected spectrophotometrically (Scheme 3).

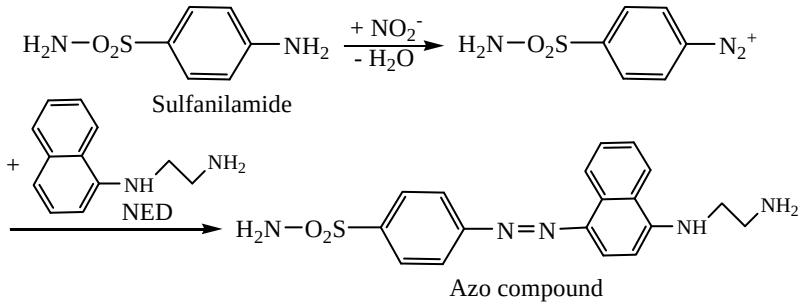

Scheme 3. Chemical reactions involved in the measurement of NO_2^- using the Griess reagent system.

The absorbance of the TSP-81 solution increased with the concentration and the amount of NO released related to a theoretical maximum release of 1 mol NO mol^{-1} of test compound was found to be around 0.5 mol (Table V). The results

confirm the ability of the TSP-81 to release NO and also the implication of the NO in the expression of the anti-inflammatory effect of the tested compound.

TABLE V. The nitric oxide releasing effect of the TSP-81 (data represent average ± *SEM*, $n = 3$, $P < 0.05$)

Volume, mL	Concentration, μg mL^{-1}	Absorbance	NO_2^- released, mol
0.05	330	0.2748±0.0052	0.4763±0.04314
0.1	650	0.57313±0.0144	
0.2	1250	0.95207±0.0310	

CONCLUSIONS

A new xanthine nitric oxide donor (TSP-81) was synthesized and characterized from spectral, thermal and biological viewpoints. The thermo-oxidative decomposition of the TSP-81 occurred in four steps. As was expected, this new NO-donor compound was less stable than its intermediate (D6) and parent drugs (theophylline and acetaminophen). The results of the biological evaluation of the compound support its lower toxicity, its higher anti-inflammatory effect and its ability to release nitric oxide. As a result, it could be supposed that the anti-inflammatory effect of TSP-81 is due to the inhibition of phosphodiesterase activity and also to its nitric oxide releasing properties. In conclusion, TSP-81 could become an important drug in the management of asthma and chronic obstructive pulmonary diseases.

SUPPLEMENTARY MATERIAL

Physical, analytic and spectral data for the synthesised compounds are available electronically from http://www.shd.org.rs/JSCS/, or from the corresponding author on request.

ИЗВОД

СИНТЕЗА, КАРАКТЕРИЗАЦИЈА И ИСПИТИВАЊЕ БИОЛОШКЕ АКТИВНОСТИ НОВОГ ДОНОРА АЗОТ-МОНОКСИДА

LENUTA PROFIRE[1], MARIA APOTROSOAEI[1], ANCA OPREA[2], MIHAI BREBU[2], FLORENTINA LUPASCU[1], CATALINA ELENA LUPUSORU[3] и CORNELIA VASILE[2]

[1]Department of Pharmaceutical Chemistry, Faculty of Pharmacy, "Grigore T. Popa" University of Medicine and Pharmacy, 16 University Str., 700115, Iasi, Romania, [2]Department of Physical Chemistry of Polymers, "P. Poni" Institute of Macromolecular Chemistry, Romanian Academy, 41A Grigore Ghica Voda Alley, 700487, Iasi, Romania и [3]Department of Pharmacology, Faculty of Medicine, "Grigore T. Popa" University of Medicine and Pharmacy, 16 University Str., 700115, Iasi, Romania

Описана је синтеза ксантинског донора (TSP-81) азот-моноксида. Једињење је осмишљено да садржи две структурне целине – теофилин (1,3-диметилксантин) и ацетаминофен (4-хидроксиацетанилид), повезане линкером који садржи извор азот-моноксида. Једињење је окарактерисано микроанализом, спектралним методама ^{1}H-NMR, ^{13}C- NMR, FT-IR, UV–Vis као и TG и DTG техникама. Термални профил показује да се TSP-81 топи у четири корака, уз распадање, од којих су најважнији други корак (детектован губитак масе 17,6 %) и трећи корак (регистрован губитак масе 30,4 %). Такође, испитана је токсичност, анти-инфламаторни ефекат и способност отпуштања

азот-моноксида. Биолошки тестови показују да TSP-81 има ниску токсичност и изражен анти-инфламаторни ефекат, у поређењу са теофилином и ацетаминофеном, једињењима из којих је изведен. TSP-81 је око 2 пута активнији од теофилина и око 4 пута активнији од ацетаминофена. Осим тога, резултати указују да ослобађање азот-моноксида доприноси анти-инфламаторном ефекту.

(Примљено 24. јануара, ревидирано 1. јула 2013)

REFERENCES

1. M. Biava, C. Battilocchio, G. Poce, S. Alfonso, S. Consalvi, G. C. Porretta, S. Schenone, V. Calderone, A. Martelli, L. Testai, C. Ghelardini, L. Mannelli, L. Sautebin, A. Rossi, A. Giordani, P. Patrignani, M. Anzini, *Eur. J. Med. Chem.* **58** (2012) 287
2. R. A. Serafim, M. C. Primi, G. H. Trossini, E. I. Ferreira, *Curr. Med. Chem.* **19** (2012) 386
3. E. Gkaliagkousi, A. Ferro, *Front. Biosci.* **16** (2011) 1873
4. J. Kaur, A. Bhardwaj, Z. Huang, D. Narang, T. Y. Chen, F. Plane, E. E. Knaus, *J. Med. Chem.* **55** (2012) 7883
5. N. Borhade, A. R. Pathan, S. Halder, M. Karwa, M. Dhiman, V. Pamidiboina, M. Gund, J. J. Deshattiwar, S. V. Mali, N. J. Deshmukh, S. P. Senthilkumar, P. Gaikwad, S. G. Tipparam, J. Mudgal, M. C. Dutta, A. U. Burhan, G. Thakre, A. Sharma, S. Deshpande, D. C. Desai, N. P. Dubash, A. K. Jain, S. Sharma, K. V. Nemmani, A. Satyam, *Chem. Pharm. Bull.* **60** (2012) 465
6. Y. Li, X. Wang, R. Fu, W. Yu, X. Wang, Y. Lai, S. Peng, Y. Zhang, *Bioorg. Med. Chem. Lett.* **21** (2011) 4210
7. F. Stefano, E. Distrutti, *Curr. Top. Med. Chem.* **7** (2007) 277
8. E. Koc, S. G. Kucukguzel, *Mini Rev. Med. Chem.* **9** (2009) 611
9. S. Fiorucci, E. Distrutti, *Curr. Med. Chem.* **18** (2011) 3494
10. M. Marshall1, J. Keeble, P. K. Moore, *Brit. J. Pharmacol.* **149** (2006) 516
11. P. J. Barnes, *Proc. Am. Thorac. Soc.* **2** (2005) 334
12. K. H. Banner, C. P. Page, *Eur. Respir. J.* **8** (1995) 996
13. G. Danila, L. Profire, G. G. Bumbu, C. Vasile, *Thermochim. Acta* **343** (2000) 69
14. L. Profire, G. G. Bumbu, M. Costuleanu, G. Danila, C. Vasile, *Thermochim. Acta* **381** (2002) 19
15. L. Profire, V. Sunel, D. Lupascu, M. C. Baican, N. Bibire, C. Vasile, *Farmacia* **58** (2010) 170
16. L. Profire, D. Lupascu, V. Sunel, N. Bibire, C. Vasile, *Rev. Chim. (Bucharest*) **61** (2010) 1150
17. S. Bhardwaj, D. Gupta, *Int. J. Pharm. Bio. Sci.* **1** (2012) 103
18. J. S. Akhila, S. Deepa, M. C. Alwar, *Curr. Sci.* **93** (2007) 917
19. European Parliament and the Council: *Directive 2010/63/EU on the protection of animals used for scientific purposes* (2010)
20. A. A Bekhit, H. M. Ashour, A.-D. Bekhit, S. A. Bekhit, *Med. Chem.* **5** (2009) 103
21. A. H. Abadi, G. H. Hegazy, A. A. El-Zaher, *Bioorg. Med. Chem.* **13** (2005) 5759
22. M. F. F. Pedrosa, D. M. Araujo Melo, H. Scatena, F. M. M. Borges, L. B. Zinner, A. O. Silva, *J. Alloys Compò.* **303** (2000) 142
23. S. Y. Yorulmaz, A. T. Atimtay, *Fuel Process. Technol.* **90** (2009) 939
24. A. Ahmadi, M. Khalili, A. Nafarie, A. Yazdani, B. Nahri-Niknafs, *Mini Rev. Med. Chem.* **12** (2012) 1282

25. A. A. Bekhit, H. T. Fahmy, S. A. Rostom, A. El-Din, A. Bekhit, *Eur. J. Med. Chem*. **45** (2010) 6027.
26. S. Huerta, S. Chilka, B. B. Vida, *Int. J. Oncol*. **33** (2008) 909.

Journal of the Serbian Chemical Society
JSCS@tmf.bg.ac.rs • www.shd.org.rs/JSCS
J. Serb. Chem. Soc. 79 (4) S44–S45 (2014) *Supplementary material*

SUPPLEMENTARY MATERIAL TO

The synthesis, characterization and biological evaluation of a new nitric oxide donor agent

LENUTA PROFIRE[1]*, MARIA APOTROSOAEI[1], ANCA OPREA[2], MIHAI BREBU[2], FLORENTINA LUPASCU[1], CATALINA ELENA LUPUSORU[3] and CORNELIA VASILE[2]

[1]*Department of Pharmaceutical Chemistry, Faculty of Pharmacy, "Grigore T. Popa" University of Medicine and Pharmacy, 16 University Str., 700115, Iasi, Romania,* [2]*Department of Physical Chemistry of Polymers, "P. Poni" Institute of Macromolecular Chemistry, Romanian Academy, 41A Grigore Ghica Voda Alley, 700487, Iasi, Romania and* [3]*Department of Pharmacology, Faculty of Medicine, "Grigore T. Popa" University of Medicine and Pharmacy, 16 University Str., 700115, Iasi, Romania*

J. Serb. Chem. Soc. 79 (4) (2014) 389–400

PHYSICAL, ANALYTIC AND SPECTRAL DATA FOR THE SYNTHESISED COMPOUNDS

*7-[3-(4-(Acetylamino)phenoxy)-2-hydroxypropyl]-1,3-dimethyl-8-(morpholin-4-yl)xanthine (**5**)*. Yield: 68.6 %; m.p. 228–230 °C; Anal. Calcd. for $C_{22}H_{28}N_6O_6$: C, 55.92, H, 5.92, N, 17.78. Found: C, 56.14; H, 6.21, N, 18.03; IR (KBr, cm^{-1}): 3400, 1200 (linked OH), 3120, 2968 (>N–CH_3), 2900 (CH_3, –CH_2–), 2884 (–CH<), 1720 (>C=N), 1620 (–NH–CO), 1660 (>C=C<N–), 1580 (>C=C<CO), 1480, 780, 710 (–C_6H_4–), 1350 (–O–CH_2), 1370 (–CO–CH_3); ^{1}H-NMR (400 MHz, DMSO-d_6, δ / ppm): 2.02 (1H, *d*, OH, *J* = 7.2 Hz), 2.10 (3H, *s*, CH_3–CO), 2.68 (6H, *s*, 2CH_3–N<), 2.90 (4H, *m*, 2CH_2–N<, *J* = 7.4 Hz), 3.77 (4H, *m*, 2CH_2–O, *J* = 7.4 Hz), 3.88 (2H, *d*, CH_2–C, *J* = 7.6 Hz), 4.15 (2H, *d*, CH_2–O, *J* = 7.6 Hz), 4.38 (1H, *m*, CH), 6.78 (2H, *d*, aromatic, *J* = 8.4 Hz), 7.53 (2H, *d*, aromatic, *J* = 8.4 Hz), 8.05 (1H, *s*, NH); ^{13}C-NMR (100 MHz, DMSO-d_6, δ / ppm): 17.62, 28.34, 36.71 (CH_3), 38.56, 58.84, 58.92, 71.42, 71.68, 77.60 (CH_2), 74.91 (CH), 136.81, 141.04, 149.80 (xanthine), 114.42, 114.68, 121.08, 121.25, 132.40, 154.70 (aromatic), 156.81, 166.84, 168.23 (CO); Mass (*m*/*z*): 472 [M^+].

*7-[-3-(4-(acetylamino)phenoxy)-2-((2-chloroacetyl)oxy)propyl]-1,3-dimethyl-8-(morpholin-4-yl)xanthine (**6**)*. Yield: 74.6 %; m.p. 189–192 °C; Anal. Calcd. for $C_{24}H_{29}ClN_6O_7$: C, 52.50, H, 5.32, N, 15.30. Found: C, 52.12; H, 5.80, N, 14.84; IR (KBr, cm^{-1}): 3141, 2954 (>N–CH_3), 2908 (CH_3, –CH_2–), 2875

* Corresponding author. E-mail: nprofire@yahoo.com

(–CH<), 1704 (>C=N), 1740 (–CO–O), 1658 (–NH–CO), 1606 (>C=C<N–), 1540 (>C=C<CO), 1511, 751, 675 (–C_6H_4–), 1453 (–O–CH_2), 1363 (–CO–CH_3), 690 (C–Cl); ^{1}H-NMR (400 MHz, DMSO-d_6, δ / ppm): 2.05 (3H, *s*, CH_3–CO), 2.75 (6H, *s*, 2CH_3–N<), 2.95 (4H, *m*, 2CH_2–N<, *J* = 7.4 Hz), 3.70 (4H, *m*, 2CH_2–O, *J* = 7.4 Hz), 3.95 (2H, *d*, CH_2–C, *J* = 7.3 Hz), 4.15 (2H, *d*, CH_2–O, *J* = = 7.3 Hz), 4.45 (2H, *s*, CH_2–CO), 4.55 (1H, *m*, CH), 6.78 (2H, *d*, aromatic, *J* = = 8.5 Hz), 7.59 (2H, *d*, aromatic, *J* = 8.5 Hz), 8.05 (1H, *s*, NH); ^{13}C-NMR (100 MHz, DMSO-d_6, δ / ppm): 18.24, 29.26, 37.41 (CH_3), 41.23, 50.57, 59.18, 59.34, 71.48, 71.81, 74.49 (CH_2), 75.34 (CH), 136.47, 140.52, 149.67 (xanthine), 114.38, 114.87, 121.72, 122.15, 132.48, 154.83 (aromatic), 156.95, 166.54, 168.82, 172.47 (CO); Mass (*m*/*z*): 549 [M^+].

*7-[-3-(4-(acetylamino)phenoxy)-2-((2-(nitrooxy)acetyl)oxy)propyl]-1,3-dimethyl-8-(morpholin-4-yl)xanthine (**7**, TSP-81)*. Yield: 63.5 %, m.p. 161–163 °C; Anal. Calcd. for $C_{24}H_{29}N_7O_{10}$: C, 50.08, H, 5.07 N, 17.03. Found: C, 50.36, H, 4.78, N, 17.36; IR (KBr, cm^{-1}): 3144, 2957 (>N–CH_3), 2914 (CH_3, –CH_2–), 2872 (–CH<), 1755 (–CO–O), 1712 (>C=N), 1648 (–NH–CO), 1610 (>C=C<N–), 1548 (>C=C<CO), 1524, 743, 684 (–C_6H_4–), 1457 (–O–CH_2), 1371 (–CO–CH_3), 1314 (–O–NO_2); ^{1}H-NMR (400 MHz, DMSO-d_6, δ / ppm): 2.08 (3H, *s*, CH_3– –CO), 2.72 (6H, *s*, 2CH_3–N<), 2.92 (4H, *m*, 2CH_2–N<, *J* = 7.5 Hz), 3.64 (4H, *m*, 2CH_2–O, *J* = 7.5 Hz), 3.91 (2H, *d*, CH_2–C, *J* = 7.4 Hz), 4.12 (2H, *d*, CH_2–O, *J* = = 7.4 Hz), 4.41 (2H, *s*, CH_2–CO), 4.52 (1H, *m*, CH), 6.69 (2H, *d*, aromatic, *J* = = 8.4 Hz), 7.52 (2H, *d*, aromatic, *J* = 8.4 Hz), 8.11 (1H, *s*, NH). ^{13}C-NMR (100 MHz, DMSO-d_6, δ / ppm): 17.82, 28.67, 37.23 (CH_3), 40.84, 58.67, 58.84, 68.81, 71.76, 72.08, 74.75 (CH_2), 75.21 (CH), 137.12, 141.24, 149.36 (xanthine), 115.12, 115.54, 122.46, 122.83, 133.08, 155.23 (aromatic), 158.23, 167.48, 169.52, 171.87 (CO); Mass (*m*/*z*): 575 [M^+]; UV–Vis (ethanol:water, 9:1, λ_{max} / / nm): 277, 248.

Journal of the Serbian Chemical Society
JSCS-info@shd.org.rs • www.shd.org.rs/JSCS
J. Serb. Chem. Soc. 79 (4) 401–409 (2014)
JSCS–4594
UDC 547.458.6+547.831+547.495.1+ 542.913:544.478
Original scientific paper

β-Cyclodextrin–polyurethane polymer: a neutral and eco-friendly heterogeneous catalyst for the one-pot synthesis of 1,4-dihydropyridine and polyhydroquinoline derivatives *via* the Hantzsch reaction under solvent-free conditions

ALI REZA KIASAT*, SIMIN NAZARI and JAMAL DAVARPANAH

Chemistry Department, Faculty of Sciences, Shahid Chamran University, Ahvaz 61357-4-3169, Iran

(Received 12 January, revised 25 May 2013)

Abstract: An efficient synthesis of 1,4-dihydropyridine and polyhydroquinoline derivatives using a *β*-cyclodextrin–polyurethane polymer (*β*-CDPU) as a stationary micro-vessel and neutral heterogeneous catalyst *via* a four component coupling of aldehydes, *β*-ketoester (2 mol) and ammonium acetate under solvent-free conditions is described. Compared with the classical Hantzsch reaction, this new method has the advantages of good yield, short reaction time and methodological simplicity. *β*-CDPU was proved to be an efficient heterogeneous catalyst that could be easily handled and removed from the reaction mixture by simple filtration, and also recovered and reused without loss of reactivity.

Keywords: *β*-cyclodextrin–polyurethane polymer; 1,4-dihydropyridine and polyhydroquinoline derivatives; heterogeneous catalyst; four-component coupling; solvent-free.

INTRODUCTION

The development of simple synthetic routes for complex organic molecules from readily available reagents is an important task in organic synthesis. In recent years, the development of new multicomponent reactions (MCRs) and the improvement of known MCRs are important areas of research in organic, combinatorial and medicinal chemistry.[1–3] As opposed to the classical route to synthesize complex molecules by sequential synthesis, MCRs allow the assembly of complex molecules in one-pot and offer a facile execution, high atom-economy and high selectivity and yields.[4–7]

Dihydropyridines and their derivatives (DHPs) have received considerable attention of synthetic and medicinal chemists because of their broad spectrum of

* Corresponding author. E-mail: akiasat@scu.ac.ir
doi: 10.2298/JSC130112130K

biological and pharmaceutical activities.[8–15] These derivatives show antihypertensive, vasodilator, antimutagenic, antitumor, anticonvulsant, antidiabetic, anti-anxiety, antidepressive, analgesic, seditative, bronchodilator, hypnotic and anti--inflammatory activities.[16–20] Furthermore, these compounds are used as calcium channel blockers for the treatment of cardiovascular diseases including hypertension.[21] Recent studies have shown that 1,4-DHPs exhibit several other medicinal properties, which indicates the remarkable potential of novel DHP derivatives as a source of valuable drug candidates.[22]

Due to the biological importance associated with these compounds, numerous methods have been reported for their synthesis. However, many of these methodologies suffer from several drawbacks, such as a long reaction time, an excess of organic solvent, low product yields, expensive reagents, harsh conditions and the occurrence of several side products and difficulties in the recovery and reusability of the catalysts. Due to these problems, the development of an efficient, novel and versatile method for the preparation of 1,4-DHPs is an important aspect and is an active on-going research area. There is also scope for further improvement towards mild reaction conditions and higher yields.

With the increasing public concern over environmental degradation, the elimination of volatile and toxic organic solvents in chemical processes represents very powerful procedures for green chemical technology from both the economic and synthetic points of view.[23–25] They have many advantages, such as reduced pollution, lower cost, and simplicity in processing, which are beneficial to the industry as well as to the environment. There is also another route to combine economic aspects with environmental protection, *i.e.*, the use of heterogeneous catalysts.

Recently, the use of solid supported catalysts[26] has received considerable importance in organic synthesis because of their ease of handling, reduced reaction times, greater selectivity, simple workup, and recoverability of the catalysts. With this goal in mind and in continuation of on-going research into the employment of *β*-cyclodextrin–polyurethane as a stationary micro-vessel and heterogeneous catalyst in organic transformations,[27–32] herein, a green approach is reported for the synthesis of 1,4-dihydropyridine and polyhydroquinoline derivatives *via* the Hantzsch reaction catalyzed by *β*-CDPU resin as a neutral and eco-friendly polymeric catalyst under solvent-free neat conditions.

EXPERIMENTAL

The chemicals were purchased from Fluka, Merck or Aldrich. *β*-Cyclodextrin was heated at 80 °C under vacuum for 30 min before use to remove traces of moisture. The yields refer to the isolated crude products. The NMR spectra were recorded in acetone-d_6 or $CDCl_3$ on a Bruker Avance DPX 400 MHz spectrometer using TMS as the internal standard. The purity determination of the products and the reaction monitoring were accomplished by TLC on silica gel polygram SILG/UV 254 plates. The FT-IR spectra of the *β*-cyclodextrin–polyure-

thane were recorded as potassium bromide discs on a BOMEM MB-Series1998 FT-IR spectrophotometer.

Preparation of β*-cyclodextrin–polyurethane polymer*

The *β*-cyclodextrin–polyurethane polymer (*β*-CDPU) was synthesized by reacting *β*-CD with hexamethylene diisocyanate, HMDI, in dry DMF according to Yilmaz *et al.*[33] Briefly, two grams of *β*-CD (1.76 mmol) were dissolved in 15 mL of dry DMF in a 100 mL round bottom flask at room temperature. To the solution, 17.6 mmol of HMDI in 5 mL of dry DMF was added dropwise. Then the mixture was stirred at 70 °C for 3 h. The resin was filtered off and washed with acetone several times. The polymer was dried under vacuum at 80 °C overnight.

General procedure for the synthesis of 1,4-DHPs

The *β*-CDPU resin (0.15 g) was added to a magnetically stirred mixture of aromatic aldehyde **1** (1 mmol), ethyl acetoacetate **2** (2 mmol) and ammonium acetate **3** (1.2 mmol). The resulting reaction mixture was stirred at 80 °C for the appropriate time. After completion of the reaction, as indicated by TLC (using *n*-hexane/ethyl acetate (5:1)), the reaction mixture was cooled to room temperature and the crude product extracted with CH_2Cl_2. The organic solvent was removed by simple evaporation. Finally, the crude product was recrystallized from EtOH/H_2O to afford the corresponding pure 1,4-dihydropyridine derivatives in high yields. All the compounds were characterized based on spectroscopic data (IR, ^{1}H- and ^{13}C--NMR) and by comparison with those reported in the literature. The spectral data is given in the Supplementary material to this paper.

General procedure for the synthesis of polyhydroquinolines

A mixture of aromatic aldehyde (1 mmol), dimedone (1 mmol), ammonium acetate (1.5 mmol), ethyl acetoacetate (1 mmol), and *β*-CDPU resin (0.15 g) was heated at 80 °C with stirring for 10–30 min. After completion of the reaction, as indicated by TLC, the reaction mixture was washed with CH_2Cl_2 and the catalyst was filtered off. The organic solvent was removed by simple evaporation and the pure product was obtained by recrystallization from ethanol. The catalyst was recovered by filtration, washed with water and methanol, dried at room temperature and reused several times for the same reaction.

The spectral data are given in the Supplementary material to this paper.

RESULTS AND DISCUSSION

β-Cyclodextrin (*β*-CD) is a torus-shaped cyclic oligosaccharide composed of seven D-glucopyranose units connected by *α*-(1,4)-linkages. These macromolecules possess a characteristic toroidal shape with a well-defined lipophilic cavity and a hydrophilic exterior that is suitable for the inclusion binding of appropriately sized guest compounds. This outstanding property has long been utilized in the pharmaceutical, food, cosmetic and textile industries and has found applications in the field of catalysis, environmental remediation, chemical sensing, and enantiomeric separations. Various methods for insoluble CD production and/or immobilization on solid supports have been successfully developed and used. Hexamethylene diisocyanate (HMDI) is a widely used linker for the fabrication of drug delivery vehicles with reportedly a very low degree of toxicity.

Bearing all this in mind, in the present work, *β*-CD was incorporated into a cross-linked polymeric form using hexamethylene diisocyanate. Using this strategy, the recycling of *β*-CD would become feasible and its discharge into the environment significantly minimized to non-harmful levels. The polymeric network was synthesized in the reaction depicted in Scheme 1.

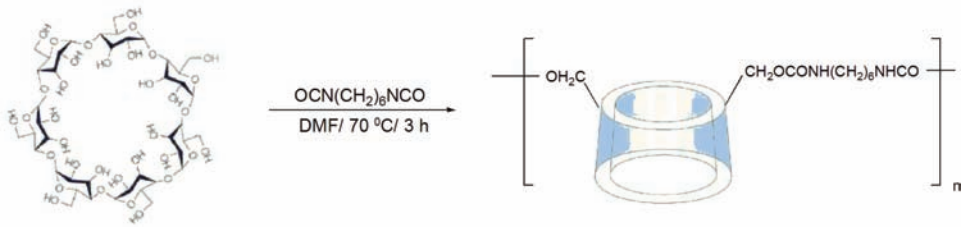

Scheme 1. Synthesis of the *β*-CD based polymer.

The polymerization of *β*-CD molecules with the assistance of hexamethylene diisocyanate (HMDI) was confirmed by FT-IR analysis. Evidence of polymerization was the disappearance of the isocyanate peak in the IR spectrum at about 2280 cm^{-1}. The IR spectrum of the polymer showed characteristic absorption bands at 3360 and 1718 cm^{-1}, corresponding to NH and C=O groups. NHCO stretching was also observed at 1570 cm^{-1}.

In order to investigate the possible catalytic properties of the *β*-CDPU resin in the Hantzsch reaction, the four-component coupling of aldehydes, *β*-ketoester and ammonium acetate under solvent-free conditions was chosen (Scheme 2).

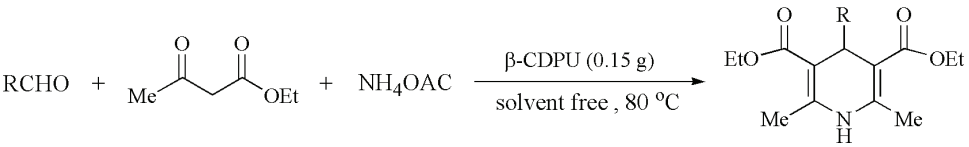

Scheme 2. Synthesis of the 1,4-dihydropyridine derivatives.

Initially, a mixture of benzaldehyde, ethyl acetoacetate and ammonium acetate was studied as the model reaction to determine whether the use of the polymeric catalyst was efficient and to determine the optimized conditions. The results are given in Table I.

The temperature had a critical effect on the reaction yield and no reaction occurred at room temperature, even after two hours. However, heating the reaction mixture at 80 °C afforded the product in 89 % yield (reaction conditions 3). For yield improvement, the effect of the catalyst loading was also studied. Increasing the catalyst loading from 0.15 to 0.20 g did not significantly affect the yield, while the reaction in the absence of the polymeric catalyst at 80 °C gave the product in only 10 % yield after 3 h.

TABLE I. Optimization of reaction conditions for the four-component coupling of benzaldehyde, ethyl acetoacetate and ammonium acetate

Entry	β-CDPU amount, g	Temperature, °C	Ammonium acetate amount, mmol	Time, min	Yield, %
1	0.00	80	1.5	180	10
2	0.1	80	1.5	30	89
3	0.15	80	1.5	15	89
4	0.2	80	1.5	15	90
5	0.15	25	1.5	120	Trace
6	0.1 5	60	1.5	45	72
8	0.15	90	1.5	15	87
9	0.15	80	1	55	68
10	0.15	80	2	15	90

With the optimized conditions in hand, an array of aromatic aldehydes were treated with ethyl acetoacetate and ammonium acetate using 0.15 g of β-CDPU at 80 °C whereby the desired products were afforded in high to excellent isolated yields (86–94 %) (Table II). Aromatic aldehydes, however, provided better yields in comparison with their aliphatic counterparts. With regard to substituents, both aldehydes with electron-withdrawing and electron-donating groups participated in the reaction, but the former reacted better.

TABLE II. Synthesis of the 1,4-dihydropyridine derivatives catalyzed by β-CDPU under solvent-free conditions at 80 °C

Compound	R	Time, min	Yield, %
1	C_6H_5	15	89
2	4-$CH_3OC_6H_4$	20	92
3	4-OHC_6H_4	30	86
4	4-ClC_6H_4	20	87
5	4-CNC_6H_4	15	92
6	4-$EtOC_6H_4$	35	88
7	4-$(CH_3)_2NC_6H_4$	45	92
8	4-$NO_2C_6H_4$	15	94
9	2-ClC_6H_4	20	90
10	2-$NO_2C_6H_4$	25	88

In view of environmentally friendly methodologies, recovery and reuse of a catalyst is highly desired. The β-CDPU polymer did not suffer from extensive mechanical degradation and was quantitatively recovered by simple filtration and washing with water and methanol. It could be reused for subsequent reactions. Recycled β-CDPU showed no loss of efficiency with regard to yield after four successive runs (Table III).

The high reaction rate observed in the present method could be attributed to the fact that the hydrophobic central cavities of β-CD units in the β-CDPU polymer acted as a micro-vessel and accommodated the nonpolar compounds. In

addition, the hydrophilic exterior due to the outer OH of the *β*-CD cavity promoted the reaction *via* hydrogen bonding (Scheme 3).

TABLE III. Recyclability of the *β*-CDPU polymer

Entry	Yield, %
1	89
2	87
3	87
4	84

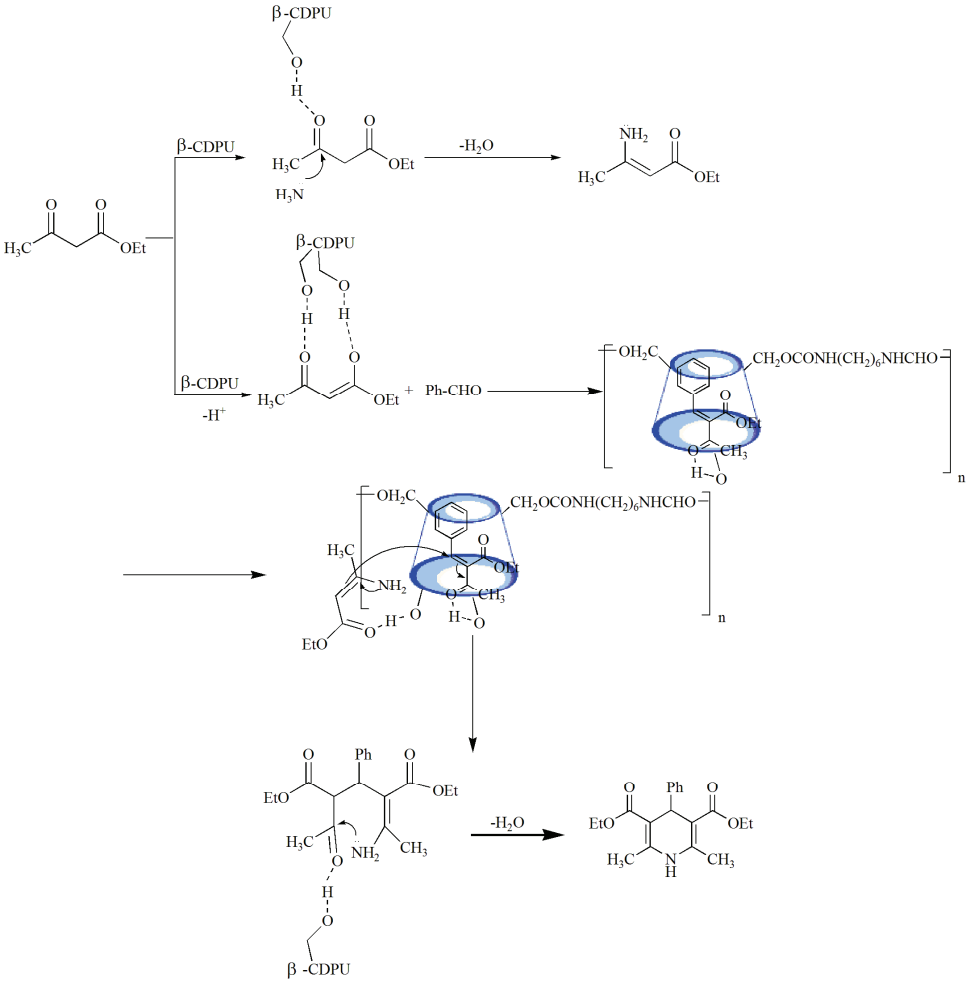

Scheme 3. A plausible mechanism of the reaction.

After the success of this first set of Hantzsch reactions catalyzed by *β*-CDPU resin, the reaction was extended to the synthesis of polyhydroquinoline deri-

vatives. Thus, various aromatic aldehydes were treated with dimedone, ammonium acetate and ethyl acetoacetate under the optimized reaction conditions for preparation of 1,4-dihydropyridines derivatives (Scheme 4). The results are summarized in Table IV, which indicate that the desired products were formed in high isolated yields and in appropriative times.

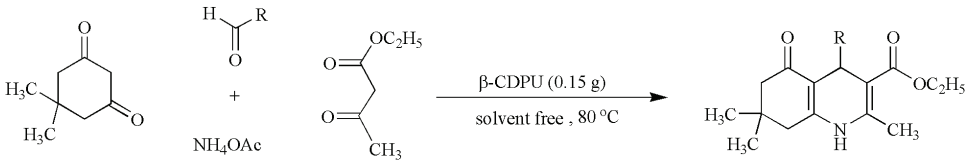

Scheme 4. Synthesis of the polyhydroquinoline derivatives.

TABLE IV. Synthesis of the polyhydroquinoline derivatives *via* unsymmetrical Hantzsch reactions catalyzed by *β*-CDPU

Compound	R	Time, min	Yield, %	M.p. / °C (found)	M.p. / °C (reported)
11	C_6H_5	10	90	224–226	227–229[34]
12	4-ClC_6H_4	10	84	242–243	245–246[35]
13	4-OHC_6H_4	25	90	237–238	238–240[36]
14	4-$CH_3C_6H_4$	15	89	260–262	260–262[34]
15	4-$N(CH_3)_2C_6H_4$	30	92	227–230	229–231[37]
16	4-$NO_2C_6H_4$	10	86	242–246	242–244[38]
17	2-ClC_6H_4	15	93	208–211	–
18	2-$NO_2C_6H_4$	15	87	202–206	–

CONCLUSIONS

In conclusion, an easy, efficient and green protocol for the synthesis of 1,4--dihydropyridines and polyhydroquinoline derivatives under solvent-free neat conditions *via* an improved Hantzsch reaction catalyzed by *β*-CDPU polymer has been reported. The method offers marked improvement with its operational simplicity, short reaction time and high yields of pure products without use of any organic solvent.

SUPPLEMENTARY MATERIAL

Spectral data for the synthesized compounds are available electronically from http:// //www.shd.org.rs/JSCS/, or from the corresponding author on request.

Acknowledgment. We are grateful to the Research Council of Shahid Chamran University, Iran, for financial support.

И З В О Д

β-ЦИКЛОДЕКСТРИН–ПОЛИУРЕТАНСКИ ПОЛИМЕР: НЕУТРАЛАН И ЕКОЛОШКИ ПРИХВАТЉИВ ХЕТЕРОГЕНИ КАТАЛИЗАТОР У СИНТЕЗИ ДЕРИВАТА 1,4-ДИХИДРОПИРИДИНА И ПОЛИХИДРОХИНОЛИНА ХАНЧОВОМ (*HANTZSCH*) РЕАКЦИЈОМ У ЈЕДНОМ РЕАКЦИОНОМ КОРАКУ У ОДСУСТВУ РАСТВАРАЧА

ALI REZA KIASAT, SIMIN NAZARI и JAMAL DAVARPANAH

Chemistry Department, Faculty of Science, Shahid Chamran University, Ahvaz 61357-4-3169, Iran

Описана је примена циклодекстрин–полиуретанског полимера (*β*-CDPU) у синтези деривата 1,4-дихидропиридина и полихидрохинолина. *β*-CDPU је присутан као стационарна микропосуда и хетерогени катализатор у реакцији купловања четири реакционе компоненте, алдехида, *β*-кетоестра (2 mol) и амонијум-ацетата, без присутног растварача. У поређењу са класичним реакционим условима Ханчове (*Hantzsch*) реакције, описани поступак као предност има бољи принос, кратко реакционо време и једноставнију методологију. *β*-CDPU је ефикасан хетерогени катализатор, лак за коришћење и лако се уклања из реакционе смесе филтрирањем, а може се поново користити без губитка активности.

(Примљено 12. јануара, ревидирано 25 маја 2013)

REFERENCES

1. J. Zhu, H. Bienayme, *Multi Component Reactions*, Wiley–VCH, Weinheim, Germany, 2005
2. A. Domling, *Chem. Rev*. **106** (2006) 17
3. A. R. Kiasat, A. Mouradezadegun, S. J. Saghanezhad, *J. Serb. Chem. Soc.* **77** (2012) 1
4. C. B. Sangani, N. M. Shah, M. P. Patel, R. G. Patel, *J. Serb. Chem. Soc.* **77** (2012) 1165
5. R. R. Nagawade, D. B. Shinde, *Acta Chim. Slov*. **54** (2007) 642
6. D. M. D'Souza, T. J. Mueller, *Chem. Soc. Rev*. **36** (2007) 3169
7. C. C. A. Cariou, G. J. Clarkson, M. Shipman, *J. Org. Chem*. **73** (2008) 9762
8. G. M. Reddy, M. Shiradkar, A. K. Chakravarthy, *Curr. Org. Chem*. **11** (2007) 484
9. R. Gupta, R. Gupta, S. Paul, A. Loupy, *Synthesis* (2007) 2835
10. O. De Paolis, J. Baffoe, S. M. Landge, B. Török, *Synthesis* (2008) 3423
11. A. Debache, R. Boulcina, A. Belfaitah, S. Rhouati, B. Carboni, *Synlett* (2008) 509
12. A. Debache, W. Ghalem, R. Boulcina, A. Belfaitah, S. Rhouati, B. Carboni, *Tetrahedron Lett*. **50** (2009) 4248
13. E. Rafiee, S. Eavani, S. Rashidzadeh, M. Joshaghani, *Inorg. Chim. Acta* **362** (2009) 3555
14. F. Tamaddon, Z. Razmi, A. A. Jafari, *Tetrahedron Lett*. **51** (2010) 1187
15. N. K. Ladani, D. C. Mungra, M. P. Patel, R. G. Patel, *Chin. Chem. Lett.* **22** (2011) 1407
16. R. A. Janis, D. A. Triggle, *J. Med. Chem*. **25** (1983) 775
17. R. H. Bocker, F. P. Guengerich, *J. Med. Chem*. **28** (1986) 1596
18. A. C. Gaudio, A. Korolkovas, Y. Tkahata, *J. Pharm. Sci*. **83** (1994) 1110
19. R. S. Kumar, A. Idhayadhulla, A. J. Abdulnaser, J. Selvin, *J. Serb. Chem. Soc.* **76** (2011) 1
20. R. Mannhold, B. Jablonka, W. Voigdt, K. Schoenafinger, K. Schravan, *Eur. J. Med. Chem*. **27** (1992) 229
21. H. Nakayama, Y. Kasoaka, *Heterocycles* **42** (1996) 901
22. V. Klusa, *Drugs Future* **20** (1995) 135
23. O. Carp, C. L. Huisman, A. Reller, *Prog. Solid State Chem.* **32** (2004) 33
24. Z. Predojević, B. Škrbić, N. D. Đurišić, *J. Serb. Chem. Soc*. **77** (2012) 815

25. V. Homem, L. Santos, *J. Environ. Manage.* **92** (2011) 2304
26. C. Ramesh, G. Mahender, N. Ravindranath, D. Biswanath, *Tetrahedron Lett.* **44** (2003) 1465
27. A. R. Kiasat, S. Nazari, *Catal. Commun.* **18** (2012) 102
28. A. R. Kiasat, S. Nazari, *Catal. Sci. Technol.* **2** (2012) 1056
29. A. R. Kiasat, M. Fallah Mehrjardi, *Catal. Commun.* **9** (2008) 1497
30. A. R. Kiasat, R. Badri, B. Zargar, S. Sayyahi, *J. Org. Chem.* **73** (2008) 8382
31. A. R. Kiasat, S. Sayyahi, *Mol. Divers.* **14** (2010) 155
32. A. R. Kiasat, M. Zayadi, *Catal. Commun.* **9** (2008) 2063
33. E. Y. Ozmen, M. Sezgin, M. Yilmaz, *J. Mol. Catal., B* **57** (2009) 109
34. L. J. Donelson, R. A. Gibbs, S. De, *J. Mol. Catal., A* **256** (2006) 309
35. A. Kumar, R. A. Maurya, *Tetrahedron* **63** (2007) 1946
36. G. Song, B. Wang, X. Wu, Y. Kang, L. Yang, *Synth. Commun.* **35** (2005) 2875
37. A. Kumar, R. A. Maurya, *Tetrahedron Lett.* **48** (2007) 3887
38. M. Heravi, K. Bakhtiari, N. M. Javadi, F. Bamoharam, M. Saeedi, H. Oskooie, *J. Mol. Catal., A* **264** (2007) 50.

Journal of the Serbian Chemical Society
JSCS@tmf.bg.ac.rs • www.shd.org.rs/JSCS
J. Serb. Chem. Soc. 79 (4) S46–S49 (2014) *Supplementary material*

SUPPLEMENTARY MATERIAL TO

β-Cyclodextrin–polyurethane polymer: a neutral and eco-friendly heterogeneous catalyst for the one-pot synthesis of 1,4-dihydropyridine and polyhydroquinoline derivatives *via* the Hantzsch reaction under solvent-free conditions

ALI REZA KIASAT*, SIMIN NAZARI and JAMAL DAVARPANAH

Chemistry Department, Faculty of Sciences, Shahid Chamran University, Ahvaz 61357-4-3169, Iran

J. Serb. Chem. Soc. 79 (4) (2014) 401–409

SPECTRAL DATA FOR THE SYNTHESIZED COMPOUNDS

Diethyl 2,6-dimethyl-4-phenyl-1,4-dihydropyridine-3,5-dicarboxylate (***1***). Pale yellow solid; IR (KBr, cm^{-1}): 3378, 3016, 1714, 1692, 1502, 1334, 1300, 1204, 1118, 1072, 1009, 730; ^{1}H-NMR (400 MHz, acetone-d_6, δ / ppm): 1.26 (6H, *t*, J = 6.8 Hz, $2CH_3$), 2.29 (6H, *s*, $2CH_3$), 4.22 (4H, *q*, J = 7.2 Hz, $2CH_2$), 5.05 (1H, *s*, ArCH), 5.68 (1H, *brs*, NH), 7.20–7.62 (5H, *m*, ArH); ^{13}C-NMR (100 MHz, acetone-d_6, δ / ppm): 15.0, 20.01, 44.0, 63.3, 104.2, 116.3, 130.8, 144.8, 145.2, 150.7, 167.6.

Diethyl 4-(4-methoxyphenyl)-2,6-dimethyl-1,4-dihydropyridine-3,5-dicarboxylate (***2***). IR (KBr, cm^{-1}): 3345, 3022, 2960, 1741, 825; ^{1}H-NMR (400 MHz, acetone-d_6, δ / ppm): 1.24 (6H, *t*, J = 7.2 Hz, $2CH_3$), 2.26 (6H, *s*, $2CH_3$), 3.81 (3H, *s*, OCH_3), 4.20 (4H, *q*, J = 7.2 Hz, $2CH_2$), 4.80 (1H, *s*, ArCH), 6.35 (1H, *brs*, NH), 6.88–7.25 (4H, *m*, ArH); ^{13}C-NMR (100 MHz, acetone-d_6, δ / ppm): 15.1, 18.4, 43.8, 55.0, 61.7, 103.2, 115.1, 130.2, 136.3, 157.4, 158.6.

Diethyl 4-(4-hydroxyphenyl)-2,6-dimethyl-1,4-dihydropyridine-3,5-dicarboxylate (***3***). Pale yellow solid; IR (KBr, cm^{-1}): 3340, 3020, 2911, 1760, 1445, 812; ^{1}H-NMR (400 MHz, acetone-d_6, δ / ppm): 1.25 (6H, *t*, J = 8.5 Hz, $2CH_3$), 2.22 (6H, *s*, $2CH_3$), 4.24 (4H, *q*, J = 8.5 Hz, $2CH_2$), 4.70 (1H, *s*, ArCH), 6.30–7.27 (4H, *m*, ArH), 7.78 (1H, *brs*, NH), 8.70 (1H, *brs*, OH); ^{13}C-NMR (100 MHz, acetone-d_6, δ / ppm): 14.2, 19.8, 45.7, 63.6, 102.3, 117.8, 133.4, 139.6, 153.2, 158.7.

Diethyl 4-(4-chlorophenyl)-2,6-dimethyl-1,4-dihydropyridine-3,5-dicarboxylate (***4***). Pale yellow solid; IR (KBr, cm^{-1}): 3333, 1712, 1655, 1484, 1468,

* Corresponding author. E-mail: akiasat@scu.ac.ir

1380, 1222; ^{1}H-NMR (400 MHz, acetone-d_6, δ / ppm): 1.20 (6H, *t*, *J* = 8.5 Hz, $2CH_3$), 2.32 (6H, *s*, $2CH_3$), 4.13 (4H, *q*, *J* = 8.4 Hz, $2CH_2$), 4.88 (1H, *s*, ArCH), 5.78 (1H, *brs*, NH), 7.15 (2H, *d*, J = 8.1 Hz, ArH), 7.28 (2H, *d*, *J* = 8.1 Hz, ArH); ^{13}C-NMR (100 MHz, acetone-d_6, δ / ppm): 15.7, 19.0, 30.1, 34.9, 61.2, 105.2, 129.1, 130.4, 132.1, 143.2, 155.8.

*Diethyl 4-(4-cyanophenyl)-2,6-dimethyl-1,4-dihydropyridine-3,5-dicarboxylate (**5**)*. IR (KBr, cm^{-1}): 3345, 2229, 1701, 1680, 1207, 1109, 776; ^{1}H-NMR (400 MHz, acetone-d_6, δ / ppm): 1.24 (6H, *t*, *J* = 7.2 Hz, $2CH_3$), 2.33 (6H, *s*, $2CH_3$), 4.15 (4H, *q*, *J* = 7.3 Hz, $2CH_2$), 5.00 (1H, *s*, ArCH), 5.75 (1H, *brs*, NH), 7.30–7.65 (4H, *m*, ArH); ^{13}C-NMR (100 MHz, acetone-d_6, δ / ppm): 14.2, 19.4, 40.3, 59.9, 103.2, 109.7, 119.3, 128.8, 131.8,144.6, 153.0, 167.1.

*Diethyl 4-(4-ethoxyphenyl)-2,6-dimethyl-1,4-dihydropyridine-3,5-dicarboxylate (**6**)*. IR (KBr, cm^{-1}): 3350, 3030, 2968, 1745, 814; ^{1}H-NMR (400 MHz, acetone-d_6, δ / ppm): 1.00 (3H, *t*, *J* = 7.2 Hz, CH_3), 1.28 (6H, *t*, J = 7.2 Hz, $2CH_3$), 2.29 (6H, *s*, $2CH_3$), 4.01 (2H, *q*, *J* = 7.2 Hz, CH_2), 4.28 (4H, *q*, *J* = 7.2 Hz, $2CH_2$), 4.85 (1H, *s*, ArCH), 6.55 (1H, *brs*, NH), 6.92–7.42 (4H, *m*, ArH); ^{13}C-NMR (100 MHz, acetone-d_6, δ / ppm): 14.2, 16.2, 19.4, 42.6, 62.8, 61.7, 103.2, 117.1, 131.0, 137.3, 158.3, 160.6.

*Diethyl 4-(4-(dimethylamino)phenyl)-2,6-dimethyl-1,4-dihydropyridine-3,5--dicarboxylate (**7**)*. Pale yellow solid; IR (KBr, cm^{-1}): 3340, 3030, 2960, 1763, 810; ^{1}H-NMR (400 MHz, acetone-d_6, δ / ppm): 1.30 (6H, *t*, *J* = 8.4 Hz, $2CH_3$), 2.26 (6H, *s*, $2CH_3$), 3.14 (6H, *s*, $N(CH_3)_2$), 4.25 (4H, *q*, *J* = 8.5 Hz, $2CH_2$), 4.65 (1H, *s*, ArCH), 7.12–7.29 (4H, *m*, ArH), 8.08 (1H, *brs*, NH); ^{13}C-NMR (100 MHz, acetone-d_6, δ / ppm): 14.1, 17.8, 40.3, 44.2, 61.0, 103.4, 114.0, 128.2, 134.3, 149.0, 152.1.

*Diethyl 2,6-dimethyl-4-(4-nitrophenyl)-1,4-dihydropyridine-3,5-dicarboxylate (**8**)*. Pale yellow solid; IR (KBr, cm^{-1}): 3039, 2975, 1768, 1537, 818; ^{1}H--NMR (400 MHz, acetone-d_6, δ / ppm): 1.34 (6H, *t*, *J* = 8.4 Hz, $2CH_3$), 2.29 (6H, *s*, $2CH_3$), 4.25 (4H, *q*, *J* = 8.5 Hz, $2CH_2$), 4.73 (1H, *s*, ArCH), 7.50–8.10 (4H, *m*, ArH), 8.15 (1H, *brs*, NH); ^{13}C-NMR (100 MHz, acetone-d_6, δ / ppm): 14.5, 19.0, 32.2, 44.1, 60.2, 104.1, 123.4, 127.1, 145.2, 151.8, 153.2.

*Diethyl 4-(2-chlorophenyl)-2,6-dimethyl-1,4-dihydropyridine-3,5-dicarboxylate (**9**)*. Pale yellow solid; IR (KBr, cm^{-1}): 3342, 1722, 1664, 1473, 1472, 1375, 1218; ^{1}H-NMR (400 MHz, acetone-d_6, δ /ppm): 1.10 (6H, *t*, *J* = 8.6 Hz, $2CH_3$), 2.28 (6H, *s*, $2CH_3$), 4.12 (4H, *q*, *J* = 8.4 Hz, $2CH_2$), 4.85 (1H, *s*, ArCH), 6.12 (1H, *brs*, NH), 7.10–7.32 (4H, *m*, ArH); ^{13}C-NMR (100 MHz, acetone-d_6, δ / ppm): 16.1, 19.8, 31.2, 35.3, 63.2, 104.9, 129.9, 132.5, 132.9, 144.1, 156.2.

*Diethyl 2,6-dimethyl-4-(2-nitrophenyl)-1,4-dihydropyridine-3,5-dicarboxylate (**10**)*. Pale yellow solid; IR (KBr, cm^{-1}): 3042, 2978, 1762, 1541, 820; ^{1}H--NMR (400 MHz, acetone-d_6, δ / ppm): 0.98 (3H, *t*, *J* = 7.4 Hz, CH_3), 1.36 (3H, *t*, *J* = 7.4 Hz, CH_3), 1.89 (1H, *brs*, NH), 2.24 (3H, *s*, CH_3), 2.55 (3H, *s*, CH_3),

4.12 (2H, *q*, *J* = 7.4 Hz, CH_2), 4.40 (2H, *q*, *J* = 7.4 Hz, CH_2), 7.42–8.31 (4H, *m*, ArH); ^{13}C-NMR (100 MHz, acetone-d_6, δ / ppm): 13.6, 14.4, 27.4, 32.1, 61.2, 63.0, 122.3, 124.0, 128.4, 131.0, 135.0, 139.4, 164.2, 167.2.

*Ethyl 1,4,5,6,7,8-hexahydro-2,7-dimethyl-5-oxo-4-phenylquinoline-3-carboxylate (**11**)*. Pale yellow solid; IR (KBr, cm^{-1}): 3299, 2998, 1680, 1645, 1609, 1465, 1380, 1228, 1175; ^{1}H-NMR (400 MHz, $CDCl_3$, δ / ppm): 0.94 (3H, *s*, CH_3), 1.07 (3H, *s*, CH_3), 1.21 (3H, *t*, *J* = 7.2 Hz), 2.14–2.45 (7H, *m*, $2CH_2$, CH_3), 4.08 (2H, *q*, *J* = 7.2 Hz, CH_2), 5.06 (1H, *s*, ArCH), 6.18 (1H, *brs*, NH), 7.12 (1H, *t*, J = 7.6 Hz, ArH), 7.18 (2H, *t*, *J* = 7.6 Hz, ArH), 7.33 (2H, *d*, *J* = 7.6 Hz, ArH); ^{13}C-NMR (100 MHz, $CDCl_3$, δ / ppm): 15.1, 19.4, 28.2, 29.3, 33.4, 37.3, 40.3, 50.6, 58.7, 106.6, 114.5, 126.9, 128.7, 128.8, 144.6, 146.2, 149.7, 168.6, 197.7.

*Ethyl 4-(4-chlorophenyl)-1,4,5,6,7,8-hexahydro-2,7,7-trimethyl-5-oxoquinoline-3-carboxylate (**12**)*. Pale yellow solid; IR (KBr, cm^{-1}): 3300, 2998, 1688, 1650, 1608, 1480, 1384, 1228, 1187; ^{1}H-NMR (400 MHz, $CDCl_3$, δ / ppm): 0.94 (3H, *s*, CH_3), 1.08 (3H, *s*, CH_3), 1.20 (3H, *t*, *J* = 7.2 Hz, CH_3), 2.41–2.55 (7H, *m*, $2CH_2$, CH_3), 4.07 (2H, *q*, *J* = 7.2 Hz, CH_2), 5.04 (1H, *s*, ArCH), 6.09 (1H, *brs*, NH), 7.10 (2H, *d*, *J* = 8.0 Hz, ArH), 7.33 (2H, *d*, *J* = 8.0 Hz, ArH); ^{13}C-NMR (100 MHz, $CDCl_3$, δ / ppm): 15.1, 19.3, 27.2, 29.8, 33.5, 37.2, 41.9, 50.8, 58.6, 107.6, 112.8, 129.7, 129.3, 132.7, 145.8, 148.7, 169.5, 198.5.

*Ethyl 1,4,5,6,7,8-hexahydro-4-(4-hydroxyphenyl)-2,7,7-trimethyl-5-oxoquinoline-3-carboxylate (**13**)*. Yellow solid; IR (KBr, cm^{-1}): 3435, 3305, 3045, 2968, 1679, 1624, 1500, 1371, 1210, 758; ^{1}H-NMR (400 MHz, $CDCl_3$, δ / ppm): 0.96 (3H, *s*, CH_3), 1.09 (3H, *s*, CH_3), 1.25 (3H, *t*, *J* = 7.1 Hz), 2.27 (3H, *s*, CH_3), 2.41–2.55 (4H, *m*, $2CH_2$), 4.10 (2H, *q*, *J* = 7.1 Hz, CH_2), 5.05 (1H, *s*, ArCH), 5.70 (1H, *brs*, OH), 6.01 (1H, *brs*, NH), 6.85 (2H, *d*, *J* = 8.5 Hz, ArH), 7.33 (2H, *d*, *J* = 8.5 Hz, ArH); ^{13}C-NMR (100 MHz, $CDCl_3$, δ / ppm): 16.0, 20.0, 19.2, 27.5, 33.5, 37.0, 43.0, 52.3, 57.8, 62.2, 109.3, 115.6, 118.5, 132.2, 134.3, 140.3, 148.3, 152.7, 158.6, 170.4, 197.6.

*Ethyl 1,4,5,6,7,8-hexahydro-2,7,7-trimethyl-4-(4-methylphenyl)-5-oxoquinoline-3-carboxylate (**14**)*. Yellow powder; IR (KBr, cm^{-1}): 3281, 3027, 3001, 1640, 1600, 1485, 1333, 1210, 761; ^{1}H-NMR (400 MHz, $CDCl_3$, δ / ppm): 1.0 (3H, *s*, CH_3), 1.14 (3H, *s*, CH_3), 1.19 (3H, *t*, *J* = 7.1 Hz, CH_3), 2.20 (3H, *s*, CH_3), 2.39–2.50 (7H, *m*, $2CH_2$, CH_3), 4.16 (2H, *q*, *J* = 7.1 Hz, CH_2), 5.24 (1H, *s*, ArCH), 6.05 (1H, *brs*, NH), 7.50 (2H, *d*, *J* = 8.7 Hz, ArH), 8.08 (2H, *d*, *J* = 8.3 Hz, ArH); ^{13}C-NMR (100 MHz, $CDCl_3$, δ / ppm): 16.2, 19.6, 28.6, 30.3, 33.6, 38.1, 40.4, 49.9, 57.9, 106.4, 115.0, 127.9, 127.8, 129.2, 145.6, 147.1, 150.1, 169.1, 195.9.

*Ethyl 4-(4-(dimethyamino)phenyl)-1,4,5,6,7,8-hexahydro-2,7,7-trimethyl-5--oxoquinoline-3-carboxylate (**15**)*. Yellow powder; IR (KBr, cm^{-1}): 3280, 3010, 2944, 1598, 1505, 1380, 1220, 772; ^{1}H-NMR (400 MHz, $CDCl_3$, δ / ppm): 1.10

(3H, *s*, CH_3), 1.15 (3H, *s*, CH_3), 1.30 (3H, *t*, *J* = 7.0 Hz, CH_3), 2.21 (3H, *s*, CH_3), 2.35–2.47 (4H, *m*, $2CH_2$), 4.17 (2H, *q*, *J* = 7.0 Hz, CH_2), 5.16 (1H, *s*, ArCH), 6.10 (1H, *brs*, NH), 7.19 (2H, *d*, *J* = 8.3 Hz, ArH), 7.23 (2H, *d*, *J* = 8.4 Hz, ArH); ^{13}C-NMR (100 MHz, $CDCl_3$, δ / ppm): 16.5, 21.0, 21.6, 27.3, 27.8, 35.7, 37.8, 43.4, 45.0, 53.7, 58.0, 61.8, 109.6, 117.1, 118.8, 133.0, 135.1, 140.9, 148.9, 153.0, 159.1, 170.6, 196.2.

*Ethyl 1,4,5,6,7,8-hexahydro-2,7,7-trimethyl-4-(4-nitrophenyl)-5-oxoquinoline-3-carboxylate (**16**)*. Yellow solid; IR (KBr, cm^{-1}): 3298, 2990, 1695, 1650, 1617, 1468, 1373, 1221, 1182; ^{1}H-NMR (400 MHz, $CDCl_3$, δ / ppm): 0.92 (3H, *s*, CH_3), 1.08 (3H, *s*, CH_3), 1.23 (3H, *t*, *J* = 7.2 Hz), 2.15–2.39 (4H, *m*, $2CH_2$), 2.41 (3H, *s*, CH_3), 4.10 (2H, *q*, *J* = 7.2 Hz, CH_2), 5.14 (1H, *s*, ArCH), 6.69 (1H, *brs*, NH), 7.50 (2H, *d*, *J* = 8.8 Hz, ArH), 8.12 (2H, *d*, *J* = 8.8 Hz, ArH); ^{13}C--NMR (100 MHz, $CDCl_3$, δ / ppm): 14.08, 17.0, 19.19, 20.94, 27.12, 32.5, 36.88, 37.13, 43.4, 57.3, 60.1, 104.6, 111.8, 123.3, 128.9, 134.8, 144.9, 146.4, 151.6, 154.7, 167.0, 196.2.

*Ethyl 4-(2-chlorophenyl)-1,4,5,6,7,8-hexahydro-2,7,7-trimethyl-5-oxoquinoline-3-carboxylate (**17**)*. Yellow solid; IR (KBr, cm^{-1}): 3103, 2966, 1733, 1645, 1621, 1471, 1390,1230, 1025, 745; ^{1}H-NMR (400 MHz, $CDCl_3$, δ / ppm): 0.99 (3H, *s*, CH_3), 1.12 (3H, *s*, CH_3), 1.25 (3H, *t*, *J* = 7.2 Hz), 2.10–2.35 (4H, *m*, $2CH_2$), 2.46 (3H, *s*, CH_3), 4.10 (2H, *q*, *J* = 7.1 Hz, CH_2), 5.05 (1H, *s*, ArCH), 6.21 (1H, *brs*, NH), 7.30–7.48 (4H, *m*, ArH); ^{13}C-NMR (100 MHz, $CDCl_3$, δ / / ppm): 27.5, 29.8, 32.3, 35.3, 43.1, 48.8, 51.0, 51.5, 52.9, 56.1, 103.3, 110.0, 115.2, 127.9, 128.1, 128.9, 131.1, 133.3, 143.0, 169.4, 196.8.

*Ethyl 1,4,5,6,7,8-hexahydro-2,7,7-trimethyl-4-(2-nitrophenyl)-5-oxoquinoline-3-carboxylate (**18**)*. Yellow solid; IR (KBr, cm^{-1}): 3300, 2992, 1698, 1652, 1614, 1465, 1376, 1227, 1180; ^{1}H-NMR (400 MHz, $CDCl_3$, δ / ppm): 0.95 (3H, *s*, CH_3), 1.10 (3H, *s*, CH_3), 1.27 (3H, *t*, *J* = 7.1 Hz), 2.20–2.42 (4H, *m*, $2CH_2$), 2.44 (3H, *s*, CH_3), 4.18 (2H, *q*, *J* = 7.1 Hz, CH_2), 5.19 (1H, *s*, ArCH), 7.0 (1H, *brs*, NH), 7.45–8.10 (4H, *m*, ArH); ^{13}C-NMR (100 MHz, $CDCl_3$, δ /ppm): 15.2, 17.8, 19.3, 21.2, 27.5, 33.1, 37.3, 36.9, 42.9, 57.8, 60.5, 105.0, 113.1, 125.3, 130.2, 135.3, 146.1, 147.4, 153.2, 155.1, 169.0, 195.2.

Journal of the Serbian Chemical Society
JSCS-info@shd.org.rs • www.shd.org.rs/JSCS
J. Serb. Chem. Soc. 79 (4) 411–420 (2014) UDC 579.8+664.644.5+543.544:664.24(497.11)
JSCS–4595 *Original scientific paper*

A thin layer chromatographic comparison of raw and soluble starch hydrolysis patterns of some α-amylases from *Bacillus* sp. isolated in Serbia

NIKOLA GLIGORIJEVIĆ[1], NIKOLA STEVANOVIĆ[1#], NIKOLA LONČAR[1], RADA BAOŠIĆ[1#], ZORAN VUJČIĆ[1] and NATAŠA BOŽIĆ[2]*

[1]*Faculty of Chemistry, University of Belgrade, Studentski trg 12–16, Belgrade, Serbia and* [2]*Institute of Chemistry, Technology and Metallurgy – Center of Chemistry, University of Belgrade, Studentski trg 12–16, Belgrade, Serbia*

(Received 9 September, revised 16 December 2013)

Abstract: Several natural isolates of *Bacillus* strains namely 5B, 12B, 16B, 18 and 24B were grown at two different temperatures in submerged fermentation for the production of raw-starch-digesting α-amylases. All strains except *Bacillus* sp. 18 produced more α-amylase at 37 °C. The hydrolysis of raw cornstarch followed the same pattern. Efficient hydrolysis was obtained with α-amylases from *Bacillus* sp. 5B, 12B, 16B and 24B grown at 37 °C and *Bacillus* sp. 18 grown at 50 °C. Zymography after isoelectric focusing showed that α-amylases were produced in multiple forms, from 2 to 6, depending on the strain when they were growing at 37 °C, while growth at 50 °C induced only 1 or 2 isoforms. Thin layer chromatography (TLC) analysis of the hydrolysis products of raw corn and soluble starch by α-amylases revealed the production of various mixtures of oligosaccharides. In most cases, G3 was the most dominant product from soluble starch while G2, G3 and G5 were the main products of raw starch hydrolysis. This indicates that the obtained α-amylases could be used for starch liquidification or short-chain-oligosaccharide formation, depending on the type of starch (raw or soluble) used for the hydrolysis.

Keywords: bacterial amylase; raw starch digestion; TLC; zymogram.

INTRODUCTION

Starch is the dominant carbohydrate reserve material of higher plants, being found in leaf chloroplasts and in the amyloplasts of storage organs such as seeds and tubers.[1] It constitutes an inexpensive source for the production of syrups containing glucose, fructose or maltose, which are widely used in the food, sweetener and ethanol industries.[2,3] Starch is a mixture of two polysaccharides,

* Corresponding author. E-mail: nbozic@chem.bg.ac.rs
# Serbian Chemical Society member.
doi: 10.2298/JSC130909155G

amylose and amylopectin, and contains small amounts of non-carbohydrate constituents, such as lipids, phosphates and proteins.[4] Starch granules from different botanical sources are of different sizes, shapes and physical properties.[5] Starch is insoluble in cold water and often resistant to chemical and enzymatic treatments.[6]

Conventionally, conversion of starch to glucose is a high temperature, liquid-phase enzymatic hydrolysis process that requires a high-energy input, resulting in increased production costs of starch-based products.[7] In view of energy costs, effective utilization of natural resources and viscosity problems, direct hydrolysis of starch below its gelatinization temperature is desirable.[2,6,7]

α-Amylases (E.C. 3.2.1.1.) are starch-degrading enzymes that catalyze the hydrolysis of the internal α-1,4-*O*-glycosidic bonds in polysaccharides with retention of the α-anomeric configuration in the products.[8] They are typical endoamylases and are often divided into two categories according to the degree of hydrolysis of the substrate. Saccharifying α-amylases hydrolyze 50 to 60 % while liquefying α-amylases cleave about 30 to 40 % of the glycosidic linkages of starch.[9] The end products of α-amylase action are oligosaccharides of varying length with the α-configuration and α-limit dextrins, which constitute branched oligosaccharides.[9] Amylases account for about 30 % of the world's enzyme production, with potential applications in starch liquefaction, the manufacture of maltose, high fructose-containing syrups, maltotetraose syrups, in the removal of starch from textiles, direct fermentation of starch to ethanol and in the treatment of starch processing water.[10] α-Amylases can be produced by different species of microorganisms, but for commercial applications, α-amylase is mainly derived from the genus *Bacillus*. *B. stearothermophilus*, *B. licheniformis* and *B. amyloliquefaciens* are known to be good producers of thermostable α-amylase, and these have been widely used for commercial production of the enzyme for various applications.[11] α-Amylase with suitable properties can be very useful in a specific industry; thus, it has become essential to characterize all available microbial strains for their productivity. Since almost all microorganisms of the *Bacillus* genus synthesize α-amylase, this genus has the potential to dominate the enzyme industry.[12] Various factors affect the efficiency of raw starch hydrolysis by amylases. They include granule dimensions and shape, amylose content, lipid and phosphate content, architecture of starch granules and the amylase source.[13]

Quantitative and qualitative estimation of malto-oligosaccharides produced by the action of α-amylases can be achieved by thin layer chromatography (TLC).[14] This method is very convenient for the characterization of amylase types defined by their mode of action that can be derived from the starch hydrolysis patterns. Based on the products from the hydrolysis visualized by TLC, selection of the amylase for application in a specified industry, such as production of ethanol or sweeteners, can be achieved.

The aim of this work was to compare raw corn and soluble starch hydrolysis patterns of some Serbian *Bacillus* sp. α-amylases in order to elucidate their potential industrial application.

EXPERIMENTAL

Chemicals

All reagents and solvents were of the highest available purity and at least of analytical grade. They were purchased from Merck (Darmstadt, Germany) and Sigma–Aldrich (St. Louis, MO, USA) unless otherwise stated. Raw cornstarch was isolated in our laboratory according to standard recommended procedure.

Production of α-amylase

Different soil and milk samples were taken from various regions of Serbia as a source of microorganisms that were identified as *Bacillus* sp.[15] according to the methods described in Bergey's Manual of Systematic Bacteriology.[16] α-Amylase was produced from different strains of *Bacillus* using a submerged fermentation described previously.[7] The strains were grown at 37 °C and 50 °C for the comparison of the effect of each temperature on the α-amylase production. Fermentation mediums containing α-amylase were used for the experiments.

α-Amylase activity assay

The α-amylase activity was determined by measuring the formation of reducing sugars released during starch hydrolysis. The reaction mixture containing 0.05 mL of appropriately diluted enzyme and 0.45 mL of 1.0 % (w/v) soluble starch (Merck) in 50 mM phosphate buffer (pH 6.5) was incubated at 65 °C for 30 min. The amount of liberated reducing sugar was determined by the dinitrosalicylic acid (DNSA) method.[17] One unit of α-amylase activity was defined as the amount of enzyme that released 1 μmol of reducing end groups per min at 65 °C. Maltose was used to construct a standard curve.

Isoelectric focusing of α-amylase isoforms

Analytical isoelectric focusing was performed using Multiphor II Electrophoresis system (Pharmacia LKB, Uppsala, Sweden) according to the manufacturer's instruction. Focusing was realized on a 7.5 % acrylamide gel with ampholytes in the pH range 3.0–10.0, at 7 W constant power for 1.5 h at 10 °C. After isoelectric focusing, the α-amylases were detected by zymogram detection with I_2/KI staining solution according to a previously published method.[18] The α-amylase activity appeared as clear bands on a dark background.

Hydrolysis of raw corn and commercial soluble starch

The raw starch digestion ability of crude α-amylase extracts (10 % v/v) was investigated by measuring the hydrolysis of 1 % raw cornstarch granules in a short time period of 6 h at pH 6.5 and 65 °C. The degradation of the raw starch was monitored as previously described using the DNSA method, with maltose as the standard.[7] At appropriate time intervals, the hydrolysis reactions were stopped by centrifugation at 14000 rpm for 1 min in order to separate the non-hydrolyzed raw starch from the solution. Aliquots for TLC analysis were withdrawn and kept at –20 °C. Hydrolysis of the soluble starch was performed in the same way as the hydrolysis of raw starch, except that the hydrolysis lasted for 2 h since this was the time when the percent of hydrolysis was comparable to that obtained for the raw starch. After this time, the starches were no longer significantly hydrolyzed. The reaction of soluble starch hydrolysis was stopped by mixing aliquots with DNSA and further monitored as for the raw starch degradation.[7] Aliquots for TLC analysis were withdrawn and kept at –20 °C.

TLC analysis

Oligosaccharide separation was performed by horizontal thin layer chromatography on silica plates, 10 cm×10 cm (Silica Gel 60 F_{254}, Merck, Darmstadt, Germany), using a Camag horizontal HPTLC development chamber in the tank configuration. All plates were pre-washed with a mixture of methanol and water (7/1, v/v). Standard solution of the oligosaccharides (0.33 mg/mL each) was prepared in deionized water. Standard solutions and samples in appropriate dilution (20 μL) were applied in bands using an autosampler (Linomat 5, Camag). The employed mobile phase was mixture of *n*-butanol, ethanol and 0.1 % water solution of boric acid (5/4/3, v/v/v). All separations were realized at ambient temperature (22±2 °C). After drying, the plates were sprayed with diphenylamine–aniline–phosphoric acid reagent and then heated at 110 °C for 10 min.[19]

RESULTS AND DISCUSSION

The most commonly used *Bacillus* strains, such as *B. amyloliquefaciens*, *B. subtilis*, *B. licheniformis* and *B. stearothermophilus*, are reported to produce α-amylase usually at temperatures between 37 °C and 60 °C depending on the strain.[20–22] For this reason, it was necessary to test the growth of different wild type *Bacillus* sp. strains as well as the production of different α-amylase isoforms at 37 °C and 50 °C. The results showed that the production of α-amylases was dependant on the growth temperature for all tested strains, Fig. 1. When strains were grown at 37 °C, the highest enzyme activity was detected in a *Bacillus* sp. 16B fermentation broth. On the other hand, when the strains were grown at 50 °C, the highest enzyme activity was detected in the fermentation medium of *Bacillus* sp. 18. Moreover, all strains, except *Bacillus* sp. 18, produced more α-amylase when grown at 37 °C than when grown at 50 °C. The differences in α-amylase production between the strains regarding the temperatures used for their growth were expected. Different strains have different optimal conditions for the growth and enzyme production and individual optimization of cultural conditions is important for maximum production of the microbial strains.[12]

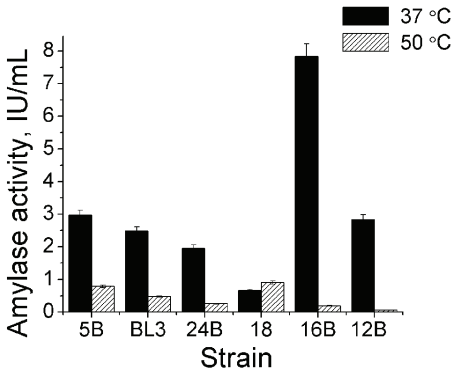

Fig. 1. Extracellular α-amylase activities of different *Bacillus* sp. strains. Each data point represents the mean of three independent assays.

The production of α-amylase isoforms by the specified strains were analyzed using zymography after isoelectric focusing. As could be seen from Fig. 2, diffe-

rent *Bacillus* sp. strains produced different isoforms of α-amylase. All the tested strains produced multiple forms of α-amylase, from 2 to 6, depending on the strain when growing at 37 °C, while only 1 or 2 isoforms were induced when growing at 50 °C.

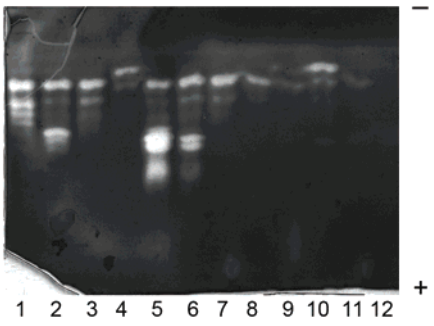

Fig. 2. Zymogram of α-amylases of different *Bacillus* sp. strains obtained after isoelectric focusing. Lanes 1–6: strains grown at 37 °C, lanes 7–12: strains grown at 50 °C. Lanes 1 and 7: *Bacillus* sp. 5B, lanes 2 and 8: *Bacillus* sp. BL3, lanes 3 and 9: *Bacillus* sp. 24B, lanes 4 and 10: *Bacillus* sp. 18, lanes 5 and 11: *Bacillus* sp. 16B and lanes 6 and 12: *Bacillus* sp. 12B.

The production of multiple isoforms of α-amylase by *Bacillus* sp., such as two extracellular α-amylase isoenzymes produced by *Bacillus* species WN11;[23] three extracellular α-amylase isoenzymes produced by *Bacillus* species B-3881[24] or six extracellular α-amylase isoenzymes produced by *B. licheniformis* ATCC 9945a,[7] was reported previously. The present study concerning *Bacillus* sp. α-amylase isoforms showed that isoforms were also detected when the strains were grown at different temperatures in solid-state fermentation on triticale (results not shown). Moreover, same strains produced different isoforms even at the same growth temperature due to different fermentation conditions. All these results are important from the viewpoint of the ability of specific isoforms to hydrolyze raw starch in comparison to the crude α-amylase activities obtained from the fermentation broth.

Many factors contribute to the efficiency of raw starch hydrolysis and one of them is the source of the employed enzyme.[13] The amount of hydrolysis of raw cornstarch by α-amylase produced by specified strains after 6 h at 65 °C are shown in Fig. 3. As expected, more starch was hydrolyzed by α-amylases produced by strains that were grown at 37 °C, since their α-amylases had higher activities. The exception was again *Bacillus* sp. 18 grown at 50 °C, when the α-amylase was more efficient in the hydrolysis of cornstarch than that obtained when the strain was grown at 37 °C.

The α-amylases from *Bacillus* sp. strains 5B and 18 were the most efficient in the hydrolysis of raw cornstarch when the strains were grown at 50 °C. On the other hand, the α-amylases from all *Bacillus* sp. strains grown on 37 °C were very efficient in the hydrolysis of raw starch; slightly better results were obtained for strains designated as 5B, 12B, 16B and 24B. Although the *Bacillus* sp. strain 16B produced the most active amylases at 37 °C (its activity was almost three

times higher that the activity of the amylases produced by the other strains), the degree of raw starch hydrolysis was not proportional. This is probably because the most active amylase isoforms produced by the strain 16B might not be the ones responsible for raw starch hydrolysis. In a previous study, it was found that only one isoform amongst several produced by SSF of strain 12B had the ability to hydrolyze raw starch.[15] It is very important to notice that the control strain in this study (BL3), *B. licheniformis* ATCC9945a, which was already shown to produce highly efficient α-amylase for the digestion of raw starch,[7] was less efficient than the tested wild type strains.

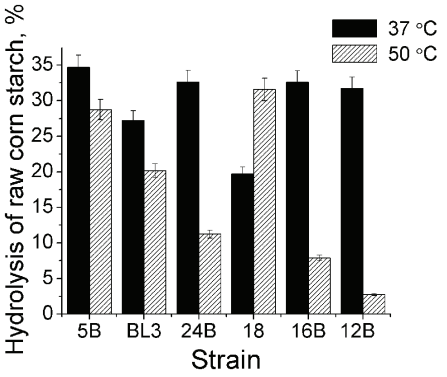

Fig. 3. Hydrolysis of raw cornstarch by α-amylases of different *Bacillus* sp. strains. Each data point represents the mean of three independent assays.

Due to the different reaction conditions used, comparison with other published results on the α-amylases from *Bacillus* sp. was difficult. However, for example, hydrolysis yields in a period of 5 h of raw cornstarch were 62 % for the α-amylase from *B. amyloliquefaciens*,[25] while after 6 h of hydrolysis at 60 °C, 15 % of cornstarch was digested by the α-amylase from *Bacillus* sp. GRE1.[26] Nevertheless, it is very important to emphasize that approximately 10–100 times lower enzyme doses were applied in the present study where 35 % of raw cornstarch was hydrolyzed after 6 h of incubation at 65 °C.

To determine hydrolysis products of soluble and raw corn starch by *Bacillus* sp. that were more efficient α-amylase producers (all strains grown at 37 °C except *Bacillus* sp. 18, for which the one grown at 50 °C was used for the analysis), distributions of the reaction products were analyzed by TLC.

From the results obtained and shown in Fig. 4, it can be seen that maltose (G2) and maltotriose (G3) were among the first produced when both starches were hydrolyzed. They were observed after only 15 minutes of hydrolysis. Other products appeared after 15 or 30 min and their concentrations only increased as the hydrolysis continued. They include oligosaccharides from G2 to G7 and minor amounts of G1 for all strains in the case of raw starch hydrolysis, while only α-amylase from *Bacillus* sp. 16B released glucose from soluble starch. As expected, the hydrolysis profiles differed between strains since they represent

different sources for the production of α-amylase. α-Amylases from *Bacillus* sp. 16B did not produce oligosaccharides > G5 regardless of the starch type (raw or soluble), while those from *Bacillus* sp. 24B produce only G2 and G3 when soluble starch was used.

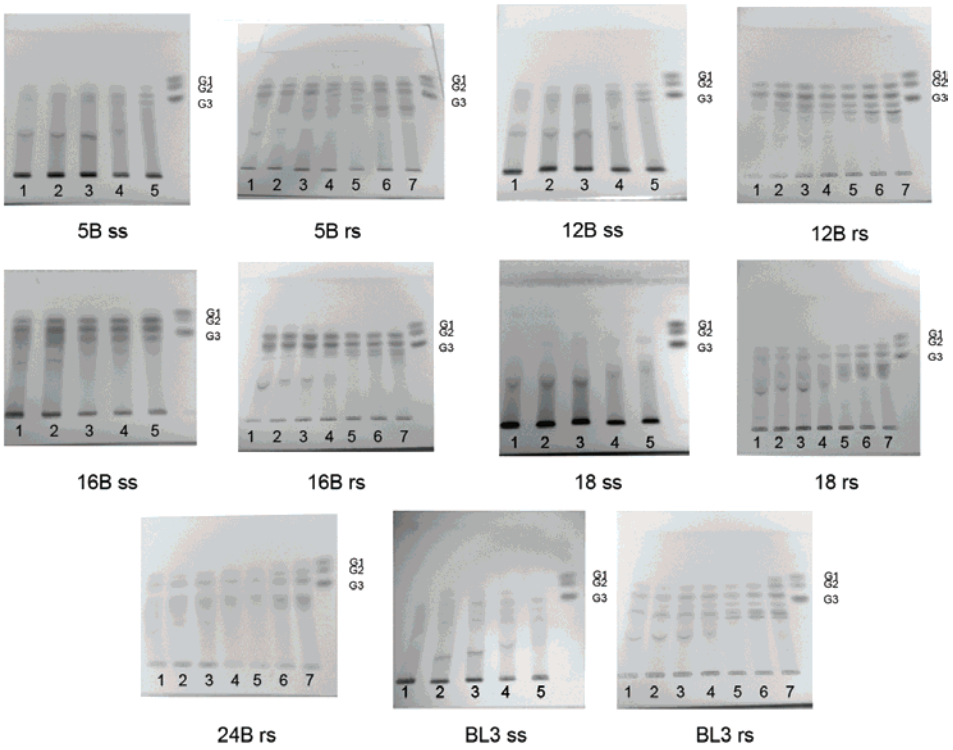

Fig. 4.TLC analysis of the time course of the hydrolytic products of soluble starch (ss) and raw starch (rs) by α-amylases of different *Bacillus* sp. strains at 37 °C and *Bacillus* sp. 18 at 50 °C. Lane 1: 15, lane 2: 30, lane 3: 45, lane 4: 60, lane 5: 120, lane 6: 240 and lane 7: 360 min. G1, G2, G3 represent standards. The curve-shaped bands visible at the area of slower mobility originated from the enzyme solutions, which was confirmed by TLC analysis of the fermentation broths alone (results not shown). The time course the hydrolytic products of soluble starch by α-amylases of *Bacillus* sp. 24B is not presented due to the very high background with hydrolysis product clearly visible only after 2 h of hydrolysis as shown in Fig. 5.

In general, less G4 was produced when the raw starch was hydrolyzed by the different amylases, Fig. 5. The end product profiles of the hydrolysis of soluble and raw starch by all the tested strains showed the formation of malto-oligosaccharides, Fig. 5, which indicates that the endo-mode of action was operative for all of the tested α-amylases on both raw and soluble starch. This random mode of action is typical for α-amylases.[27,28] Endo-amylases produce oligosaccharides of

different length, which was observed in this work and is in agreement with other published results.[27,29–31] The hydrolysis products ranged from G1 to G7 and these products are typical for endoamylolytic hydrolysis.[32] First products to appear were G2 and G3 for both raw and soluble starch. This was also observed for the α-amylase from *Geobacillus thermoleovorans*.[31] However, in the present study, the concentrations of all other products increased as the hydrolysis proceeded, especially in the hydrolysis of raw starch when finally G5 became dominant with G2 and G3 for all the strains, except for *Bacillus* sp. 16B. This observation was similar to those of others,[14,33] where G3 and G6 were the main products of hydrolysis of native cornstarch by α-amylase from *B. subtilis*. On the other hand, the hydrolysis patterns for soluble starch revealed that G3 was the most dominant product for all the strains, except for *Bacillus* sp. 16B where G2 and G3 were dominant.

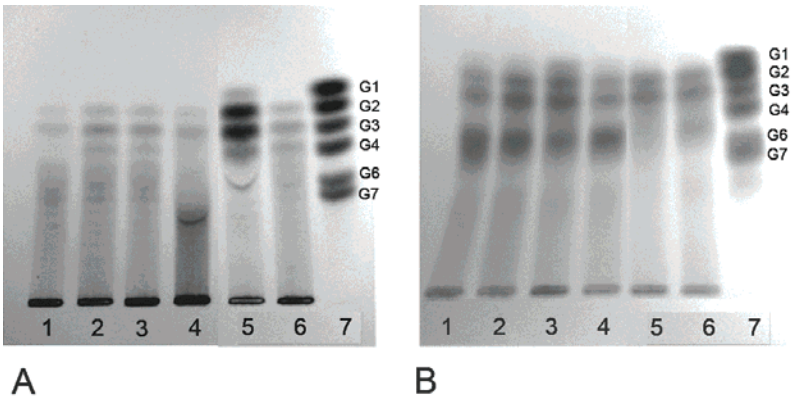

Fig. 5. TLC analysis of hydrolytic products of A) soluble starch and B) raw starch by α-amylases of different *Bacillus* sp. strains. Lane 1: *Bacillus* sp. 18 (50 °C), lane 2: *Bacillus* sp. 5B (37 °C), lane 3: *Bacillus* sp. BL3 (37 °C), lane 4: *Bacillus* sp. 24B (37 °C), lane 5: *Bacillus* sp. 16B (37 °C) and lane 6: *Bacillus* sp. 12B (37 °C). Lane 7: G1, G2, G3, G4, G6 and G7 represent standards. The curve-shaped bands visible in samples 4 and 5, panel A, originated from the enzyme solutions, which was confirmed by TLC analysis of the fermentation broths alone (results not shown).

Based on the described results, it seems that the α-amylases described in this study belong to the liquefying α-amylase type since there are many end products from hydrolysis of both types of starch. The liquefying α-amylase from *B. amyloliquefaciens* was reported to produce maltosaccharides predominantly while the saccharifying enzyme from *B. subtilis* yielded mostly glucose and maltose from starch.[34] With respect to the major products of hydrolysis, the α-amylases tested here might be useful for starch liquefaction or formation of short-chain-oligosaccharide, and specific application might be directed by the type of starch (raw or soluble) that was to be hydrolyzed.

CONCLUSIONS

The present study showed that the tested *Bacillus* sp. strains produced highly efficient raw starch digesting α-amylases able to hydrolyze raw cornstarch at a temperature below the temperature of gelatinization. TLC analysis of the hydrolyzed products showed that oligosaccharides from G2 to G7 were obtained when raw or soluble starches were used for the hydrolysis,. In most cases, G3 was preferentially produced from soluble starch while G2, G3 and G5 were the main products of raw starch hydrolysis. G1 was produced from raw starch only by the α-amylase from *Bacillus* sp. 16B. The advantages of the α-amylases from *Bacillus* sp. 5B, 12B, 16B, 18 and 24B compared to the previously reported ones are related to a high hydrolytic affinity towards raw cornstarch granules, the wide range of oligosaccharides produced by their action on starch as well as different hydrolysis pattern obtained after digestion of raw and soluble starch. This indicates that obtained α-amylases could be used for starch liquefaction and the formation of short-chain-oligosaccharides.

Acknowledgements. This work was supported by the Ministry of Education, Science and Technological Development or the Republic of Serbia, Project No. 172048 and an ICGEB Research Grant, No. CRP/YUG11-02.

ИЗВОД

ПРИМЕНА ТАНКОСЛОЈНЕ ХРОМАТОГРАФИЈЕ ЗА ПОРЕЂЕЊЕ ПРОИЗВОДА ХИДРОЛИЗЕ СИРОВОГ И РАСТВОРНОГ СКРОБА α-АМИЛАЗАМА СОЈЕВА *Bacillus* ИЗОЛОВАНИХ У СРБИЈИ

НИКОЛА ГЛИГОРИЈЕВИЋ[1], НИКОЛА СТЕВАНОВИЋ[1], НИКОЛА ЛОНЧАР[1], РАДА БАОШИЋ[1], ЗОРАН ВУЈЧИЋ[1] и НАТАША БОЖИЋ[2]

[1]Хемијски факултет, Универзитет у Београду, Студентски трг 12–16, Београд и [2]Институт за хемију, технологију и металургију – Центар за хемију, Универзитет у Београду, Студентски трг 12–16, Београд

Неколико природних изолата сојева *Bacillus* названих 5B, 12B, 16B, 18 и 24B су гајени на две различите температуре течном ферментацијом ради продукције α-амилаза које хидролизују сирови скроб. Сви сојеви осим *Bacillus* sp. 18 су продуковали више α-амилазе на 37 °C. Хидролиза сировог скроба је пратила исту шему. Ефикасна хидролиза је остварена са α-амилазама из *Bacillus* sp. 5B, 12B, 16B и 24B који су гајени на 37 °C и *Bacillus* sp. 18 гајен на 50 °C. Зимограмска детекција након изоелектричног фокусирања је показала да су α-амилазе продуковане у више изоформи, од 2 до 6, зависно од соја када су гајени на 37 °C, док је гајење на 50 °C индуковало само 1 или 2 изоформе. TLC анализом продуката хидролизе сировог кукурузног и растворног скроба α-амилазама показана је продукција различитих смеша олигосахарида. У већини случајева G3 је био најдоминантнији продукт из растворног скроба док су G2, G3 и G5 били главни продукти хидролизе сировог скроба. Ово указује на то да се добијене α-амилазе могу користити за отечњавање скроба и продукцију кратко-ланчаних олигосахарида у зависности од тога који тип скроба (сирови или растворни) је коришћен за хидролизу.

(Примљено 9. септембра, ревидирано 16. децембра 2013)

REFERENCES

1. T. L. Wang, T. Y. Bogracheva, C. L. Hedley, *J. Exp. Bot.* **49** (1998) 481
2. N. Goyal, J. K. Gupta, S. K. Soni, *Enzyme Microb. Technol.* **37** (2005) 723
3. D. K. Apar, B. Özbek, *Process Biochem.* **39** (2004) 1137
4. Y. Chen, S. Huang, Z. Tang, X. Chen, Z. Zhang, *Carbohydr. Polym.* **85** (2011) 272
5. C. Yook, J. F. Robyt, *Carbohydr. Res.* **337** (2002) 1113
6. S. Mitsuiki, K. Mukae, M. Sakai, M. Goto, S. Hayashida, K. Furukawa, *Enzyme Microb. Technol.* **37** (2005) 410
7. N. Božić, J. Ruiz, J. López-Santín, Z. Vujčić, *Biochem. Eng. J.* **53** (2011) 203
8. S. Sivaramakrishnan, D. Gangadharan, K. M. Nampoothiri, C. R. Soccol, A. Pandey, *Food Technol. Biotechnol.* **44** (2006) 173
9. C. Chang, *Carbohydrates – Comprehensive Studies on Glycobiology and Glycotechnology*, InTech, Rijeka, Croatia, 2012, p. 459
10. B. A. Kikani, S. Pandey, S. P. Singh, *Bioprocess Biosyst. Eng.* **36** (2013) 567
11. P. Monteiro de Suoza, P. de Oliveira e Magalhães, *Braz. J. Microbiol.* **41** (2010) 850
12. N. Božić, J. Ruiz, J. López-Santín, Z. Vujčić, *J. Serb. Chem. Soc.* **76** (2011) 965
13. R. F. Tester, X. Qi, J. Karkalas, *Anim. Feed Sci. Technol.* **130** (2006) 39
14. I. Lovšin-Kukman, M. Zelenik-Blatnik, V. Abram, *Eur. Food Res. Technol.* **206** (1998) 175
15. N. Božić, M. Šokarda Slavić, A. Gavrilović, Z. Vujčić, *Bioprocess Biosyst. Eng.* (2013), in press, doi: 10.1007/s00449-013-1105-1
16. P. H. A. Sneath, N. S. Mair, E. M. Sharpe, J. G. Holt, *Bergey's Manual of Systematic Bacteriology*, Williams and Wilkins, Baltimore, MD, USA, 1986.
17. P. Bernfeld, in *Methods in Enzymology*, I. P. De Murray, Ed, Academic Press INC Deutcher, San Diego, CA, 1955, p. 149
18. B. Dojnov, N. Božić, V. Nenadović, J. Ivanović, Z. Vujčić, *Comp. Biochem. Phys., B* **149** (2008) 153
19. G. E. Morlock, F. Gamlich, *J. Planar. Chromatogr.* **25** (2012) 244
20. J. R. Mielenz, *Proc. Natl. Acad. Sci.* **80** (1983) 5975
21. D. R. Mendu, B. V. V. Ratnam, A. Purnima, C. Ayyanna, *Enzyme Microb. Technol.* **37** (2005) 712
22. S. Mishra, S. B. Noronha, G. K. Suraishkumar, *Process Biochem.* **40** (2005) 1863
23. G. Mamo, A. Gessesse, *Lett. Appl. Microbiol.* **29** (1999) 61
24. E. W. Boyer, M. B. Ingle, *J. Bacteriol.* **110** (1972) 992
25. D. Gangadharan, K. M. Nampoothiri, S. Sivaramakrishnan, A. Pandey, *Appl. Biochem. Biotech.* **158** (2009) 653
26. G. D. Haki, A. J. Anceno, S. K. Rakshit, *World J. Microb. Biot.* **24** (2008) 2517
27. F. Puspasari, Z. Nurachman, A. S. Noer, O. K. Radjasa, M. J. E. C. van der Maarel, D. Natalia, *Starch-Stärke* **63** (2011) 461
28. S. A. Mohamed, E. I. Azhar, M. M. Ba-Akdah, N. R. Tashkandy, T. A. Kumosani, *Afr. J. Microbiol. Res.* **5** (2011), 1018
29. N. Atichokudomchai, J. Jane, G. Hazlewood, *Carbohydr. Polym.* **64** (2006) 582
30. S. Dincbas, E. Demirkan, *J. Biol. Environ. Sci.* **4** (2010) 87
31. D. Mehta, T. Satyanarayana, *J. Mol. Catal., B* **85–86** (2013) 229
32. P. Ziegler, *Plant Physiol.* **86** (1988) 659
33. J. Robyt, D. French, *Arch. Biochem. Biophys.* **100** (1963) 451
34. E. S. Demirkan, B. Mikami, M. Adachi, T. Higasa, S. Utsumi, *Process Biochem.* **40** (2005) 2629.

Journal of the Serbian Chemical Society
JSCS-info@shd.org.rs • www.shd.org.rs/JSCS
J. Serb. Chem. Soc. *79* (4) 421–433 (2014)
JSCS–4596
UDC 546.562'742'732'472:547.853+547.442+547.466:542.9+547.571+547.551
Original scientific paper

Synthesis and characterization of bioactive binuclear transition metal complexes of a Schiff base ligand derived from 4-amino-1*H*-pyrimidin-2-one, diacetyl and glycine

ABHAY NANDA SRIVASTAVA, NETRA PAL SINGH* and CHANDRA KIRAN SHRIWASTAW

Department of Chemistry, Meerut College, Meerut-250001, India

(Received 23 January, revised 27 November 2013)

Abstract: A series of novel binuclear transition metal complexes was synthesized by reaction of a Schiff base ligand 2-((1-methyl-2-((2-oxo-1,2-dihydro-pyrimidin-4-yl)imino)propylidene)amino)acetic acid) (L^aH) derived from 4-amino-1*H*-pyrimidin-2-one, diacetyl, glycine and the corresponding chloride salt of Cu(II), Ni(II), Co(II) and Zn(II) metals in a 1:1 (metal:ligand) mole ratio. The compounds were characterized by elemental analyses, molar conductance measurements, magnetic moment measurements and various spectral studies *viz.* IR, UV–Vis, ^{1}H-NMR, ^{13}C-NMR, EPR and ESI-MS. The molar conductance measurements revealed the non-electrolytic nature of the metal complexes. Electronic absorption spectral data, electronic paramagnetic resonance parameters and magnetic moment values revealed an octahedral geometry for the binuclear metal complexes. A cyclic voltammetric study of Ni(II) complex shows a couple of one-electron anodic responses near 0.70 and 1.10 V. The *in vitro* biological activity of the Schiff base ligand and the binuclear complexes was assessed against bacteria (*Staphylococcus aureus*, *Bacillus subtilis*, *Escherichia coli* and *Salmonella typhi*) and fungi (*Candida albicans* and *Candida parapsilosis*) to ascertain their antibacterial and antifungal properties.

Keywords: pyrimidine; diketone; amino acid; octahedral geometry; antimicrobial properties.

INTRODUCTION

Considerable attention has been paid to pyrimidines and related *N*-heterocyclic derivatives as ligands for transition metal ions because these compounds show multifunctional coordinating ability and are present in many biological systems.[1–3] Amino heterocycles containing two or more potential donor centers play an important role in the study of the comparative reactivity of ambidentate ligand

* Corresponding author. E-mail: npsmcm.in@gmail.com
doi: 10.2298/JSC130123148S

systems.[4] Heterocyclic diazines, such as pyridazine and pyrimidine, are known to act as bidentate or tridentate ligand when coordinated to metal ions. Due to the multifunctional coordinating ability of pyrimidines and their derivatives, they have been used for the synthesis of mononuclear and binuclear transition metal complexes.[5–7] Transition metal complexes containing pyrimidine ligand are commonly found in biological media and play important role in processes such as catalysis of drug interaction with biomolecules. Recently, a number of transition metal complexes of pyrimidine derivatives were prepared that showed good biological activity *viz.* antibacterial and antifungal.[8–10] Complexes that contain glycine and its derivative as potent ligands were synthesized to assess their biological property.[11,12] Recently synthesized Cu(II), Ni(II), Co(II) and Zn(II) complexes show the current interest of researchers in the field of coordination chemistry of these metal ions.[13–15] Some other transition metal complexes were also synthesized for the study of their biological activities *viz.* antimicrobial, fluorescence quenching study in proteins, toxicity and DNA interaction.[16–22] In view of the importance of metal complexes, the preparation, characterization and *in vitro* antibacterial and antifungal properties of a new Schiff base ligand derived from 4-amino-1*H*-pyrimidin-2-one, diacetyl, glycine and its binuclear metal complexes are reported herein.

EXPERIMENTAL

All chemicals and solvents were of analytical reagent grade and used as obtained without further purification. Methanol, ethanol, diethyl ether, DMF, DMSO and metal salts were purchased from Qualigens (Mumbai, India). Diacetyl was purchased from Sigma–Aldrich. 4-Amino-1*H*-pyrimidin-2-one and glycine were purchased from SD-Fine (Mumbai). Silica gel F_{254} TLC plates (20 cm×20 cm) were purchased from Merck (India). Elemental analyses (C, H, N) were performed using a VarioEL Elementar Analysensystem. The metals and chlorides were determined volumetrically[23] and gravimetrically,[24] respectively. Melting points were recorded on an electro-thermal melting point apparatus and are uncorrected. The IR spectra were recorded as KBr discs using a Perkin-Elmer-621 spectrophotometer covering the frequency range 4000–200 cm^{-1}. The electronic absorption spectra in the 200–900 nm range were measured in DMF on a Systronic UV–visible spectrophotometer at room temperature. The ^{1}H-NMR and ^{13}C-NMR spectra were recorded at room temperature in DMSO-d_6 on a Bruker Avance II 400 NMR spectrometer. The chemical shifts (δ) were measured down-field with reference to TMS (tetramethylsilane, 0.0 ppm). The ESI-mass spectra were obtained on an AB-Sciex Q-Star LCMS-MS spectrometer. The molar conductance measurements were determined in DMSO ($\approx 10^{-3}$ M) at room temperature using a Jenway model 4070 conductivity meter. The magnetic moment measurements were realized by the Gouy method at room temperature using $Hg[Co(SCN)_4]$ as the calibrant. The electrochemical behavior of the binuclear Ni(II) complex was studied (in acetonitrile solution) on a CHI620A electrochemical analyzer using a platinum electrode. Tetraethylammonium perchlorate (TEAP) was used as the supporting electrolyte and the potentials are referenced to a saturated calomel electrode (SCE) without junction correction. The cyclic voltammgram was recorded at a scan rate of 50 mV s^{-1} with *iR* compensation. The EPR spectra of the Cu(II) and Co(II) complexes were recorded as

polycrystalline sample on a Varian E-112 spectrometer in the X-band region with a frequency of 9.1 GHz under a magnetic field strength of 3200 G using TCNE (tetracyanoethylene) as the field marker (g = 2.0027).

Synthesis of Schiff base ligand 2-((1-methyl-2-((2-oxo-1,2-dihydropyrimidin-4-yl)imino)propylidene)amino)acetic acid, L^aH

To an aqueous solution of glycine (10 mmol, 0.75 g), an ethanolic solution of diacetyl (10 mmol, 0.87 mL) was added dropwise under constant stirring. The resulting solution was stirred for 30 min and refluxed at 60 °C for 1 h. The precipitated cream-colored solid product 2-((1-methyl-2-oxopropylidene)amino)acetic acid (LH) was filtered off, washed with water, ethanol and diethyl ether and dried in vacuum desiccator over anhydrous calcium chloride. Then, an ethanolic solution of (LH) (10 mmol, 1.30 g) was stirred with an aqueous ethanolic solution of 4-amino-1*H*-pyrimidin-2-one (10 mmol, 1.40 g) for 45 min and refluxed at 65 °C for 3 h. Completion of reaction was monitored by thin layer chromatography (TLC). The reaction mixture was cooled in a refrigerator overnight. The obtained yellow solid Schiff base ligand (L^aH) was filtered off, washed with water, methanol, ethanol and diethyl ether and dried in a vacuum desiccator over anhydrous calcium chloride (Scheme 1).

Step I

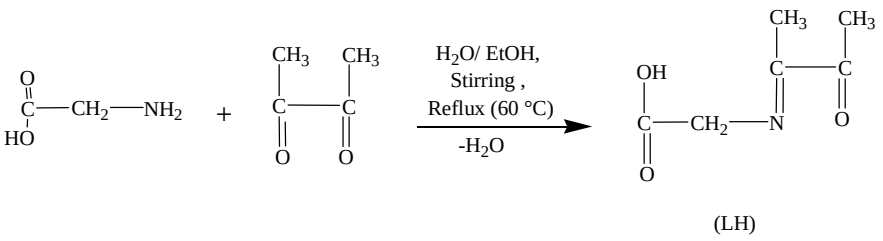

(LH)

Step II

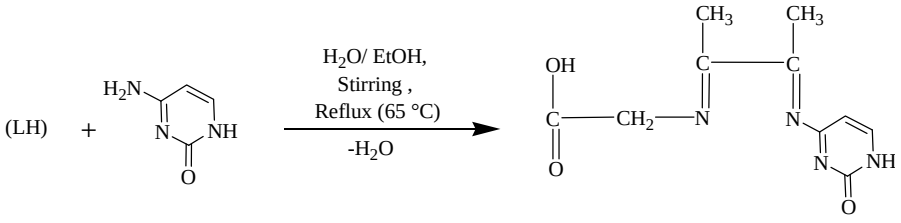

(L^aH)

Scheme 1. Synthesis of Schiff base ligand (L^aH).

Yield: 74 %; color: yellow; m.p. 204 °C; Anal. Calcd. for $C_{10}H_{12}N_4O_3$ (FW: 236.22): C, 50.84; H, 5.12; N, 23.72 %. Found: C, 50.75; H, 5.06; N, 23.62 %.

*Synthesis of binuclear metal complexes **1**–**4***

To an ethanolic solution of the Schiff base ligand (L^aH) (2 mmol, 0.47 g), a methanolic solution of metal salt (2 mmol, $CuCl_2{\cdot}2H_2O$ (0.34 g), $NiCl_2{\cdot}6H_2O$ (0.47 g), $CoCl_2{\cdot}6H_2O$ (0.48 g) or $ZnCl_2$ (0.27 g)) was added dropwise under constant stirring. The resulting solutions were

stirred for 1.5 h and refluxed at 70 °C for ≈10–12 h. Completion of the reaction was monitored by thin layer chromatography (TLC). The reaction mixture was cooled in a refrigerator over night. The colored solid products (except for the Zn(II) complex) of the metal complexes were filtered off, washed with water, methanol, ethanol and diethyl ether, and dried in a vacuum desiccator over anhydrous calcium chloride (Scheme 2).

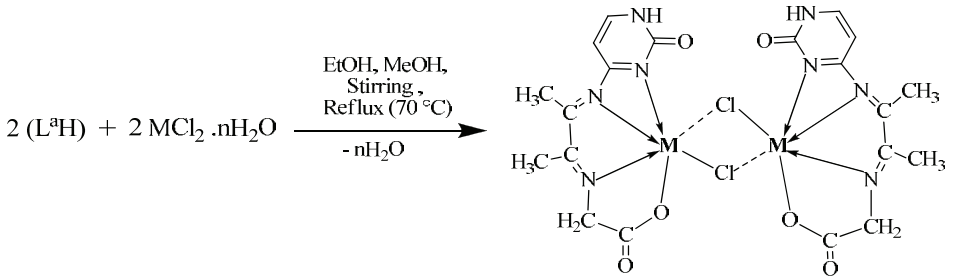

Scheme 2. Synthesis of the binuclear metal complexes $[M_2(L^a)_2Cl_2]$ (**1**–**4**) of the ligand (L^aH).

In vitro *antibacterial activity*

Antibacterial activity of synthesized ligand and binuclear complexes were screened *in vitro* against two Gram-positive (*Staphylococcus aureus* MTCC 1144 and *Bacillus subtilis* MTCC 2423) and two Gram-negative (*Escherichia coli* MTCC 739 and *Salmonella typhi* MTCC 733) bacteria using the agar well diffusion method.[25,26] Streptomycin was used as reference antibacterial drug. Bacterial strains stored in Mueller–Hinton broth (Merck) were sub-cultured for testing in the same medium and grown at 37 °C. Test compounds (ligand, metal complexes and streptomycin) were dissolved in DMSO at a concentration of 2 mg mL^{-1}. Stock solutions were prepared and dilutions were made according to the guidelines in the NCCLS approved standard document M7-A4 using the microdilution broth procedure.[27] Bacterial cells were suspended according to the 0.5 McFarland protocol in saline solution to produce a suspension of 10^4–10^6 CFU mL^{-1}. Serial dilutions of the test compounds were prepared in test tubes to final concentrations of 1024, 512, 256, 128, 64, 32, 16, 8, 4 and 2 μg mL^{-1}. All strains were incubated at 37 °C for 24 h with different concentrations of compounds in Mueller–Hinton broth. Wells were created in medium with the help of a sterile cork borer of 8 mm diameter and the nutrient agar broth was prepared by dissolving beef extract (1.0 g), yeast extract (2.0 g), peptone (5.0 g), NaCl (5.0 g), agar (15.0 g) in one liter of distilled water.. The pH of the solutions was adjusted to 7.2 by the addition of the appropriate amount of sodium hydroxide. The resulting solution was autoclaved for 25 min at 15 psi and seeded with 100 μL of prepared inocula containing approximately 10^6 CFU mL^{-1}. The Petri plates were prepared by pouring 70 mL of seeded nutrient agar. The antibacterial activity was determined by measuring the diameter of the inhibition zone (in mm). For quantitative measurement of growth inhibition, the calculation was performed according to a literature procedure.[26] Minimum inhibitary concentrations of each chemical compound were recorded as the lowest concentration of each chemical compound in the tubes with no growth (*i.e.* no turbidity) of the inoculated bacteria. Each assay was performed in duplicate and repeated three times.

In vitro *antifungal activity*

The antifungal activity of the synthesized ligand and all the binuclear complexes were tested *in vitro* against two fungi *Candida albicans* MTCC 227 and *C. parapsilosis* MTCC 2509 strains by using the poison food technique.[28] The fungal strains were grown on Sabouraud dextrose agar (SDA) at 25 °C for 7–8 days. One-week old cultures of the fungi were used as inoculums for determining the antifungal activity of test compounds. Fluconazole was used as a reference antifungal drug and the medium using DMSO as the solvent was used as a negative control. Solutions of the test compounds (ligand and metal complexes) and the reference drug were dissolved in DMSO at a concentration of 2 μg mL^{-1}. Molten SDA was poisoned by the addition of 100 μL of the prepared inocula and poured into sterile Petri plates. The prepared plates containing the test compounds were inoculated with fungal plugs (6 mm diameter) obtained from the activity growing margins of the fungal plates. The plates were incubated at 25 °C for one week. Each assay was performed in duplicate and repeated three times. Antifungal activity data of all compounds were expressed as percent inhibition calculated from the diameter of inhibition zone. The percent inhibition was determined using the formula:

$$\text{Inhibition} = 100(C - T)/C$$

where C is the diameter of the fungal colony in the control plate and T is the diameter of the microbial colony in the tested plate after the same incubation period.

RESULTS AND DISCUSSION

The Schiff base ligand was synthesized in two steps. In first step, glycine was condensed with diacetyl in a 1:1 mole ratio to form a Schiff base 2-((1--methyl-2-oxopropylidene)amino)acetic acid (LH) and in second step, condensation of LH with 4-amino-1*H*-pyrimidin-2-one produced corresponding Schiff base ligand 2-((1-methyl-2-((2-oxo-1,2-dihydropyrimidin-4-yl)imino)propylidene)amino)acetic acid (L^aH). The newly synthesized Schiff base ligand (L^aH) was effectively employed for the isolation of model binuclear metal complexes **1**–**4**. The Schiff base ligand and binuclear metal complexes were quite stable at room temperature in the solid state. The Schiff base ligand was soluble in common organic solvents but the metal complexes were soluble in DMF and DMSO. Single crystal of the compounds, suitable for X-ray diffraction studies, could not be crystallized by various methods, such as crystallization using solvent mixtures, low temperature crystallization, but the analytical and spectral data, presented in the Supplementary material to this paper, were consistent with the proposed molecular formula and structure of the Schiff base ligand and metal complexes.

The positions of the molecular ion peaks in the mass spectra of the compounds were consistent with their empirical formulae and formula weight. The molar conductance values of the metal complexes, found in the range 3.4–8.3 Ω^{-1} cm^2 mol^{-1} (in DMSO), were too low to account for any dissociation, hence the complexes were considered non-electrolyte in nature.[29] Based on the electronic

spectral data, EPR spectral data and magnetic moment values, octahedral geometry was assigned for all the binuclear metal complexes.

IR spectra

The most relevant IR absorption bands from the spectra of Schiff base ligand (L^aH) and binuclear metal complexes **1**–**4** are summarized in Table S-I of the Supplementary material to this paper.

In the IR spectrum of Schiff base ligand (L^aH), there are no bands of unreacted $–NH_2$ or ketonic groups. The absence of these bands and appearance of a new band at 1642 cm^{-1}, which may be assigned to azomethine group (ν(–C=N)) vibrations, indicates the condensation of amino groups of glycine and 4-amino-1*H*-pyrimidin-2-one with the carbonyl groups of diacetyl and the formation of the proposed Schiff base ligand.[30,31] The band in the IR spectrum of ligand at 1696 cm^{-1} may be assigned to the (N–C=O) group of the pyrimidine ring.[32] The appearance of band at 1532 cm^{-1} may arise from ν(C=N) of the pyrimidine ring. The band at 3074 cm^{-1} may be due to the characteristic stretching vibration of the heterocyclic –NH group of the pyrimidine ring.[32] The Schiff base ligand (L^aH) showed two characteristic bands at 1748 and 1236 cm^{-1}, assigned to the asymmetric and symmetric vibrations of the (–COOH) group, respectively.[33] The IR spectra of metal complexes **1**–**4** show significant changes compared to the free ligand (L^aH).

The IR spectra of the binuclear complexes exhibit characteristic bands in the range of 3072–3078 cm^{-1} due to the stretching vibration of the (–NH) groups of the pyrimidine ring. The band in the range 1688–1694 cm^{-1} may be assigned to the non-coordinated (N–C=O) group of the pyrimidine ring.[10,32] In the IR spectrum of metal complexes **1**–**4**, the absence of the bands at 1748 and 1236 cm^{-1} revealed that the (–COOH) group of the Schiff base ligand was deprotonated on complexation.[34] Instead of these bands, two new bands in the ranges 1604–1565 cm^{-1} and 1396–1348 cm^{-1} appeared that may be assigned to asymmetric and symmetric vibrations of the ($–COO^–$) group, respectively. The pragmatic $\Delta\nu$ ($\nu_{as} - \nu_s$) values for the synthesized complexes were in the range of 206–232 cm^{-1}, which, being larger than 200 cm^{-1}, indicates the unidentate fashion of coordination of carboxylato group with the central metal ion.[35] Coordination through the oxygen atom of the deprotonated carboxyl group is further supported by the appearance of a new band in the range of 508–524 cm^{-1}, which may be assigned to ν(M–O) vibrations.[36,37] The band observed at 1642 cm^{-1} in the spectrum of the free ligand was shifted to 1580–1592 cm^{-1} in the spectra of the complexes, indicating coordination of the azomethine group (–C=N).[38] The band at 1532 cm^{-1} of the ν(C=N) of the pyrimidine ring in free ligand was shifted to 1490––1506 cm^{-1}, indicating the participation of (C=N) group of the pyrimidine ring in the coordination.[39] Coordination through nitrogen atom of azomethine group and

the (C=N) group of the pyrimidine ring is further supported by the presence of a new band in the range of 462–495 cm^{-1}, which is assignable to ν(M–N) vibrations.[37,40] The bands observed in the ranges 345–338 cm^{-1} and 305–290 cm^{-1} may be assigned to ν(M–Cl) and bridged metal chloride (ν(M–Cl–M)) vibrations, respectively.[41,42]

^{1}H-NMR and ^{13}C-NMR spectra

The ^{1}H-NMR and ^{13}C-NMR spectra of Schiff base ligand (L^aH) and $Zn_2[(L^a)_2Cl_2]$ complex (**4**) were recorded in DMSO-d_6 and the resulting data are given in Table S-II of the Supplementary material to this paper.

The ^{1}H-NMR spectrum of ligand (L^aH) does not display a signal corresponding to a primary amine proton, which suggests the condensation of amino group of glycine and 4-amino-1*H*-pyrimidin-2-one with the carbonyl group of diacetyl. A sharp singlet at 11.36 ppm and broad singlet at 11.10 ppm indicate the presence of characteristics (–OH) proton of carboxyl group and (–NH) proton of pyrimidine ring in synthesized ligand (L^aH), respectively. In the ^{1}H-NMR spectrum of the $Zn_2[(L^a)_2Cl_2]$ complex, the signals of the (CH_3–C=N) protons, and the (–NH) and (–CH) protons of the pyrimidine ring were shifted compared to the corresponding protons in the spectra of the free ligand, suggesting coordination through the nitrogen atoms of the azomethine group and the (C=N) group of the pyrimidine ring. The absence of the signals of the (OH) protons indicates deprotonation of the carboxyl group present in the Schiff base.[43]

In the ^{13}C-NMR spectrum of the Zn(II) complex, the changes in the chemical shift values compared to those of the free ligand (L^aH) show coordination through nitrogen atom of the azomethine group and the (C=N) group of the pyrimidine ring and the oxygen atom of the carboxyl group present in the Schiff base. On the other hand, no change in the chemical shift value of the carbon of the carbonyl group of the pyrimidine ring indicates that the oxygen atom of this group did not participate in the coordination.

Thus, the ^{1}H-NMR and ^{13}C-NMR spectral data support the proposed structure of ligand and its Zn(II) complex, as well as the coordination behavior of ligand.[43]

Mass spectra

The formation of Schiff base ligand (L^aH) and metal complexes **1**–**4** were studied through their ESI-MS spectra. The proposed molecular formula of compounds was confirmed by comparing their molecular formula weight with the *m*/*z* values. In the mass spectra of the compounds, peaks were attributed to the molecular ions, *m/z*: 236.12 $[M]^+$ for the Schiff base compound (L^aH); 742.30 $[M+1]^+$ for complex **1**; 732.62 $[M+1]^+$ for complex **2**, 734.11 $[M+2]^+$ for complex **3** and 839.32 $[M]^+$ for complex **4**. These data are in good agreement with the proposed

molecular formula of the Schiff base compound (L^aH) and its binuclear metal complexes **1**–**4**. In addition to the peaks due to the molecular ion, the spectra exhibited peaks assignable to various fragments arising from the cleavage of the compounds in interaction with the accelerated electrons.

Electronic absorption spectra and magnetic moment measurements

The electronic absorption spectra of the binuclear metal complexes **1**–**4** were measured in DMF and the data along with their magnetic moment values are summarized in Table S-III of the Supplementary material to this paper.

The electronic absorption spectrum of $Cu_2[(L^a)_2Cl_2]$ (**1**) exhibits a band at 762 nm that was assigned to the $^2E_g \rightarrow {}^2T_{2g}$ transition, suggesting octahedral geometry around the Cu(II) ion.[44] The obtained μ_{eff} value for Cu(II) complex is 1.62 μ_B, indicating that magnetic exchange occurs between the two copper sites. The electronic absorption spectrum of the $Ni_2[(L^a)_2Cl_2]$ complex (**2**) shows a sharp peak at 242 nm which was assigned to an intra-ligand transition, while the broad peaks around 376 and 552 nm, assigned to $^3A_{2(g)} \rightarrow {}^3T_{1g}$ and $^3A_{2(g)} \rightarrow$ $\rightarrow {}^3T_{2g}$ transitions, respectively, showed d–d transition of Ni(II), consistent with an octahedral geometry of the complex.[44,45] The magnetic moment value of Ni(II) complex was 2.82 μ_B, which indicates the presence of two unpaired electrons per Ni(II) ion, that also confirmed the octahedral geometry of the binuclear Ni(II) complex. The electronic absorption spectral data of the $Co_2[(L^a)_2Cl_2]$ complex (**3**) show absorptions at 590 and 462 nm, which may be assigned to the transitions $^4T_{1g} \rightarrow {}^4A_{2g}$ and $^4T_{1g} \rightarrow {}^4T_{1g}$, respectively. These transitions revealed the octahedral geometry of Co(II) complex.[44] Furthermore, the octahedral geometry for the Co(II) complex was also proved by its magnetic moment value at room temperature of 4.56 μ_B per Co atom. The electronic absorption spectrum of $Zn_2[(L^a)_2Cl_2]$ (**4**) shows two bands at 328 and 356 nm which may be assigned to charge transfer transitions from ligand to the Zn(II) ion (LMCT). The Zn(II) complex is diamagnetic.[44]

EPR spectra

The X-band EPR spectra of the Cu(II) and Co(II) complexes were recorded and the data are given in Table S-III. The X-band EPR spectrum of $Cu_2[(L^a)_2Cl_2]$ complex (**1**) was recorded at a frequency of 9.1 GHz under a magnetic field strength of 3200 G at room temperature (298 K) while the spectrum of $Co_2[(L^a)_2Cl_2]$ complex (**3**) was recorded at liquid nitrogen temperature (77 K) as a polycrystalline sample. Their $g_{||}$ and $g_{\perp}$ were determined from EPR spectra and g_{av} values were calculated from the formula:

$$g_{av}^2 = \frac{\left(g_{||}^2 + 2g_{\perp}^2\right)}{3}$$

Analysis of the EPR spectrum of the Cu(II) complex gives $g_{||}$ 2.124, $g_{\perp}$ 2.056 and g_{av} 2.080. The trend $g_{||} > g_{\perp} > 2.002$ observed for the complex under study indicates that the unpaired electron is localized in the d_{x2-y2} orbital of the Cu(II) ion.[46] Analysis of EPR spectrum of the Co(II) complex gives $g_{||}$ 2.314, $g_{\perp}$ 2.014 and g_{av} 2.112. The trend $g_{||} > g_{\perp} > 2.002$ observed for the Co(II) complex under study was due to a large angular momentum contribution. Thus, the EPR values also support octahedral geometry for the Cu(II) and Co(II) complexes.[47]

Cyclic voltammetric study of the $[Ni_2(L^a)_2Cl_2]$ complex

The electrochemical behavior of the $Ni_2[(L^a)_2Cl_2]$ complex (**2**) was studied by cyclic voltammetry in acetonitrile solution at a platinum electrode *versus* SCE. The complex exhibits two one electron anodic responses near 0.70 and 1.10 V. The anodic responses were assigned to the Ni(II)–Ni(II) to Ni(II)–Ni(III) and Ni(II)–Ni(III) to Ni(III)–Ni(III) transitions. This result is consistent with other reported results for binuclear Ni(II) complexes.[48]

In vitro *antibacterial activity*

The newly synthesized Schiff base ligand (L^aH), its binuclear metal complexes **1–4** and the standard drug streptomycin were screened *in vitro* separately to assess their antibacterial activity against two Gram-positive bacteria (*S. aureus* and *B. subtilis*) and two Gram-negative bacteria (*E. coli* and *S. typhi*). The synthesized compounds show greater toxicity towards the Gram-positive strains than towards the Gram-negative strains. The reason is the difference in the complexity of the structure of the cell walls of Gram-positive and Gram-negative bacteria. The antibacterial screening concentrations of the compounds were estimated from the minimum inhibitory concentration (*MIC*) value, which were in the range 4–64 μg/mL^{-1}. The *MIC* values presented in Table I clearly indicate that the $Co_2[(L^a)_2Cl_2]$ complex (**3**) was the most potent antibacterial compound with *MIC* values 16, 16, 32 and 32 μg mL^{-1} and the $Cu_2[(L^a)_2Cl_2]$ complex (**1**) was the least potent antibacterial compound with *MIC* values 32, 32, 64 and 64 μg

TABLE I. Minimum inhibition concentration (*MIC* / μg mL^{-1}) values for the Schiff base ligand (L^aH), its binuclear metal complexes **1**–**4** and the standard drug; metal complexes: **1** = $Cu_2[(L^a)_2Cl_2]$, **2** = $Ni_2[(L^a)_2Cl_2]$, **3** = $Co_2[(L^a)_2Cl_2]$, **4** = $Zn_2[(L^a)_2Cl_2]$; streptomycin = standard drug

Microorganism	Ligand (L^aH)	Metal complex				Streptomycin
		1	**2**	**3**	**4**	
Gram-positive						
S. aureus	64	32	32	16	32	4
B. subtilis	64	32	16	16	16	4
Gram-negative						
E. coli	128	64	32	32	32	8
S. typhi	128	64	64	32	64	8

mL^{-1} as compared to the other studied complexes against *S. aureus*, *B. subtilis*, *E. coli* and *S. typhi*, respectively.

In vitro *antifungal activity*

The antifungal activites of synthesized Schiff base ligand (L^aH) and its binuclear metal complexes **1**–**4** were determined *in vitro* against two fungi *C. albicans* and *C. parapsilosis* and compared with the standard antifungal drug fluconazole at the same concentration. The antifungal activity data are summarized in Table II. Among all the synthesized compounds, the $Zn_2[(L^a)_2Cl_2]$ complex (**4**) was the most active against the studied fungi and showed a higher activity against *C. parapsilosis*. The activity was greatly enhanced at the higher concentration. The DMSO control showed a negligible activity as compared to the synthesized compounds. All the metal complexes exhibited good antifungal activity against *C. albicans* and *C. parapsilosis* as compared to the activity of the standard drug fluconazole. The antifungal activity data showed that the activity of complexes depended on the type of metal ion present in complex and thus, it was observed that the $Zn_2[(La)_2Cl_2]$ complex was the most active, the $Ni_2[(L^a)_2Cl_2]$ complex was the least active, while the $Cu_2[(L^a)_2Cl_2]$ and $Co_2[(L^a)_2Cl_2]$ complexes exhibited good activity against the studied fungi.

TABLE II. *In vitro* antifungal screening data of the Schiff base ligand (L^aH), its binuclear metal complexes **1**–**4** and the standard drug`

Compound	Mycelial growth inhibition, %	
	C. ablicans	*C. parapsilosis*
(L^aH)	35.3	32.6
$[Cu_2(L^a)_2Cl_2]$ (**1**)	55.4	57.4
$[Ni_2(L^a)_2Cl_2]$ (**2**)	45.3	48.6
$[Co_2(L^a)_2Cl_2]$ (**3**)	58.2	61.5
$[Zn_2(L^a)_2Cl_2]$ (**4**)	65.8	69.6
Fluconazole (standard drug)	79.2	85.8

In the present study, the low activity of some of the metal complexes may be due to their low lipophilicity because of which penetration of the complex through the lipid membrane was decreased and hence, they could neither block nor inhibit the growth of the microorganism. The variation in the antimicrobial activity of different metal complexes against different microorganisms depends on their permeability into the cell or differences in ribosomes in the microbial cell.[49] The lipid membrane surrounding the cell favors the passage of any lipid soluble material and it is known that liposolubility is an important factor controlling antimicrobial activity.[50]

CONCLUSIONS

The newly synthesized Schiff base ligand and its binuclear metal complexes were characterized by various physicochemical techniques. The data obtained from various studies are in good agreement with proposed structure of the Schiff base ligand and its metal complexes. Octahedral geometry of the complexes was proved by their electronic absorption spectra, EPR spectra and magnetic moment values. The molar conductance values show the non-electrolyte nature of all the metal complexes. *In vitro* antibacterial and antifungal studies showed that the Schiff base ligand and its binuclear metal complexes were biologically active. The $Co_2[(L^a)_2Cl_2]$ complex showed the best activity against the studied bacteria and the $Zn_2[(L^a)_2Cl_2]$ complex showed the best activity against the studied fungi.

SUPPLEMENTARY MATERIAL

Physical and analytical data for complexes **1**–**4** are available electronically from http://www.shd.org.rs/JSCS/, or from the corresponding author on request.

Acknowledgements. The authors are thankful to ACBR, Delhi for providing the spectral data, IIT Roorkee for providing the elemental analyses data, and SAIF, Punjab University, Chandigarh for providing the ^{1}H-NMR and ^{13}C-NMR spectral data. The authors are also thankful to the authorities of Meerut College, Meerut for providing the necessary research facilities.

И З В О Д

СИНТЕЗА И КАРАКТЕРИЗАЦИЈА БИОЛОШКИ АКТИВНИХ БИНУКЛЕАРНИХ КОМПЛЕКСА ПРЕЛАЗНИХ МЕТАЛА СА ШИФОВОМ БАЗОМ КАО ЛИГАНДОМ КОЈИ ЈЕ ДОБИЈЕН У РЕАКЦИЈИ ИЗМЕЂУ 4-АМИНО-1*H*-ПИРИМИДИН-2-ОНА, ДИАЦЕТИЛА И ГЛИЦИНА

ABHAY NANDA SRIVASTAVA, NETRA PAL SINGH и CHANDRA KIRAN SHRIWASTAW

Department of Chemistry, Meerut College, Meerut-250001, India

Синтетизована је серија нових бинуклеарних комплекса прелазних метала са Шифовом базом као лигандом 2-((1-метил-2-((2-оксо-1,2-дихидропиримидин-4-ил)имино)-пропилиден)амино)сирћетне киселина, L^aH, који је добијен у реакцији 4-амино-1*H*-пиримидин-2-она, диацетила и глицина. Све реакције између Шифове базе и одговарајућег хлорида прелазног метала (Cu(II), Ni(II), Co(II) или Zn(II)) су извођене у 1:1 молском односу. Комплекси су окарактерисани елементалном микроанализом, мерењем моларне проводљивости и магнетног момента, као и различитим спектроскопским методама (IR, UV–Vis, ^{1}H-NMR, ^{13}C-NMR, EPR и ESI-MS). Мерење моларне проводљивости је показало да су сви синтетисани комплекси електронеутрални. На основу спектроскопских података и вредности магнетног момента закључено је да испитивани бинуклеарни комплекси прелазних метала имају октаедарску геометрију. У цикличном волтамограму Ni(II) комплекса јављају се два анодна пика на приближно 0,70 и 1,10 V. Извршена су *in vitro* испитивања антибактеријске и антифунгалне активности лиганда Шифове базе и одговарајућих бинуклеарних комплекса на различитим сојевима бактерија (*Staphylococcus aureus*, *Bacillus subtilis*, *Escherichia coli* и *Salmonella typhi*) и гљива (*Candida albicans* и *Candida parapsilosis*).

(Примљено 23. јануара, ревидирано 27 новембра 2013)

REFERENCES

1. J. A. Joule, K. Nills, G. F. Smith, *Heterocyclic chemistry*, Chapman and Hall, London, 1995
2. I. Lakmoska, B. Gaolankiewicz, J. Wietrzyk, M. Pelczynska, A. Nasulewicz, A. Opolski, J. Sitkowski, L. Kozerski, E. Szlyk, *Inorg. Chim. Acta* **358** (2005) 1911
3. G. Ferguson, J. N. Low, M. Quiros-Olozabal, J. M. Salas-Peregrin, F. Hueso-Urena, M. N. Moreno-Carretero, *Polyhedron* **15** (1996) 3233
4. D. A. Garnovskii, M. F. C. Guedes da Silva, M. N. Kopylovich, A. D. Granovskii, J. J. R. Frausto da Silva, A. J. L. Pombeiro, *Polyhedron* **22** (2003) 1335
5. S. E. M. Khalil, H. S. Saleem, B. A. El-Shetary, M. Shebl, *J. Coord. Chem.* **55** (2002) 883
6. M. Weitzer, S. Brooker, *Dalton Trans.* (2005) 2448
7. P. O. Lumme, H. Knuuttilla, *Polyhedron* **14** (1995) 1553
8. N. P. Singh, A. N. Srivastava, *Asian J. Chem.* **25** (2013) 533
9. C. M. Sharaby, G. C. Mohamed, M. M. Omar, *Spectrochim. Acta, A* **66** (2007) 935
10. M. Sonmez, M. Celebi, I. Berber, *Eur. J. Med. Chem.* **45** (2010) 1935
11. S. Tabassum, G. C. Sharma, F. Arjmand, A. Azam, *Nanotechnology* **21** (2010) 195102
12. A. Arbaoui, C. Redshaw, N. M. Sanchez-Ballester, M. R. J. Elsegood, D. L. Hughes, *Inorg. Chim. Acta* **365** (2011) 96
13. S. Tabassum, S. Amir, F. Arjmand, C. Pettinari, F. Marchetti, N. Masciocchi, G. Lupidi, R. Pettinari, *Eur. J. Med. Chem.* **60** (2013) 216
14. A. Alagha, L. Parthasrathi, D. Gaynor, H. M. Bunz, Z. A. Starikova, E. Farkas, E. C. O. Brien, M. J. Gil, K. B. Nolan, *Inorg. Chim. Acta* **368** (2011) 58
15. K. Zelga, M. Leszczynski, I. Justyniak, A. Kornowicz, M. Cabaj, A. E. H. Wheatley, J. Lewinski, *Dalton Trans*. **41** (2012) 5934
16. G. Psomas, D. P. Kessissoglou, *Dalton Trans.* **42** (2013) 6252
17. N. P. Singh, A. N. Srivastava, *E-J. Chem.* **8** (2010) 809
18. S. Tabassum, N. P. Singh, J. Mussarat, *Synth. React. Inorg. Met.-Org. Chem.* **33** (2003) 509
19. S. Tabassum, N. P. Singh, F. Arjmand, *Synth. React. Inorg. Met.-Org. Chem.* **31 (**2001) 1803
20. F. Arjmand, M. Muddassir, R. H. Khan, *Eur. J. Med. Chem.* **45** (2010) 3549
21. K. Singh, Y. Kumar, P. Puri, M. Kumar, C. Sharma, *Eur. J. Med. Chem.* **52** (2012) 313
22. N. P. Singh, A. N. Srivastava, *J. Serb. Chem. Soc.* **77** (2012) 637
23. C. N. Reilley, R. W. Schmidt, F. A. Sadek, *J. Chem. Educ.* **36** (1959) 619
24. A. I. Vogel, *A Text Book of Quantitative Inorganic Analysis,* Longmans, London, 1961
25. A. K. Sadan, Y. Mirza, A. R. Aneja, O. Prakash, *Eur. J. Med. Chem.* **38** (2003) 533
26. A. Rahman, M. I. Choudhary, W. J. Thomsen, *Bioassay Techniques for Drug Development*, Harwood Academic Publishers, The Netherlands, 2001
27. National Committee for Clinical Laboratory Standards. *Methods for Dilution Antimicrobial Susceptibility Tests for Bacteria that Grow Aerobically*, Approved Standard M7-A4, NCCLS: Villanova, PA, 1997
28. S. K. S. Al-Burtamani, M. O. Fatope, R. G. Marwah, A. K. Onifade, S. H. Al-Saidi, *J. Ethnopharmacol.* **96** (2005) 107
29. W. J. Geary, *Coord. Chem. Rev.* **7** (1971) 81
30. M. Dolze, M. Tumer, M. Digrak, *Transition Met. Chem.* **29** (2004) 516
31. K. Majumdar, R. J. Butcher, S. Bhattacharya, *Inorg. Chem.* **49** (2002) 4605
32. M. S. Masoud, E. A. Khalil, A. A. Hindawy, A. E. Ali, E. F. Mohamed, *Spectrochim. Acta, A* **60** (2004) 2807

33. J. Iqbal, M. Imran, S. Iqbal, S. Latif, *J. Chem. Soc. Pak.* **29** (2007) 151
34. F. Gao, P. Yang, J. Xie, H. Wang, *J. Inorg. Biochem*. **60** (1995) 61
35. G. B. Deacon, R. J. Phillips, *Coord. Chem. Rev*. **33** (1980) 227
36. G. Kumar, D. Kumar, S. Devi, R. Johari, C. P. Singh, *Eur. J. Med. Chem.* **45** (2010) 3056
37. A. A. Alemi, B. Shaabni, *Acta Chim. Slov.* **47** (2000) 363
38. K. Singh, P. Patil, B. V. Agarwal, *Spectrosc. Lett.* **28** (1995) 747
39. K. Nakamoto, *Infrared and Raman Spectra of Inorganic and Coordination Compounds*, Wiley, New York, 1986
40. L. J. Bellamy, *The Infrared Spectra of Complex Molecules*, Chapman and Hall, London, 1978
41. L. Mishra, K. K. Upadhyay, *Indian J. Chem., A* **31** (1992) 169
42. M. Shakir, O. S. M. Nasman, S. P. Varkey, *Polyhedron* **15** (1996) 309
43. R. M. Silverstein, C. M. Bassler, T. C. Morrill, *Spectrometric Identification of Organic Compounds*, Wiley, New York, 1974
44. A. B. P. Lever, *Inorganic Electronic Spectroscopy*, Elsevier, New York, 1968
45. F. F. Jian, L. Pang, H. L. Xiao, P. P. Sun, *Chin. J. Struct. Chem.* **23** (2004) 975
46. A. M. Herrera, R. J. Staples, S. V. Kryotov, A. Y. Nazarenko, E. Vakimova, *Dalton Trans*. (2003) 846
47. D. R. Lorenz, J. R. Wasson, D. K. Johonson, D. A. Thorpe, *J. Inorg. Chem.* **37** (1975) 2297
48. A. Banerjee, R. Singh, D. Chopra, E. Colacio, K. K. Rajak, *Dalton Trans.* (2008) 6539
49. S. K. Sengupta, O. P. Pandey, B. K. Srivastava, V. K. Sharma, *Transition Met. Chem*. **23** (1998) 349
50. J. Parekh, P. Inamdhar, R. Nair, S. Baluja, S. Chandra, *J. Serb. Chem. Soc.* **70** (2005) 1155.

Journal of the Serbian Chemical Society
JSCS@tmf.bg.ac.rs • www.shd.org.rs/JSCS
J. Serb. Chem. Soc. 79 (4) S50–S52 (2014) *Supplementary material*

SUPPLEMENTARY MATERIAL TO

Synthesis and characterization of bioactive binuclear transition metal complexes of a Schiff base ligand derived from 4-amino-1*H*-pyrimidin-2-one, diacetyl and glycine

ABHAY NANDA SRIVASTAVA, NETRA PAL SINGH* and CHANDRA KIRAN SHRIWASTAW

Department of Chemistry, Meerut College, Meerut-250001, India

J. Serb. Chem. Soc. 79 (4) (2014) 421–433

PHYSICAL AND ANALYTICAL DATA FOR COMPLEXES **1**–**4**

$[Cu_2(L^a)_2Cl_2]$ ***(1)***. Yield: 62 %; color: reddish brown; m.p. (dec.): 262 °C; Anal. Calcd. for $C_{20}H_{22}Cl_2Cu_2N_8O_6$ (FW: 668.43): C, 35.94; H, 3.32; N, 16.76; Cu, 19.01; Cl, 10.61 %. Found: C, 35.89; H, 3.30; N, 16.72; Cu, 18.98; Cl, 10.58 %; Molar conductance (Λ_M / Ω^{-1} cm^2 mol^{-1}): 8.3.

$[Ni_2(L^a)_2Cl_2]$ ***(2)***. Yield: 68 %; color: dark brown; m.p. (dec.): 280 °C; Anal. Calcd. for $C_{20}H_{22}Cl_2N_8Ni_2O_6$ (FW: 658.73): C, 36.47; H, 3.36; N, 17.01; Ni, 17.82; Cl, 10.76 %. Found: C, 36.43; H, 3.31; N, 16.96; Ni, 17.79; Cl, 10.70 %; Molar conductance (Λ_M / Ω^{-1} cm^2 mol^{-1}): 7.2.

$[Co_2(L^a)_2Cl_2]$ ***(3)***. Yield: 60 %; color: brown; m.p. (dec.): 252 °C; Anal. Calcd. for $C_{20}H_{22}Cl_2Co_2N_8O_6$ (FW: 659.21): C, 36.44; H, 3.36; N, 16.99; Co, 17.88; Cl, 10.75 %. Found: C, 36.38; H, 3.32; N, 16.94; Co, 17.85; Cl, 10.72 %; Molar conductance (Λ_M / Ω^{-1} cm^2 mol^{-1}): 5.4.

$[Zn_2(L^a)_2Cl_2]$ ***(4)***. Yield: 65 %; colorless; m.p. (dec.): 220 °C; Anal. Calcd. for $C_{20}H_{22}Cl_2N_8O_6Zn_2$ (FW: 672.17): C, 35.74; H, 3.30; N, 16.67; Zn, 19.46; Cl, 10.55 %. Found: C, 35.68; H, 3.27; N, 16.62; Zn, 19.44; Cl, 10.52 %. Molar conductance (Λ_M / Ω^{-1} cm^2 mol^{-1}): 3.4.

* Corresponding author. E-mail: npsmcm.in@gmail.com

TABLE S-I. Characteristic IR bands (cm^{-1}) of the Schiff base ligand (L^aH) and its binuclear metal complexes **1**–**4**; azo. = azomethine group, pym. = pyrimidine, ν_{as} = asymmetric vibration, ν_s = symmetric vibration

Compound	ν(–C=N) azo.	υ(C=N) pym.	ν_{as} ($-CO_2H$)	ν_s ($-CO_2H$)	ν_{as} ($-CO_2^-$)	ν_s ($-CO_2^-$)	ν (M–N)	ν (M–O)	ν (M–Cl)
(L^aH)	1642	1532	1748	1236	–	–	–	–	–
1	1592	1490	–	–	1604	1396	495	508	334 305
2	1588	1506	–	–	1580	1348	462	518	338 296
3	1580	1498	–	–	1574	1368	475	524	345 302
4	1584	1502	–	–	1565	1352	488	516	342 290

TABLE S-II. ^{1}H-NMR and ^{13}C-NMR spectral data for the Schiff base ligand (L^aH) and the $Zn_2[(L^a)_2Cl_2]$ complex (in DMSO-d_6) at room temperature with reference to TMS; pym. = pyrimidine

Compound	^{1}H-NMR (δ / ppm)	^{13}C-NMR (δ / ppm)
(L^aH) 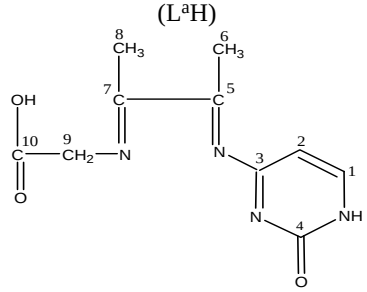	1.62 (6H, *s*, CH_3), 3.54 (2H, *s*, CH_2), 5.64 (1H, *d*, *J* = 4.2 Hz, CH=C pym.), 6.82 (1H, *d*, *J* = 1.4 Hz, =CH–N pym.), 11.10 (1H, *brs*, –NH pym.), 11.36 (1H, *s*, –OH)	20.20 (C-8), 23.50 (C-6), 46.90 (C-9), 93.90 (C-2), 148.10 (C-1), 156.10 (C-5), 161.80 (C-7), 166.90 (C-4), 169.80 (C-3), 172.60 (C-10)
$[Zn_2(L^a)_2Cl_2]$ (4) 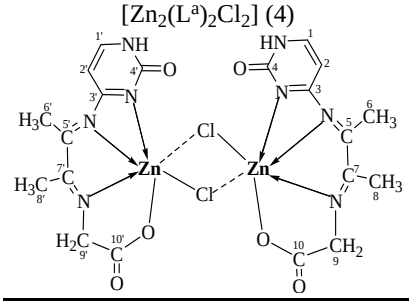	1.18 (12H, s, $-CH_3$), 3.48 (4H *s*, $-CH_2$), 5.68 (2H, *d*, *J* = 4.2 Hz, –CH=C pym.), 6.94 (2H, *d*, *J* = 1.4 Hz, =CH–N (pym.), 10.94 (2H, *brs*, –NH pym.)	19.90 [C-(8, 8′)], 23.10 [C-(6, 6′)], 46.34 [C-(9, 9′)], 93.74 [C-(2, 2′)], 147.92 [C-(1, 1′)], 154.60 [C-(5, 5′)], 158.40 [C-(7, 7′)], 166.70 [C-(4, 4′)], 167.22 [C-(10, 10′)], 169.18 [C-(3, 3′)]

TABLE S-III. Electronic absorption spectral data (in DMF), magnetic moment values and EPR spectral parameters of the metal complexes

Compound	λ_{max} / nm	Assignment	μ_{eff} / μ_B	EPR values		
				$g_{\|\|}$	$g_{\perp}$	g_{av}
1	762	$E_g \rightarrow {}^2T_{2g}$	1.62	2.124	2.056	2.080
2	242	INCT	2.82	–	–	–
	376	${}^3A_{2(g)} \rightarrow {}^3T_{1g}$				
	552	${}^3A_{2(g)} \rightarrow {}^3T_{2g}$				
3	462	${}^4T_{1g} \rightarrow {}^4T_{1g}$	4.56	2.314	2.014	2.112
	590	${}^4T_{1g} \rightarrow {}^4A_{2g}$				
4	328	LMCT	Diamagnetic	–	–	–
	356	LMCT				

Journal of the Serbian Chemical Society
JSCS-info@shd.org.rs • www.shd.org.rs/JSCS
J. Serb. Chem. Soc. *79* (4) 435–443 (2014)
JSCS–4597
UDC 547.587.51:519.677:579:615.1.8
Original scientific paper

DFT study and microbiology of some coumarin-based compounds containing a chalcone moiety

SELMA ŠPIRTOVIĆ-HALILOVIĆ[1]*, MIRSADA SALIHOVIĆ[2], HURIJA DŽUDŽEVIĆ-ČANČAR[2], SNEŽANA TRIFUNOVIĆ[3], SUNČICA ROCA[4], DŽENITA SOFTIĆ[5] and DAVORKA ZAVRŠNIK[1]

[1]*Department of Pharmaceutical Chemistry, Faculty of Pharmacy, University of Sarajevo, Zmaja od Bosne 8, 71000 Sarajevo, Bosnia and Herzegovina,* [2]*Department of Organic Chemistry, Faculty of Pharmacy, University of Sarajevo, Zmaja od Bosne 8, 71000 Sarajevo, Bosnia and Herzegovina,* [3]*Faculty of Chemistry, University of Belgrade, Studentski trg 12–16, 11000 Belgrade, Serbia,* [4]*NMR Centre, Ruđer Bošković Institute, Bijenička cesta 54, 10000 Zagreb, Croatia and* [5]*Agency for Medicinal Product and Medical Devices of Bosnia and Herzegovina, Titova 9, 71000 Sarajevo, Bosnia and Herzegovina*

(Received 28 June 2013)

Abstract: In the present investigation, a series of coumarin-based compounds containing a chalcone moiety were studied for their *in vitro* and *in silico* properties. The DFT global chemical reactivity descriptors (chemical hardness, total energy, electronic chemical potential and electrophilicity) were calculated for four synthesized compounds and used to predict their relative stability and reactivity. The antibacterial activities of all compounds were screened against *Bacillus subtilis* (ATCC 6633) and *Bacillus cereus* (ATCC 11778). The quantum-chemical calculations indicated that the antibacterial activity correlates well with chemical reactivity descriptors of the molecules.

Keywords: coumarins; chemical reactivity descriptors; antimicrobial activity; HOMO and LUMO studies.

INTRODUCTION

Problem of multi-drug resistant microorganisms has reached an alarming level around the world and the synthesis of new efficient anti-infective compounds has become an urgent need for the treatment of microbial infections.[1]

In previous works, by the nucleophilic addition reaction of the synthesized precursor 3-acetyl-4-hydroxycoumarin with different aromatic aldehydes, in the presence of basic catalysts pyridine and piperidine, a series of 3-substituted derivatives of 4-hydroxycoumarins containing a chalcone moiety were synthesized and their structures were confirmed. The results of previous studies sug-

* Corresponding author. E-mail: selmaspirtovic@yahoo.com
doi: 10.2298/JSC130628077S

gested interesting biological and physicochemical properties of synthesized compounds.[2–5] The lipophilicity of synthesized compounds was determined in order to predict their chemical behavior toward living organisms. The results of *in silico* and *in vitro* investigations for the lipophilicity parameters of the synthesized derivatives showed that this group of compounds has an optimal range of values (log *D7.4* from 1 to 3) for good absorption *in vivo* and for *per os* application.[5] All of the above was the stimulus for this new research. The reactivity of a molecule is always governed by its electronic properties and kinetic and thermodynamic stability. In this computational study, the structural and electronic properties of four compounds of some coumarin-based molecules containing a chalcone moiety were investigated and used to predict their relative stability and reactivity. The density functional theory (DFT) has been accepted by the chemistry community as a reliable and effective approach for the computation of molecular structure, vibration frequencies and energies of chemical reactions.[6–9] The DFT provides an efficient method to include correlation energy in electronic calculations.[10] In addition, it constitutes a solid support to reactivity models.[11] Besides the total energy (ε), global chemical reactivity description, such as electronic chemical potentials (μ),[12] chemical hardness (η)[13] and electrophilicity (ω),[14] can be calculated. Reactivity parameters have been associated with the response of the electronic properties and the microbiology of compounds **1** to **4**. Then, the reactivity parameters are identified with response functions and they are represented by derivates of the electronic properties.

MATERIALS AND METHODS

Investigated compounds

Four 3-substituted derivatives of 4-hydroxycoumarins containing a chalcone moiety, *i.e.*, 3-(3-(2-chlorophenyl)prop-2-enoyl)-4-hydroxy-2*H*-1-benzopyran-2-one (**1**), 3-(3-(3-chlorophenyl)prop-2-enoyl)-4-hydroxy-2*H*-1-benzopyran-2-one (**2**), 3-(3-(4-chlorophenyl)prop-2--enoyl)-4-hydroxy-2*H*-1-benzopyran-2-one (**3**) and 3-(3-(4-bromophenyl)prop-2-enoyl)-4--hydroxy-2*H*-1-benzopyran-2-one (**4**), were studied for their *in vitro* and *in silico* properties.

The structures of the tested compounds are presented in Fig. 1.

Chemical reactivity

The computations were performed using Spartan 10. The geometries of **1** to **4** were optimized at the semi-empirical AM1 level. The structures are minima on the potential energy surface with positive harmonic vibrational frequencies.

The chemical reactivity descriptors calculated using DFT are: total energy (ε), chemical hardness (η), electronic chemical potential (μ) and electrophilicity (ω).

The antimicrobial activity of the 3-substituted derivatives of 4-hydroxycoumarin

The microbiological activity of the compounds was tested by the diffusion method on the *Bacillus subtilis* (ATCC 6633) and *Bacillus cereus* (ATCC 11778) species of bacteria. For the determination of the antimicrobial activity, Müller–Hinton and nutritious bases A, B, and F were used. The diffusion method is based on monitoring the growth inhibition of a specific microorganism caused by certain concentrations of a tested compound. The results of tests are

shown as inhibition zones (*I*) expressed in mm. When using the diffusion method, the test samples were dissolved in dimethyl sulfoxide (99.5 % DMSO) to obtain 1 mg mL^{-1} stock solutions. The inhibition zones for bacteria were measured in mm at the end of an 18-hour incubation period at 37 °C with 100 μL of the solution per well. Compounds **3** and **4**, which were previously investigated against *B. subtilis* (ATCC No. 6633), were also included in the antimicrobial activity evaluations.[2]

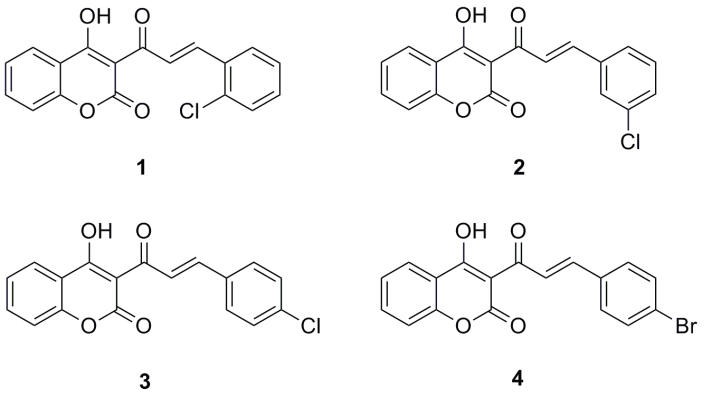

Fig. 1. Structures of the synthesized compounds **1**–**4**.

RESULTS AND DISCUSSION

Structural and electronic properties

The chemical hardness is associated with the stability and reactivity of a chemical system. In a molecule, it measures the resistance to change in the electron distribution or charge transfer. Based on frontier molecular orbitals, chemical hardness corresponds to the gap between the highest occupied molecular orbital (HOMO) and lowest unoccupied molecular orbital (LUMO). Chemical hardness is approximated using the equation:[15]

$$\eta = \frac{(\varepsilon_{\mathrm{LUMO}} - \varepsilon_{\mathrm{HOMO}})}{2} \quad (1)$$

where $\varepsilon_{\mathrm{LUMO}}$ and $\varepsilon_{\mathrm{HOMO}}$ are the LUMO and HOMO energies.

The larger the HOMO–LUMO energy gap, the harder and more stable/less reactive is the molecule.[16,17]

The electronic chemical potential is defined as the negative of electronegativity of a molecule[13] and is determined using the equation:

$$\mu = \frac{(\varepsilon_{\mathrm{HOMO}} + \varepsilon_{\mathrm{LUMO}})}{2} \quad (2)$$

Physically, μ describes the escaping tendency of electrons from an equilibrium system.

The global electrophilicity index (ω), introduced by Parr, is calculated using the electronic chemical potential and chemical hardness:[18]

$$\omega = \frac{\mu^2}{2\eta} \tag{3}$$

Electrophilicity index measures the propensity or capacity of a species to accept electrons. It is a measure of the stabilization in energy after a system accepts an additional amount of electronic charge from the environment.

Table I (row 5) contains the computed chemical hardness values for compounds **1** to **4**. The results indicate that compound **4** is harder and less reactive than **3**, which is harder and less reactive than **2**, which is harder and less reactive than **1**.

The values of μ for compounds **1** to **4** are presented in Table I. The trend in the electronic chemical potential for the compounds is **1** > **3** > **2** and **4**. The greater the electronic chemical potential, the less stable or more reactive is the compound. Therefore, **1** is the most reactive, and **2** and **4** are the least reactive of these compounds.

TABLE I. Global chemical reactivity indices for compounds **1**–**4**

Energy	Compound			
	1	**2**	**3**	**4**
Hartree	–4155.82	–4092.4	–4094.51	–4132.41
HOMO / eV*	–7.92	–8.09	–8.08	–8.12
LUMO / eV	–2.45	–2.44	–2.41	–2.41
μ / eV	–5.19	–5.27	–5.24	–5.27
η / eV	2.73	2.8	2.84	2.86
ω / eV	4.93	4.96	4.83	4.86

The electrophilicity values (Table I) for the compounds are 4.93 eV for **1**, 4.96 eV for **2**, 4.83 eV for **3** and 4.86 eV for **4**. Among these compounds, **3** is the strongest nucleophile while **2** is the strongest electrophile.

A molecule of compound **4** has the highest HOMO–LUMO energy gap, which indicates that it is the most stable and less reactive than the molecules of compounds **3**, **2** and **1**, as shown in Fig. 2.

*Atomic charges for compounds **1**–**4***

The synthesized compounds were studied theoretically and the atomic charges, heat of formation and stereochemistry were estimated. It was found that the compounds are planar (Table II).

The double bond bridge, the link between the planar benzopyrane heterocycle from the one side and the planar phenyl ring on the other side, gives rigi-

* 1 eV ≈ 1.60218×10^{-19} J

dity to all the investigated coumarins and is probably the reason for the planarity of these compounds.

Furthermore, the data show that the charge in the large atomic ligand compounds **1**–**4** are (O(11): –0.750 to –0.755). The following values are: O(22), –0.962 to –0.971. These data clearly show that these are the two most reactive atoms for substitution reactions.

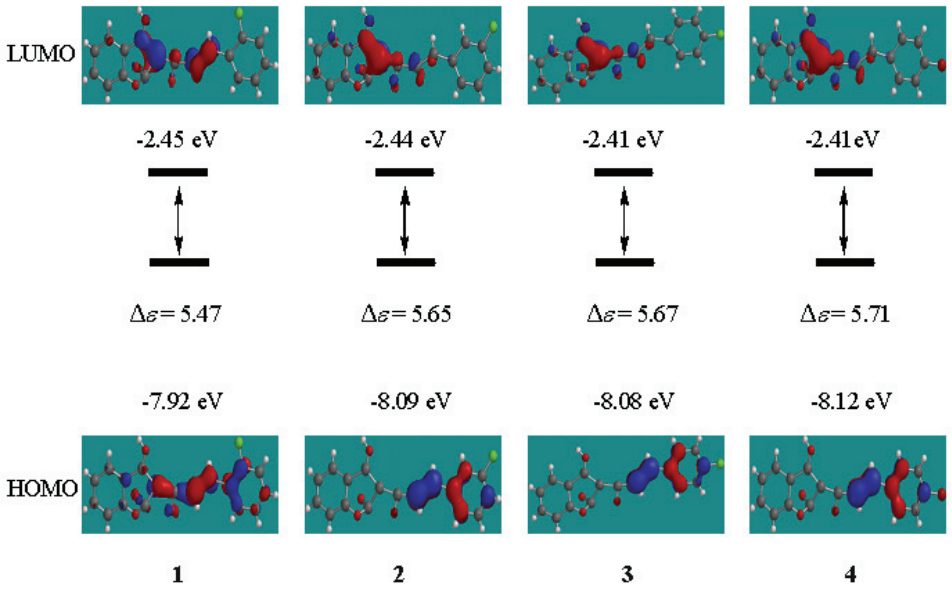

Fig. 2. Frontier molecular orbitals of compounds **1**–**4**.

TABLE II. Atomic charges for compounds **1**–**4**; All charges MM2 are 0

Atom	Atom type (MM2)	Charge Hückel	Atom	Atom type (MM2)	Charge Hückel	Atom	Atom type (MM2)	Charge Huckel
Compound **1**								
C(1)	C Alkene	–0.068	C(13)	C Carbonyl	0.120	H(25)	H	0.020
C(2)	C Alkene	–0.056	C(14)	C Alkene	0.106	H(26)	H	0.024
C(3)	C Alkene	–0.097	C(15)	C Alkene	–0.047	H(27)	H	0.026
C(4)	C Alkene	0.269	C(16)	C Alkene	0.221	H(28)	H	0.052
C(5)	C Alkene	–0.040	C(17)	C Alkene	–0.141	H(29)	H	0.343
C(6)	C Alkene	–0.055	C(18)	C Alkene	–0.186	H(30)	H	0.020
O(7)	O Enol	–0.033	C(19)	C Alkene	–0.081	H(31)	H	0.020
C(8)	C Carbonyl	0.538	C(20)	C Alkene	–0.181	H(32)	H	0.021
C(9)	C Alkene	–0.153	O(21)	O Enol	0.612	H(33)	H	0.029
C(10)	C Alkene	0.285	O(22)	O Carbonyl	–0.962	H(34)	H	0.244
O(11)	O Carbonyl	–0.753	Cl(23)	Cl	0.159			

TABLE II. Continued

Atom	Atom type (MM2)	Charge Hückel	Atom	Atom type (MM2)	Charge Hückel	Atom	Atom type (MM2)	Charge Huckel
				Compound **1**				
C(12)	C Alkene	–0.277	H(24)	H	0.020			
				Compound **2**				
C(1)	C Alkene	–0.068	C(13)	C Carbonyl	0.122	H(25)	H	0.020
C(2)	C Alkene	–0.051	C(14)	C Alkene	–0.234	H(26)	H	0.024
C(3)	C Alkene	0.097	C(15)	C Alkene	–0.008	H(27)	H	0.023
C(4)	C Alkene	0.272	C(16)	C Alkene	0.213	H(28)	H	0.052
C(5)	C Alkene	–0.037	C(17)	C Alkene	0.165	H(29)	H	0.017
C(6)	C Alkene	–0.042	C(18)	C Alkene	–0.250	H(30)	H	0.343
O(7)	O Enol	–0.033	C(19)	C Alkene	–0.028	H(31)	H	0.020
C(8)	C Carbonyl	0.537	C(20)	C Alkene	–0.194	H(32)	H	0.021
C(9)	C Alkene	–0.152	O(21)	O Enol	0.771	H(33)	H	0.030
C(10)	C Alkene	0.289	O(22)	O Carbonyl	–0.962	H(34)	H	0.216
O(11)	O Carbonyl	–0.755	Cl(23)	Cl	0.036			
C(12)	C Alkene	–0.279	H(24)	H	0.0210			
				Compound **3**				
C(1)	C Alkene	–0.068	C(13)	C Carbonyl	0.103	H(25)	H	0.020
C(2)	C Alkene	–0.074	C(14)	C Alkene	–0.117	H(26)	H	0.024
C(3)	C Alkene	–0.102	C(15)	C Alkene	–0.024	H(27)	H	0.023
C(4)	C Alkene	0.262	C(16)	C Alkene	0.225	H(28)	H	0.052
C(5)	C Alkene	–0.044	C(17)	C Alkene	–0.095	H(29)	H	0.017
C(6)	C Alkene	–0.063	C(18)	C Alkene	0.550	H(30)	H	0.343
O(7)	O Enol	–0.036	C(19)	C Alkene	–0.090	H(31)	H	0.020
C(8)	C Carbonyl	0.543	C(20)	C Alkene	–0.133	H(32)	H	0.021
C(9)	C Alkene	–0.152	O(21)	O Enol	0.749	H(33)	H	0.029
C(10)	C Alkene	0.246	O(22)	O Carbonyl	–0.971	H(34)	H	0.216
O(11)	O Carbonyl	–0.750	Cl(23)	Cl	0.009			
C(12)	C Alkene	–0.261	H(24)	H	0.021			
				Compound **4**				
C(1)	C Alkene	–0.068	C(13)	C Carbonyl	0.107	H(25)	H	0.020
C(2)	C Alkene	–0.068	C(14)	C Alkene	–0.120	H(26)	H	0.024
C(3)	C Alkene	–0.100	C(15)	C Alkene	–0.020	H(27)	H	0.023
C(4)	C Alkene	0.264	C(16)	C Alkene	0.221	H(28)	H	0.052
C(5)	C Alkene	–0.042	C(17)	C Alkene	–0.087	H(29)	H	0.017
C(6)	C Alkene	–0.057	C(18)	C Alkene	–0.004	H(30)	H	0.343
O(7)	O Enol	–0.035	C(19)	C Alkene	–0.077	H(31)	H	0.021
C(8)	C Carbonyl	0.542	C(20)	C Alkene	–0.138	H(32)	H	0.021
C(9)	C Alkene	–0.152	O(21)	O Enol	0.754	H(33)	H	0.030
C(10)	C Alkene	0.257	O(22)	O Carbonyl	–0.969	H(34)	H	0.216
O(11)	O Carbonyl	–0.751	Br(23)	Br	0.015			
C(12)	C Alkene	–0.265	H(24)	H	0.021			

Comparison of the DFT analysis with the antibacterial activity

The results of the antibacterial activities are summarized in Table III.

The diffusion method showed that almost all the synthesized compounds, to a greater or lesser extent, inhibit the growth of the Gram-positive aerobic bacteria *B. subtilis* ATCC 6633 and *B. cereus* ATCC 11778.

TABLE III. Antimicrobial activity of tested derivatives expressed as the inhibition zone, *I* (mm)

Compound	Microorganism	
	B. subtilis (ATCC 6633)	*B. cereus* (ATCC 11778)
$C_{18}H_{11}ClO_4$ (**1**)	16.0	19.5
$C_{18}H_{11}ClO_4$ (**2**)	21.0	22.5
$C_{18}H_{11}ClO_4$ (**3**)	21.5	22.75
$C_{18}H_{11}BrO_4$ (**4**)	22.5	23.75
DMSO (control)	–	–
Erythromycin	32.0	23.0
Gentamicin	32.2	27.8

Compound **4**, having the largest chemical potential (η), is the most stable and the least reactive by DFT analysis (Fig. 3). Compound **4** has the best antimicrobial activity. An examination of the mechanism of the antimicrobial action of these compounds remains for the future.

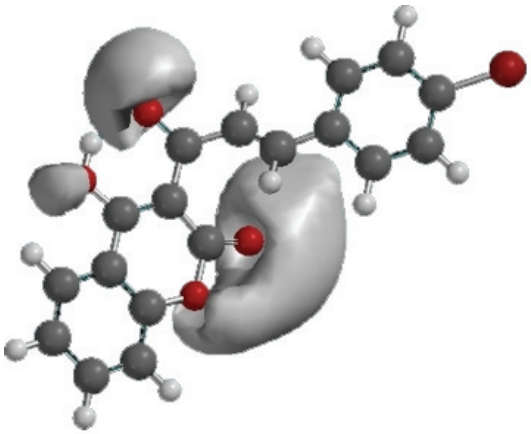

Fig. 3. Potential for compound **4**.

An increase in ε_{HOMO} and a decrease in ε_{LUMO} increase the reactivity of the synthesized compounds and decrease their activity against the tested microorganisms.

The most reactive derivative, compound **1**, showed the lowest activity against both the tested microorganisms, while the most stable compound **4** showed the best activity against both the tested microorganisms.

Bromine is less electronegative than chlorine, and as such increases the stability of the system (DFT confirmed), which contributes to a better activity (the derivative with bromine as a substituent exhibited the best antimicrobial activity).

CONCLUSION

The quantum-chemical and physicochemical calculations indicated that the calculated chemical reactivity descriptors of the molecules correlated well with antibacterial activity.

Reduction of ε_{HOMO} and increase of ε_{LUMO}, that is, a reduction in the reactivity and an increase in the stability of the synthesized compounds increased their activity against the tested microorganisms. The most reactive derivative, compound **1**, showed the lowest activity, indicating that the most chemically stable compound had the best antibacterial activity.

The promising antibacterial activity of the compounds could be helpful in the synthesis of a large number of analogues for extensive antimicrobial studies, which could be used to develop more appropriate drug candidates. It could be concluded that these classes of compounds certainly hold promise towards good active leads in medicinal chemistry.

ИЗВОД

СТУДИЈА ГУСТИНЕ И МИКРОБИОЛОГИЈЕ НЕКИХ КУМАРИНСКИХ ДЕРИВАТА КОЈИ САДРЖЕ ХАЛКОНСКИ ФРАГМЕНТ ПОМОЋУ ТЕОРИЈЕ ФУНКЦИОНАЛА

SELMA ŠPIRTOVIĆ-HALILOVIĆ[1], MIRSADA SALIHOVIĆ[2], HURIJA DŽUDŽEVIĆ-ČANČAR[2], СНЕЖАНА ТРИФУНОВИЋ[3], SUNČICA ROCA[4], DŽENITA SOFTIĆ[5] и DAVORKA ZAVRŠNIK[1]

[1]*Department of Pharmaceutical Chemistry, Faculty of Pharmacy, University of Sarajevo, Zmaja od Bosne 8, 71000 Sarajevo, Bosnia and Herzegovina,* [2]*Department of Organic Chemistry, Faculty of Pharmacy, University of Sarajevo, Zmaja od Bosne 8, 71000 Sarajevo, Bosnia and Herzegovina,* [3]*Хемијски факултет, Универзитет у Београду, Студентски трг 12–16, 11000 Београд,* [4]*NMR Centre, Ruđer Bošković Institute, Bijenička cesta 54, 10000 Zagreb, Croatia и* [5]*Agency for Medicinal Product and Medical Devices of Bosnia and Herzegovina, Titova 9, 71000 Sarajevo, Bosnia and Herzegovina*

Серија кумаринских деривата који садрже халконски фрагмент истраживана је с обзиром на њихова *in vitro* и *in silico* својства. За синтетизована једињења израчунати су DFT методом глобални хемијски реакциони дескриптори (хемијска тврдоћа, укупна енергија, електронски хемијски потенцијал и електрофилност) који су употребљени за предвиђање стаблиности и реактивности. Антибактеријска активност свих једињења одређена је у односу на *Bacillus subtilis* (ATCC 6633) и *Bacillus cereus* (ATCC 11778). Нађена антибактеријска активност се добро слаже са израчунатим дескрипторима хемијске реактивности.

(Примљено 28. јуна 2013)

REFERENCES

1. M. A. Hosny, H. A. Radwan, E. A. El-Sawi, *E-J. Chem.* **9** (2012) 1737
2. D. Završnik, S. Špirtović-Halilović, Dž. Softić, *Period. Biol.* **113** (2011) 93
3. S. Špirtović-Halilović, D. Završnik, *J. Serb. Chem. Soc.***75** (2010) 243

4. E. Bečić, M. Šober, B. Imamović, D. Završnik, S. Špirtović-Halilović, *Pigm. Resin Technol.* **40** (2011) 292
5. S. Špirtović-Halilović, D. Završnik, B. Imamović, E. Bečić, *Int. J. Pharm. Teach. Practices* **4** (2013) 489I
6. A. Beyramabadi, A. Morsali, *Int. J. Phys. Sci*. **6** (2011) 1780
7. C. A. Mebi, *J. Chem. Sci.* **123** (2011) 727
8. M. Monajjemi, M. Sayadian, K. Zare, A. R. Ilkhani, F. Mollaamin, *Int. J. Phys. Sci.* **6** (2011) 4063
9. A. A. H. Kadhum, A. A. Al-Amiery, M. Shikara, A. B. Mohamad, *Int. J. Phys. Sci.* **6** (2011) 6692
10. W. Koch, M. C. Holthausen, *A Chemist's Guide to Density Functional Theory*, 2nd Ed., Wiley–VCH, Weinheim, 2001
11. R. G. Pearson, *Chemical hardness: Application from molecules to solid*, Wiley–VCH, Weinheim, 1997
12. A. Vektariene, G. Vektaris, J. Svoboda, *ARKIVOC* (2009) 311
13. R. G. Parr, R. G. Pearson, *J. Am. Chem. Soc*. **105** (1983) 7512
14. R. G. Parr, L. Szentpaly, S. B. Liu, *J. Am. Chem. Soc*. **121** (1999) 1922
15. J. W. Peters, W. N. B. Lanzilotta, J. Lemon, L. C. Seefeldt, *Science* **282** (1998) 1853
16. P. K. Chattaraj, B. Maiti, *J. Am. Chem. Soc.* **125** (2003) 2705
17. S. Liu, *J. Chem. Sci.* **117** (2005) 477
18. C.J. Zirngibl, R. Hedderich, R.K. Thauer, *FEBS Lett.* **112 (**1990) 261.

Journal of the Serbian Chemical Society
JSCS-info@shd.org.rs • www.shd.org.rs/JSCS
J. Serb. Chem. Soc. 79 (4) 445–456 (2014)
JSCS–4598
UDC *Clonazepam*diazepam:547.441–036.7+54–145.2+532.14:544.032.1
Original scientific paper

Solubility of clonazepam and diazepam in binary and ternary mixtures of polyethylene glycols 400 or 600, propylene glycol and water at 298.2 K. Experimental data and modeling

ZAHRA BASTAMI[1], SHAHLA SOLTANPOUR[1]*, VAHID PANAHI-AZAR[2] and ABOLGHASEM JOUYBAN[3,4]

[1]Faculty of Pharmacy, Zanjan University of Medical Sciences, Zanjan 45139, Iran, [2]Liver and Gastrointestinal Diseases Research Center, Tabriz University of Medical Sciences, Tabriz 51664, Iran, [3]Drug Applied Research Center, Tabriz University of Medical Sciences, Tabriz 51664, Iran and [4]Pharmaceutical Engineering Laboratory, School of Chemical Engineering, College of Engineering, University of Tehran, P. O. Box 11155/4563, Tehran, Iran

(Received 12 December 2012, revised 7 March 2013)

Abstract: Experimental molar solubilities of clonazepam and diazepam in binary and ternary mixtures of polyethylene glycols (PEGs) 400 or 600, propylene glycol (PG) and water (138 data points) along with the density of the saturated solutions at 298.2 K were reported. The Jouyban–Acree Model was used to fit to the measurements for providing a computational method. Employing the solubilities in the mono-solvents, the measured solubilities in mixed solvents were back-calculated and the overall mean percentage deviations (*OMPD*s) of the model were 16.0 and 19.2 % for diazepam and clonazepam, respectively. Addition of the Hansen solubility parameters to the model helped in the training of all the data sets (clonazepam and diazepam) at once and the back-calculated *OMPD* for this analysis was 19.3 %.

Keywords: clonazepam; diazepam; solubility; density; PEGs 400 and 600; propylene glycol; Jouyban–Acree Model.

INTRODUCTION

Knowledge of solubility is important in drug development investigations. Regardless of the administration route, solubility is essential for the therapeutic effectiveness of drugs. Many of the pharmaceutical candidates despite their high biological activity fail in the drug development processes, because they have low bioavailability; hence, these candidates are never used clinically. For expanding the utility of such compounds for various applications, it is necessary to establish a technique for solubilizing them and controlling their bio-distributions. Several

* Corresponding author. E-mail: shahla.soltanpour@gmail.com
doi: 10.2298/JSC121212079B

methods have been established for increasing the drug solubility in pharmaceutical formulations, such as co-solvency, micellar solubilization, inclusion complexes, solid dispersion and change in polymorphs.[1]

Choosing the solubilization method depends on the dosage form of the drug. In solid dosage form, it is possible to enhance the solubility by altering the solid phase, while in parenterals, pH adjustment, co-solvent addition, surfactant addition and complexation are most common and useful methods for enhancing solubility.[1]

Polyethylene glycols (PEGs) are produced from trace hydroxide ions acting as an initiator, and since this functional polymer grows at both ends, it has a higher molecular weight than monomethyl ether, which grows at only one end. Since PEG is usually prepared by an anionic initiation process with a few chain transfer and termination steps, the molecular weight distributions are generally narrow.[2] At molecular weights less than 1000, PEGs are viscous, colorless liquids; higher molecular weight PEGs are waxy, white solids. The molecular weights commonly used in pharmaceutical and biomedical applications range from a few hundred to approximately 20000. Some of the properties of the PEGs are: soluble in water, toluene, dichloromethane and many other organic solvents, insoluble in diethyl ether, hexane and ethylene glycol, complex formation with metal cations, can be used to precipitate proteins and nucleic acids, non-toxic, hospitable to biological materials, cause cell fusion and are weakly immunogenic.[2]

PG (1,2-propanediol), one of the safe co-solvents, is used in oral, intravenous and topical pharmaceutical formulations.[3] It is a safe co-solvent unless in high doses, especially if given over a short period.

Diazepam and clonazepam are commonly used drugs for various purposes such as hypnotic–sedative effects, neuropathic pains and epilepsies. These drugs are very poorly soluble in water and are classified as class II of the BCS (Biopharmaceutical Classification System), which are low soluble and high permeable compounds.[4,5] In order to formulate diazepam and clonazepam in the desired dosage forms, such as parenteral or other liquid forms, it is necessary to enhance their solubility in a pre-determined volume of a vehicle.

PEGs and PG are the most popular freely water soluble pharmaceutical co-solvents that have already been used for solubilizing insoluble drugs, such as lorazepam, loratadine, clofazimine, nimodipine, *etc*., in different formulation forms, such as soft and hard gelatin capsules, oral solutions, elixir solutions, syrups and parenterals (IM and IV forms).[6] Therefore, in this study, PEGs 400, 600 and PG were chosen for investigating their effect on the solubility of the selected drugs, diazepam and clonazepam.

MATERIALS AND METHODS

Materials

Clonazepam (99.8 mass %) and diazepam (99.8 mass %) were purchased from Sobhan Pharmaceutical Company (Rasht, Iran). PEGs 400 and 600 (99.5 mass %), methanol (99.8 mass %), and PG (99.5 mass %), were purchased from Merck (Germany). Purified water was used for the preparation of the solutions.

Preparation of the solvent mixtures

The determined mass fractions of the solvents in the binary and ternary mixtures were prepared with an accuracy of 0.001.

Solubility determinations

The solubilities of clonazepam and diazepam were determined using the saturation shake-flask method of Higuchi and Connors.[7] Briefly, excess amounts of the drugs were added to the solvent mixtures separately. Then the solutions were equilibrated for at least 72 h on a shaker (Behdad, Tehran, Iran) in an equipped incubator, the temperature of which was maintained constant at 298.2±0.2 K. The saturated solutions were centrifuged at a speed of 13000 rpm for 10 min and the supernatant was diluted with methanol. The diluted samples were then assayed at 309 nm for clonazepam and 250 nm for diazepam, using a UV–Vis spectrophotometer (Beckman DU-650, Fullerton, USA). The concentration of each solution was determined from an appropriate absorbance *versus* concentration calibration curve (clonazepam: $A_c = 25458c_c + 0.007$; diazepam: $A_d = 30193c_d + 0.101$, where A_c and A_d are the absorbances and c_c and c_d the concentration for clonazepam and diazepam, respectively). Each experimental data point measurement was repeated three times and the final data are the averages of the repetitions, which were reproducible within ±3.7 %. A 5 mL calibrated pycnometer was used for determining the densities of the saturated solutions.

Computational method

For correlating and predicting the solubility of drugs in mixed solvents, several models were produced. The Jouyban–Acree Model is one of these models which has the most accurate results in correlating and predicting the data.[8] The solubility of clonazepam and diazepam in the mixed solvents were calculated using the Jouyban–Acree Model and its accuracies are discussed by comparing the mean percentage deviations (*MPD*) between the calculated and experimental solubilities.

The Jouyban–Acree Model provides mathematical descriptions for a variety of solute solubility in dependence on both temperature and solvent composition:[8]

$$\log c_{m,T}^{\mathrm{Sat}} = w_1 \log c_{1,T}^{\mathrm{Sat}} + w_2 \log c_{2,T}^{\mathrm{Sat}} + \left[\frac{w_1 w_2}{T} \sum_{i=0}^{2} J_i (w_1 - w_2)^i \right] \quad (1)$$

where $c_{m,T}^{\mathrm{Sat}}$ is the molar solubility of the solute in the solvent mixtures at temperature T, w_1 and w_2 are the mass fractions of the solvents 1 and 2 in the absence of the solute, respectively. $c_{1,T}^{\mathrm{Sat}}$ and $c_{2,T}^{\mathrm{Sat}}$ are the molar solubility of the solute in the neat solvents 1 and 2, respectively, and the J_i terms are the constants of the model computed by regression analysis. The model for representing the solubility of drugs in ternary solvent mixtures based on sub-binary interaction terms is:

$$\log c_{m,T}^{\mathrm{Sat}} = w_1 \log c_{1,T}^{\mathrm{Sat}} + w_2 \log c_{2,T}^{\mathrm{Sat}} + w_3 \log c_{3,T}^{\mathrm{Sat}} + \left[\frac{w_1 w_2}{T} \sum_{i=0}^{2} J_i (w_1 - w_2)^i \right] + \left[\frac{w_1 w_3}{T} \sum_{i=0}^{2} J_i^{'} (w_1 - w_3)^i \right] + \left[\frac{w_2 w_3}{T} \sum_{i=0}^{2} J_i^{''} (w_2 - w_3)^i \right] \quad (2)$$

where $c_{3,T}^{\mathrm{Sat}}$ is the molar solubility of the solute in neat solvent 3 (water in this work) at temperature T, and w_3 is the mass fraction of the solvent 3 in the absence of the solute. The $J_i^{'}$ and $J_i^{''}$ terms are computed using the same procedure as for the J_i terms. The numbers of the solvents are defined as $c_{1,T}^{\mathrm{Sat}} \rangle c_{2,T}^{\mathrm{Sat}} \rangle c_{3,T}^{\mathrm{Sat}}$. This model is a predictive version and is able to predict the solubility of solutes in ternary solvents based on sub-binary data. To provide more accurate data, it is possible to include ternary interaction terms, such as:

$$\log c_{m,T}^{\mathrm{Sat}} = w_1 \log c_{1,T}^{\mathrm{Sat}} + w_2 \log c_{2,T}^{\mathrm{Sat}} + w_3 \log c_{3,T}^{\mathrm{Sat}} + \left[\frac{w_1 w_2}{T} \sum_{i=0}^{2} J_i (w_1 - w_2)^i \right] + \left[\frac{w_1 w_3}{T} \sum_{i=0}^{2} J_i^{'} (w_1 - w_3)^i \right] + \left[\frac{w_2 w_3}{T} \sum_{i=0}^{2} J_i^{''} (w_2 - w_3)^i \right] + \left[\frac{w_1 w_2 w_3}{T} \sum_{i=0}^{2} J_i^{'''} (w_1 - w_2 - w_3)^i \right] \quad (3)$$

The $J_i^{'''}$ terms are computed by regressing:

$$\left\{ \log c_{m,T}^{\mathrm{Sat}} - w_1 \log c_{1,T}^{\mathrm{Sat}} - w_2 \log c_{2,T}^{\mathrm{Sat}} - w_3 \log c_{3,T}^{\mathrm{Sat}} - \left[\frac{w_1 w_2}{T} \sum_{i=0}^{2} J_i (w_1 - w_2)^i \right] - \left[\frac{w_1 w_3}{T} \sum_{i=0}^{2} J_i^{'} (w_1 - w_3)^i \right] - \left[\frac{w_2 w_3}{T} \sum_{i=0}^{2} J_i^{''} (w_2 - w_3)^i \right] \right\}$$

against:

$$\frac{w_1 w_2 w_3}{T}, \quad \frac{w_1 w_2 w_3 (w_1 - w_2 - w_3)}{T} \text{ and } \frac{w_1 w_2 w_3 (w_1 - w_2 - w_3)^2}{T}.$$

In the Jouyban–Acree Model when there is one solute in binary solvent mixtures, the $w_1 \log c_{1,T}^{\mathrm{Sat}}$ and $w_2 \log c_{2,T}^{\mathrm{Sat}}$ terms represent the ideal mixing behavior of saturated solutions composed of solvent 1 and 2 without any additional interactions, and for describing the interactions between the solute and the solvents in the mixtures, the J_i terms are used. Therefore, the model can cover the probable interactions that occur in a mixture.

However, for covering the physicochemical properties of the solute or solvents, this model can be combined with the parameters that are used for determining the properties of the substances. By combining the Jouyban–Acree Model and the Hansen solubility parameters, Eq. (1) could be obtained as:

$$\log c_{m,T}^{\mathrm{Sat}} = w_1 \log c_{1,T}^{\mathrm{Sat}} + w_2 \log c_{2,T}^{\mathrm{Sat}} +$$
$$+\frac{w_1 w_2}{T}\left[W_0 + W_1\delta_{\mathrm{ds}}(\delta_{\mathrm{d1}} - \delta_{\mathrm{d2}})^2 + W_2\delta_{\mathrm{ps}}(\delta_{\mathrm{p1}} - \delta_{\mathrm{p2}})^2 + W_3\delta_{\mathrm{hs}}(\delta_{\mathrm{h1}} - \delta_{\mathrm{h2}})^2\right] +$$
$$+\frac{w_1 w_2 (w_1 - w_2)}{T}\left[W_0' + W_1'\delta_{\mathrm{ds}}(\delta_{\mathrm{d1}} - \delta_{\mathrm{d2}})^2 + W_2'\delta_{\mathrm{ps}}(\delta_{\mathrm{p1}} - \delta_{\mathrm{p2}})^2 + W_3'\delta_{\mathrm{hs}}(\delta_{\mathrm{h1}} - \delta_{\mathrm{h2}})^2\right] + \quad (4)$$
$$+\frac{w_1 w_2 (w_1 - w_2)^2}{T}\left[W_0'' + W_1''\delta_{\mathrm{ds}}(\delta_{\mathrm{d1}} - \delta_{\mathrm{d2}})^2 + W_2''\delta_{\mathrm{ps}}(\delta_{\mathrm{p1}} - \delta_{\mathrm{p2}})^2 + W_3''\delta_{\mathrm{hs}}(\delta_{\mathrm{h1}} - \delta_{\mathrm{h2}})^2\right]$$

where δ_{ds}, δ_{ps} and δ_{hs} are the Hansen solubility parameters for the solute, δ_{d1}, δ_{p1} and δ_{h1}, and δ_{d2}, δ_{p2} and δ_{h2} are the Hansen parameters for solvent 1 and 2, respectively.

For ternary solvent mixtures, Eq. (4) could be modified as:

$$\log C_{m,T}^{\mathrm{Sat}} = w_1 \log C_{1,T}^{\mathrm{Sat}} + w_2 \log C_{2,T}^{\mathrm{Sat}} + w_3 \log C_{3,T}^{\mathrm{Sat}} +$$
$$+\frac{w_1 w_2}{T}\left[W_0 + W_1\delta_{\mathrm{ds}}(\delta_{\mathrm{d1}} - \delta_{\mathrm{d2}})^2 + W_2\delta_{\mathrm{ps}}(\delta_{\mathrm{p1}} - \delta_{\mathrm{p2}})^2 + W_3\delta_{\mathrm{hs}}(\delta_{\mathrm{h1}} - \delta_{\mathrm{h2}})^2\right] +$$
$$+\frac{w_1 w_2 (w_1 - w_2)}{T}\left[W_0' + W_1'\delta_{\mathrm{ds}}(\delta_{\mathrm{d1}} - \delta_{\mathrm{d2}})^2 + W_2'\delta_{\mathrm{ps}}(\delta_{\mathrm{p1}} - \delta_{\mathrm{p2}})^2 + W_3'\delta_{\mathrm{hs}}(\delta_{\mathrm{h1}} - \delta_{\mathrm{h2}})^2\right] +$$
$$+\frac{w_1 w_2 (w_1 - w_2)^2}{T}\left[W_0'' + W_1''\delta_{\mathrm{ds}}(\delta_{\mathrm{d1}} - \delta_{\mathrm{d2}})^2 + W_2''\delta_{\mathrm{ps}}(\delta_{\mathrm{p1}} - \delta_{\mathrm{p2}})^2 + W_3''\delta_{\mathrm{hs}}(\delta_{\mathrm{h1}} - \delta_{\mathrm{h2}})^2\right] + \quad (5)$$
$$+\frac{w_1 w_2 w_3 (w_1 - w_2 - w_3)^2}{T}[W_0''' + W_1'''\delta_{\mathrm{ds}}(\delta_{\mathrm{d1}} - \delta_{\mathrm{d2}} - \delta_{\mathrm{d3}})^2 + W_2'''\delta_{\mathrm{ps}}(\delta_{\mathrm{p1}} - \delta_{\mathrm{p2}} - \delta_{\mathrm{p3}})^2 +$$
$$+W_3'''\delta_{\mathrm{hs}}(\delta_{\mathrm{h1}} - \delta_{\mathrm{h2}} - \delta_{\mathrm{h3}})^2]$$

where δ_{d3}, δ_{p3} and δ_{h3} are the Hansen parameters for solvent 3.

Mean percentage deviation (*MPD*) value was used to check the accuracy of the fitted and predicted values and was calculated using:

$$MPD = \frac{100}{N}\sum\left[\frac{|\mathrm{Calculated} - \mathrm{Experimental}|}{\mathrm{Experimental}}\right] \quad (6)$$

where N is the number of data points in each set.

Data analysis

In numerical analysis I, the model constants of Eq. (1) for clonazepam and diazepam were calculated by fitting the experimental solubility data of each drug in binary solvents to Eq. (1), and then the back-calculated solubilities were used to calculate the *MPD* values. In the second part of numerical analysis I, for predicting the solubility of the drugs in ternary mixtures, the determined model constants in Eq. (1) were included in Eq. (2). The ternary interaction terms of Eq. (3) were calculated using a linear regression analysis, for providing better computations.

In numerical analysis II, the combined form of the Jouyban–Acree Model and the Hansen solubility parameters was used for training all the data sets at once. In the second part of analysis II, the Jouyban–Acree Model was used for training all data and the produced *OMPD*s from these two parts were compared.

For converting the molar solubilities into the mole fraction solubilities, the densities of the saturated solutions were required. By introducing a way to predict the densities of the

saturated solutions, time and cost of the experimental efforts can be saved. The applicability of the Jouyban–Acree Model for prediction of the density of liquid mixtures at various temperatures was shown in previous papers.[9,10]

In numerical analysis III, for showing the applicability of the model in predicting the density of the saturated solutions, first the densities of the solute-free binary and ternary solutions ($\rho_{m,T}$) were fitted to Eq. (7):

$$\log \rho_{m,T} = w_1 \log \rho_{1,T} + w_2 \log \rho_{2,T} + w_3 \log \rho_{3,T} + \left[\frac{w_1 w_2}{T}\sum_{i=0}^{2} J_i (w_1 - w_2)^i\right] + \left[\frac{w_1 w_3}{T}\sum_{i=0}^{2} J_i^{'} (w_1 - w_3)^i\right] + \left[\frac{w_2 w_3}{T}\sum_{i=0}^{2} J_i^{''} (w_2 - w_3)^i\right] \quad (7)$$

where $\rho_{m,T}$ is the density of the solute-free solvent mixtures, ρ_{1T}, ρ_{2T} and ρ_{3T} are the densities of the solute free mono-solvents 1 to 3 at temperature T, respectively.[11]

Then, by using these calculated sub-binary constants, the ternary constants of Eq. (8) were obtained:

$$\log \rho_{m,T} = w_1 \log \rho_{1,T} + w_2 \log \rho_{2,T} + w_3 \log \rho_{3,T} + \left[\frac{w_1 w_2}{T}\sum_{i=0}^{2} J_i (w_1 - w_2)^i\right] + \left[\frac{w_1 w_3}{T}\sum_{i=0}^{2} J_i^{'} (w_1 - w_3)^i\right] + \left[\frac{w_2 w_3}{T}\sum_{i=0}^{2} J_i^{''} (w_2 - w_3)^i\right] + \left[\frac{w_1 w_2 w_3}{T}\sum_{i=0}^{2} J_i^{'''} (w_1 - w_2 - w_3)^i\right] \quad (8)$$

Using the calculated sub-binary and ternary model constants and the densities of the saturated mono-solvents, trained versions of the Jouyban–Acree Model were produced, and the densities of the saturated solutions were predicted by these trained versions, in which the produced prediction errors were within an acceptable range.[12] Then, the experimental and calculated densities can be used for converting the molar solubilities to mole fraction data.

RESULTS AND DISCUSSION

The experimental molar solubilities of clonazepam and diazepam in the binary and ternary solvent mixtures along with the measured density of the saturated solution and solute-free solvent mixtures at 298.2 K are listed in Table I. The minimum solubilities of clonazepam (0.00010 M) and diazepam (0.00007 M) were observed for aqueous solutions. The maximum solubility of clonazepam (0.11110 M) among investigated solvent systems was observed for neat PEG 600 and that for diazepam (0.19510 M) was observed for PG–PEG 600 (0.4 + 0.6) solvent mixtures. The very low aqueous solubilities of clonazepam and diazepam could be explained concerning their lower polarity in comparison with the polarity of water. The Hildebrand solubility parameter (δ), can be used as a polarity index. It was shown that the maximum solubility of a solute (δ_2) is observed in a solvent with the same solubility parameter δ_1 or $(\delta_2 - \delta_1)^2 = 0$.[13,14] By adding

organic solvents to aqueous solutions, the solubility of the less polar solutes increases, because the organic solvents break the strong interactions of water molecules and reduce its polarity. This is also the case for non-aqueous mixtures, since a mixture possesses various numerical values of the solubility parameter concerning the mixture composition.

TABLE I. Experimental molar solubilities ($c_{m,T}^{Sat}$) of clonazepam and diazepam in binary and ternary mixtures of PEGs 400 or 600, PG and water (mass fraction, w) at 298.2 K and atmospheric pressure along with the density of the saturated and solute-free solutions ($\rho_{m,T}^{Sat}$)

w_1 (PEG 600)	w_2 (PEG 400)	w_3 (PG)	w_3 (H_2O) w_4	Density of the solute-free solutions, g·cm^{-3}	$c_{m,T}^{Sat}$ mol·L^{-1}	Density of the saturated solutions, g·cm^{-3}	$c_{m,T}^{Sat}$ mol·L^{-1}	Density of the saturated solutions, g·cm^{-3}
					Diazepam		Clonazepam	
–	0.0	–	1.0	0.997	0.00007	1.003	0.00010	1.016
–	0.1	–	0.9	–	0.00011	1.025	0.00016	1.031
–	0.2	–	0.8	1.017	0.00042	1.040	0.00017	1.040
–	0.3	–	0.7	–	0.00061	1.057	0.00024	1.053
–	0.4	–	0.6	1.035	0.00120	1.073	0.00030	1.070
–	0.5	–	0.5	–	0.00240	1.088	0.00069	1.085
–	0.6	–	0.4	1.067	0.00541	1.100	0.00180	1.092
–	0.7	–	0.3	–	0.01671	1.120	0.00521	1.100
–	0.8	–	0.2	1.098	0.03192	1.130	0.02240	1.190
–	0.9	–	0.1	1.114	0.04631	1.140	0.03941	1.280
–	1.0	–	0.0	1.124	0.05310	1.145	0.06561	1.141
0.0	–	1.0	–	1.027	0.02700	1.241	0.00880	1.020
0.1	–	0.9	–	1.037	0.04621	1.252	0.01514	1.054
0.2	–	0.8	–	1.047	0.06111	1.261	0.01642	1.062
0.3	–	0.7	–	1.057	0.09423	1.270	0.02302	1.071
0.4	–	0.6	–	1.067	0.11881	1.281	0.02883	1.083
0.5	–	0.5	–	1.076	0.16532	1.293	0.04502	1.093
0.6	–	0.4	–	1.086	0.19510	1.301	0.05601	1.106
0.7	–	0.3	–	1.096	0.15532	1.313	0.06394	1.116
0.8	–	0.2	–	1.106	0.13551	1.328	0.06945	1.125
0.9	–	0.1	–	1.116	0.10572	1.349	0.09110	1.139
1.0	–	0.0	–	1.129	0.09630	1.120	0.11110	1.148
–	0.0	1.0	–	1.027	0.02700	1.232	0.00880	1.020
–	0.1	0.9	–	–	0.03474	1.243	0.00781	1.050
–	0.2	0.8	–	1.057	0.04163	1.257	0.01231	1.058
–	0.3	0.7	–	1.065	0.05173	1.268	0.01934	1.069
–	0.4	0.6	–	1.073	0.07434	1.277	0.02354	1.081
–	0.5	0.5	–	–	0.09944	1.290	0.02494	1.091
–	0.6	0.4	–	1.090	0.11272	1.299	0.02805	1.102
–	0.7	0.3	–	1.098	0.07290	1.308	0.03321	1.112
–	0.8	0.2	–	1.106	0.06971	1.322	0.03823	1.119
–	0.9	0.1	–	–	0.06352	1.335	0.04172	1.135
–	1.0	0.0	–	1.124	0.05310	1.120	0.06561	1.141

TABLE I. Continued

w_1 (PEG 600)	w_2 (PEG 400)	w_3 (PG)	w_3 (H_2O) w_4	Density of the solute-free solutions, g·cm^{-3}	$c_{m,T}^{Sat}$ mol·L^{-1}	Density of the saturated solutions, g·cm^{-3}	$c_{m,T}^{Sat}$ mol·L^{-1}	Density of the saturated solutions, g·cm^{-3}
					Diazepam		Clonazepam	
–	0.8	0.1	0.1	1.112	0.05850	1.315	0.03870	1.317
–	0.7	0.2	0.1	1.096	0.03082	1.292	0.02121	1.290
–	0.5	0.4	0.1	1.078	0.05022	1.270	0.01281	1.270
–	0.3	0.6	0.1	1.061	0.03393	1.248	0.00852	1.248
–	0.1	0.8	0.1	1.086	0.01371	1.304	0.01490	1.308
–	0.6	0.2	0.2	1.078	0.02522	1.284	0.00991	1.284
–	0.3	0.5	0.2	1.067	0.02050	1.261	0.00631	1.259
–	0.1	0.7	0.2	1.090	0.01651	1.304	0.00402	1.241
–	0.5	0.2	0.3	1.076	0.00902	1.288	0.00413	1.281
–	0.3	0.4	0.3	1.057	0.00832	1.261	0.00323	1.259
–	0.1	0.6	0.3	1.086	0.00733	1.239	0.00212	1.239
–	0.4	0.2	0.4	1.073	0.00440	1.270	0.00150	1.272
–	0.2	0.4	0.4	1.071	0.00401	1.248	0.00111	1.248
–	0.4	0.1	0.5	1.067	0.00171	1.263	0.00972	1.263
–	0.2	0.3	0.5	1.057	0.00142	1.239	0.00123	1.243
–	0.3	0.1	0.6	1.051	0.00084	1.223	0.00040	1.232
–	0.1	0.3	0.6	1.037	0.00083	1.243	0.00022	1.250
–	0.1	0.2	0.7	1.023	0.00051	1.214	0.00021	1.214
0.8	–	0.1	0.1	1.121	0.07663	1.319	0.04492	1.335
0.7	–	0.2	0.1	1.112	0.05240	1.297	0.03121	1.308
0.5	–	0.4	0.1	1.092	0.06812	1.275	0.01760	1.281
0.3	–	0.6	0.1	1.075	0.05454	1.254	0.00991	1.252
0.1	–	0.8	0.1	1.057	0.02080	1.308	0.01801	1.317
0.6	–	0.2	0.2	1.110	0.03891	1.288	0.01092	1.292
0.3	–	0.5	0.2	1.079	0.03352	1.264	0.00760	1.268
0.1	–	0.7	0.2	1.059	0.01893	1.308	0.00443	1.245
0.5	–	0.2	0.3	1.102	0.01094	1.293	0.00472	1.295
0.3	–	0.4	0.3	1.079	0.00992	1.266	0.00353	1.272
0.1	–	0.6	0.3	1.061	0.00860	1.243	0.00233	1.245
0.4	–	0.2	0.4	1.086	0.00590	1.273	0.00162	1.279
0.2	–	0.4	0.4	1.063	0.00541	1.252	0.00131	1.254
0.4	–	0.1	0.5	1.082	0.00232	1.266	0.01051	1.270
0.2	–	0.3	0.5	1.061	0.00212	1.243	0.00130	1.248
0.3	–	0.1	0.6	1.065	0.00081	1.228	0.00040	1.237
0.1	–	0.3	0.6	1.046	0.00123	1.245	0.00020	1.254
0.1	–	0.2	0.7	1.036	0.00064	1.219	0.00021	1.219

The model constants and *MPD* values that were obtained by fitting the solubility data of clonazepam and diazepam to Eqs. (1) and (3) in numerical analysis I are given in Table II. Including the experimental solubility in mono-solvents, *i.e.*, $c_{1,T}^{Sat}$, $c_{2,T}^{Sat}$ and $c_{3,T}^{Sat}$, and the obtained constants, the solubility of clona-

zepam and diazepam in all composition ranges of the solvents at various temperatures could be predicted. In the binary mixtures of clonazepam, the lowest and highest *MPD* values of 2.3 and 7.2 % were found for PEG 600–water and PEG 400–water mixtures, respectively. The overall *MPD* (*OMPD*) values were 5.7 and 32.7 %, respectively, for binary and ternary mixtures. For diazepam, the lowest and highest *MPD* values of 5.7 and 11 % were observed for PEG 600–water and PG–PEG 400 mixtures, respectively. The *OMPD* values were 7.5 and 24.6 %, respectively, for binary and ternary mixtures. All the *MPD* values together with the set detail are listed in Table II.

TABLE II. The constants of the Jouyban–Acree Model (Eqs. (1) and (3)), and the mean percentage deviations (*MPD*s) of the back-calculation for the solubility of clonazepam and diazepam in binary and ternary solvent mixtures of PEGs 400 or 600, PG and water

Drug	Solvent system	*N*	J_0	J_1	J_2	*MPD*
Diazepam	PEG 400–water	11	133.634	420.255	683.600	6.3
Diazepam	PG–PEG 400	11	396.395	–[a]	–	11.0
Diazepam[b]	PG–water	11	–833.981	–	–	6.8
Diazepam	PEG 600–water	11	–195.069	192.591	283.501	5.7
Diazepam	PG–PEG 600	11	555.018	–	–	7.5
					Overall *MPD*	7.5
Diazepam	PEG 400–PG–water	18	1571.077	–	–	28.9
Diazepam	PEG 600–PG–water	18	1056.387	–5494.395	–	20.3
					Overall *MPD*	24.6
					Overall *MPD*	16.0
Clonazepam	PEG 400–water	11	–706.968	492.773	1188.381	7.2
Clonazepam	PG–PEG 400	11	73.589	–107.005	–515.002	6.5
Clonazepam[b]	PG–water	11	–105.693	543.399	–	6.3
Clonazepam	PEG 600–water	11	–570.410	265.227	1115.012	2.3
Clonazepam	PG–PEG 600	11	145.419	–	–	6.3
					Overall *MPD*	5.7
Clonazepam	PEG 400–PG–water	18	2313.360	–877.800	–7013.672	33.0
Clonazepam	PEG 600–PG–water	18	836.724	–2470.504	–8228.089	32.5
					Overall *MPD*	32.7
					Overall *MPD*	19.2

[a]Not significant; [a]data were taken from a previous paper[11]

In numerical analysis II, Eqs. (4) and (5), which are the combined form of the Jouyban–Acree Model with Hansen solubility parameters, were used for fitting the experimental solubilities. The back-calculated *OMPD* for all data of clonazepam and diazepam was 19.3 %. In the second part of this analysis, Eq. (3) was used for training all the data sets and the back-calculated *OMPD* was 41.6 %.

In the numerical analysis III, Eqs. (7) and (8) were used to produce trained versions of the Jouyban–Acree Model employing the densities of the solute-free solutions. Theses trained versions were used for predicting the density of the

saturated solutions. The model constants of the trained versions of the Jouyban–Acree Model (after excluding the constants with $p > 0.10$) for all studied data sets are listed in Table III. Using the densities of the saturated solutions in mono-solvents and the obtained model constants enables the prediction of the densities of the saturated solvent mixtures.[8,9] The experimental and calculated densities were used for converting the molar solubility to the mole fraction solubility, and the *OMPD* value for the difference in the mole fraction solubilities obtained from experimental and predicted densities was 5.0 %.

TABLE III. The model constants and the *MPD* values using the density of the solute-free binary and ternary solvent mixtures

Solvent system	J_0	J_1	J_2	*MPD*
PEG 400–water	–2.737	–[a]	–	0.3
PG–PEG 400	3.954	–58.527	–	2.4
PG–water	–0.46	–3.252	2.831	0.1
PEG 600–water	12.525	3.421	–	0.1
PG–PEG 600	–0.228	–1.398	–1.496	0.1
			OMPD	0.6
PEG 400–PG–water	140.644	348.362	444.344	1.2
PEG 600–PG–water	67.536	–67.97	–	0.9
			OMPD	1.0

[a]Not significant

CONCLUSIONS

The experimental solubilities of clonazepam and diazepam in binary and ternary mixed solvents of PEGs 400, 600, PG and water at 298.2 K are reported. These values extend the solubility database of drugs in solvent mixtures.[15]

As mentioned before, diazepam and clonazepam are poorly water-soluble drugs with widespread applications in clinical use. Thus, finding suitable solvents or solvent mixtures with high efficiency for solubilizing diazepam and clonazepam is necessary, because solubility is one of the important limiting factors in the development of liquid dosage forms of the drugs and improvement of their bioavailability. Measuring the solubility of drugs in the laboratory is a costly and time-consuming process. However, by performing systematic solubility measurements and proposing trained models, the solubility of the desired drugs in binary or ternary mixtures of the investigated solvents can be predicted without repetition of the measurements. According to the predicted solubilities, the best choice of the solvent mixtures for the determined concentration of the drug can be selected. The solubility data reported in this paper could be employed in preparation of oral liquid drug formulations and in preparation of other formulations, such as soft-gels, which is dependent on the percent of water in the solvent mixtures. The low *MPD* values for the fitting and prediction of the solubility data in modeling part showed that the Jouyban–Acree Model fits well the measured

solubility data of clonazepam and diazepam in the investigated solvent mixtures with the determined solvents mass fractions. Generally, because of the low *OMPD*s observed in these predictions, the Jouyban−Acree Model is one of the more accurate co-solvency models that can predict the solubility of the drugs in the presence of one or two co-solvents.

Acknowledgment. Financial support from Zanjan University of Medical Sciences, Iran (No. A-11-387-1), is acknowledged.

ИЗВОД

РАСТВОРЉИВОСТ КЛОНАЗЕПАМА И ДИАЗЕПАМА У БИНАРНИМ И ТЕРНЕРНИМ СМЕШАМА ПОЛИЕТИЛЕН-ГЛИКОЛА 400 ИЛИ 600 И ВОДЕ НА ТЕМПЕРАТУРИ 298,2 K. ЕКСПЕРИМЕНТАЛНИ ПОДАЦИ И МОДЕЛОВАЊЕ

ZAHRA BASTAMI[1], SHAHLA SOLTANPOUR[1], VAHID PANAHI-AZAR[2] и ABOLGHASEM JOUYBAN[3,4]

[1]Faculty of Pharmacy, Zanjan University of Medical Sciences, Zanjan 45139, Iran, [2]Liver and Gastrointestinal Diseases Research Center, Tabriz University of Medical Sciences, Tabriz 51664, Iran, [3]Drug Applied Research Center, Tabriz University of Medical Sciences, Tabriz 51664, Iran и [4]Pharmaceutical Engineering Laboratory, School of Chemical Engineering, College of Engineering, University of Tehran, P.O. Box 11155/4563, Tehran, Iran

Дати су резултати експерименталне моларне растворљивости клоназепама и диазепама у бинарним и тернерним смешама полиетилен-гликола (PEG) 400 или 600, пропилен-гликола (PG) и воде (138 података), као и густине засићених раствора на температури 298,2 K. За добијање компјутерског програма који би одговарао мерењима примењен је *Jouyban–Acree* модел. Коришћењем растворљивости у појединачном растварачима, израчунате су растворљивости у смешама са *OMPD* вредностима од 16,0 и 19,2 %, за диазепам и клоназепам, редом. Уношење Хансенових параметара растворљивости у модел помогло је третирању свих сетова података (за клоназепам и диазепам) истовремено и изведена *OMPD* вредност ове анализе била је 19,3 %.

(Примљено 12. децембра 2012, ревидирано 7. марта 2013)

REFERENCES

1. S. Kolhe, M. Chipade, P. D. Chaudhari, *Int. J. Pharm. Chem. Sci.* **1** (2012) 130
2. http://www.fao.org/ag/agn/jecfa-additives/specs/Monograph1 (accessed: 10/2012)
3. T. Zar, C. Graeber, M. A. Perazellat, *Seminars in Dialysis* **20** (2007) 217
4. G. L. Amidon, H. Lennernas, V. P. Shah, J. R. Crison, *Pharm. Res.* **12** (1995) 413
5. R. Lobenberg, L. G. Amidon, *Eur. J. Pharm. Biopharm.* **50** (2000) 3
6. R. G. Strickley, *Pharm. Res.* **21** (2004) 201
7. T. Higuchi, K. A. Connors, *Adv. Anal. Chem. Instrum.* **4** (1965) 117
8. A. Jouyban, *J. Pharm. Pharm. Sci.* **11** (2008) 32
9. Sh. Soltanpour, A. Jouyban, *J. Solution Chem.* **40** (2011) 2032
10. Sh. Soltanpour, A. Jouyban, *Chem. Pharm. Bull.* **58** (2010) 1132
11. A. Jouyban, A. Fathi-Azarbayjani, M. Khoubnasabjafari, W. E. Acree Jr., *Indian J. Chem.* **44** (2005) 1553
12. Sh. Soltanpour, A. Jouyban, *Chem. Pharm. Bull.* **58** (2010) 219
13. J. Amiran, V. Nicolosi, S. D. Bergin, O. Khan, P. E. Lyons, J. N. Coleman, *J. Phys. Chem., C* **112** (2008) 3519

14. G. D. Mills, in *Paint and Coating Testing Manual: the Gardner–Sward Handbook*, 14th ed., J. V. Koleske, Ed., ASTM, Philadelphia, PA, 1995, Ch. 35
15. A. Jouyban, *Handbook of solubility data for pharmaceuticals*. CRC Press Inc., Boca Raton, FL, 2009.

Journal of the Serbian Chemical Society
JSCS-info@shd.org.rs • www.shd.org.rs/JSCS
J. Serb. Chem. Soc. 78 (4) 457–468 (2013)
JSCS–4599
UDC 532.135.004.12:547.263–36+541.64+546.33'226:541.12.032
Original scientific paper

Rheological properties of hydroxypropylmethyl cellulose/sodium dodecylsulfate mixtures

JAROSLAV M. KATONA*#, SANDRA Đ. NJARADI, VERICA J. SOVILJ, LIDIJA B. PETROVIĆ#, BRANKICA B. MARČETA and JADRANKA L. MILANOVIĆ#

University of Novi Sad, Faculty of Technology Novi Sad, Bul. Cara Lazara 1, 21000 Novi Sad, Serbia

(Received 7 August, revised 30 October 2013)

Abstract: The rheological properties of mixtures of hydroxypropylmethyl cellulose (HPMC), a nonionic associative cellulose ether, and sodium dodecylsulfate (SDS), an anionic surfactant, were investigated by viscosity measurements performed at different shear rates (0.1–6000 s^{-1}). HPMC/SDS mixtures containing different concentrations of SDS (c_{SDS}, 0.00–3.50 mass %) and HPMC concentrations, which corresponded to the overlap parameter c/c^* of 3, 6 and 12, were prepared. All HPMC/SDS mixtures were found to be shear-thinning when examined in the low-end to mid-range of the applied shear rates. The degree of shear-thinning, *n*, and the viscosity of the mixtures were influenced by composition of the HPMC/SDS mixtures and HPMC–SDS complex formation. The changes in *n* ranged from values typical for highly shear-thinning to almost perfectly Newtonian liquids, and were more pronounced as c/c^* was increased from 3 to 6 and 12. A change in the flow profile and a buildup of the first normal stress difference (N_1) was observed in HPMC/SDS mixtures with c/c^* = 6 and 12 and c_{SDS} 0.55–1.00 and 0.55–2.50 mass %, respectively, when a critical shear rate, $\dot{\gamma}_{crit}$, was exceeded, suggesting that a shear-induced structure formation in the mixtures occurred.

Keywords: polymer–surfactant interaction; HPMC–SDS interaction; shear-thinning; shear-thickening; shear-induced structure formation.

INTRODUCTION

Polymers and surfactants are common components of many products of the food, pharmaceutical and chemical industry. An interaction between a polymer and a surfactant often occurs when they are jointly found in a solution. Polymer––surfactant interaction influences the physicochemical properties of solutions and is often employed to achieve different effects, such as emulsification, colloidal

* Corresponding author. E-mail: jkatona@uns.ac.rs
# Serbian Chemical Society member.
doi: 10.2298/JSC130807132K

stability, viscosity enhancement, gel formation, solubilization, phase separation *etc*. Details of polymer–surfactant interaction depend on the molecular characteristics and concentration of both polymer and surfactant.[1–5]

Hydroxypropylmethyl cellulose (HPMC) is a nonionic, water-soluble cellulose ether. It is obtained by partial substitution of hydroxyl groups of cellulose with hydrophobic hydroxypropyl and methyl groups. The substituents make HPMC a typical amphiphilic polymer with properties such as ability to adsorb at air–water and oil–water interfaces, emulsification, self-assembly and association with other amphiphilic molecules.[6–9] In this regard, addition of low molar mass surfactants, especially anionics such as sodium dodecylsulfate (SDS), to HPMC solution may result in a polymer–surfactant interaction. HPMC–SDS interaction takes place when the SDS concentration (c_{SDS}) exceeds the critical association concentration (*CAC*), which is the minimal surfactant concentration required for the onset of association of a surfactant and a polymer.[1,10] HPMC–SDS interaction occurs *via* hydrophobic moieties of the components, where SDS binds to the HPMC chains and thereby brings about HPMC–SDS complex formation.[11–14] The binding and complex formation supports physical cross-links between the entangled HPMC chains, which result in an increase in the viscosity of HPMC/ /SDS mixtures.[11,15] Simultaneously, the formation of negatively charged SDS micelles along the HPMC chains progressively converts the non-ionic polymer into a polyanion. As the c_{SDS} is further increased, electrostatic repulsive forces between neighboring HPMC chains start to dominate, the network structure is gradually lost and consequently, the viscosity of the HPMC/SDS mixture falls. Individual HPMC chains become fully solubilized with SDS when the c_{SDS} reaches the polymer saturation point, *PSP*. Increasing the c_{SDS} above the *PSP* causes only a slight decrease in viscosity of HPMC/SDS mixtures because of the formation of free SDS micelles in the solution, which brings about slight conformational changes of the SDS-solubilized HPMC chains.[14]

Rheological measurements are often used to study interaction of an associative polymer and a surfactant in a solution in which polymer chains are entangled, *i.e*., when the concentration of the polymer is above the overlap concentration (c^*).[12,16,17] The degree of entanglement is often expressed as the overlap parameter c/c^*, which is the ratio of the actual polymer concentration in a solution and its overlap concentration.[18] In rheological studies of polymer–surfactant interaction, a zero-shear viscosity, *i.e*., the viscosity of a polymer/ /surfactant mixture at zero shear rate, is commonly used to quantify the changes in mixtures. The influence of the shear rate on the viscous properties of HPMC/ /SDS mixtures has rarely been reported.[15,19] The goal of the present work was to investigate the rheological properties of HPMC/SDS mixtures containing different concentrations of SDS (c_{SDS}, 0.00–3.50 mass %) and different degrees of

entanglements of the HPMC chains (c/c^* of 3, 6 and 12) by measuring the viscosity of the mixtures performed at different shear rates (0–6000 s^{-1}).

EXPERIMENTAL

Materials

Hydroxypropylmethyl cellulose, HPMC (trade name Methocel K4M CR, methoxyl content 22.7 mass %, hydroxypropyl content 8.9 mass %) was obtained from Colorcon Ltd., England. The viscosity average molar mass ($\bar{M}_V$) determined at 20 °C was 91500 g mol^{-1} and the overlap concentration was c^* = 0.126 %, *w*/*V*.[15] Sodium dodecylsulfate, SDS, purity >99 %, was obtained from Merck, Germany. The critical micelle concentration (*CMC*) determined at 20 °C by conductometric titration was 0.244 % *w*/*V*.[15] All samples were used without any further purification. Demineralized water was used as the solvent.

Preparation of the solutions

A stock solution of HPMC (2.6 mass %) was prepared by dispersing HPMC in water at 80–90 °C under gentle stirring. The stock solution was left for 24 h at room temperature before further use. Stock solutions of SDS (3.00 and 7.00 % *w*/*V*) were prepared by dissolving SDS in water at 20 °C.

The stock solution of HPMC, diluted stock solution of SDS and water were mixed together to obtain HPMC/SDS mixtures of the desired composition. The HPMC concentration was set to 0.37, 0.74 and 1.49 mass %, which was equivalent to three, six and twelve times higher concentration of HPMC than its overlap concentration, *i.e*. the overlap parameter c/c^* was 3, 6, and 12. The SDS concentration was varied from 0.00 to 3.50 mass % for each of the three HPMC concentrations. The concentrations in the further text are expressed as mass %, unless otherwise noted.

Rheological measurements

Rheological measurements were performed using a RheoStress 600HP rheometer (Thermo HAAKE, Germany), at 20 °C. The cone and plate geometry was used (d = 60 mm, θ = 1 °). The steady-state method was employed to obtain viscosity curves in a shear rate range of 0.1–6000 s^{-1}, while the rheometer was operated in the controlled rate mode (CR mode).[20] The measurements were performed in triplicate and average values are reported. The measurement error was 2.5 %.

Shear-thinning regions of the experimental viscosity curves were fitted to the Ostwald de Waele Equation:

$$\eta = K\dot{\gamma}^{n-1} \text{ (Pa s)} \quad (1)$$

where: η is the viscosity, Pa s; $\dot{\gamma}$ the shear rate, s^{-1}; the K is the coefficient of consistency and n is the degree of shear-thinning. Fit quality was evaluated by the coefficient of correlation, which was always better than 0.995.

The rheometer was equipped with a sensor for measuring a force in a direction perpendicular to the shear flow, *i.e*., the normal force, F_n. The first normal stress difference, N_1 (*i.e*., the stress in a direction perpendicular to the shear flow), was calculated by the instrument software using the equation:

$$N_1 = \frac{2F_n}{\pi a^2} \text{ (Pa)} \quad (2)$$

where a is the cone radius.

RESULTS AND DISCUSSION

Low- to mid-shear rate range rheology of the HPMC/SDS mixtures

The influence of c_{SDS} on the rheological properties of the HPMC/SDS mixtures containing three different concentrations of HPMC was investigated. The HPMC concentrations in the mixtures were 0.37, 0.74 and 1.49 mass %, which corresponded to the overlap parameters, c/c^*, of 3, 6, and 12, respectively. The higher the c/c^* value was, the more entangled were the HPMC chains in the solution. The viscosity curves of the HPMC/SDS mixtures containing 0.00–0.35 mass % SDS and HPMC concentrations that correspond to the three values of the overlap parameter are shown in Fig. 1.

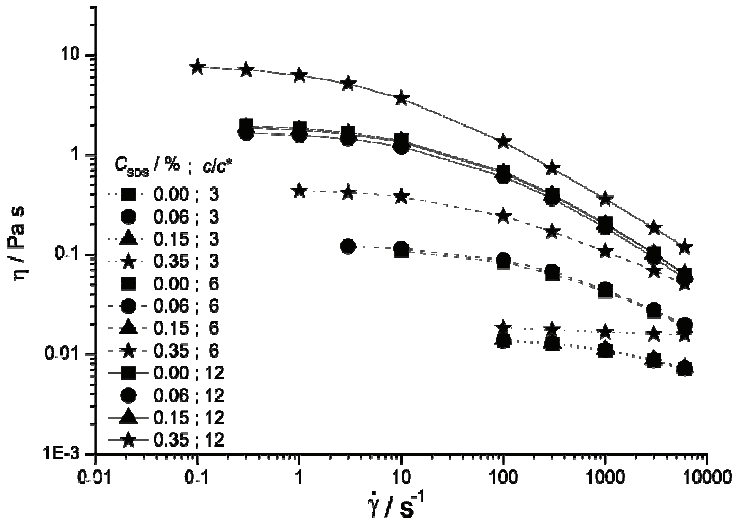

Fig. 1. Viscosity curves of HPMC/SDS mixtures containing 0.00–0.35 mass % SDS and HPMC concentrations that correspond to the overlap parameters of 3, 6 and 12.

The viscosity curves of the HPMC solutions containing no SDS showed typical shear-thinning behavior, *i.e.*, the viscosity of the solutions decreased with increasing shear rate. The decrease is due to disentanglement and orientation of HPMC macromolecules in the flow field.[18] The viscosity of the HPMC solutions increased as the number of HPMC chain entanglements increased, *i.e.*, as c/c^* increased from 3 to 6 and 12. In a like manner, the influence of the shear rate on viscosity was more pronounced and solutions become more shear-thinning as the value of c/c^* increased. This was confirmed by fitting the experimental data to the Ostwald de Waele Equation and determining the degree of shear-thinning, n, and the coefficient of consistency, K. The numerical values of the fitting parameters n and K are given in Table I. The influences of c_{SDS} on n and K are shown in Figs. 2 and 3, respectively.

TABLE I. The degree of shear-thinning, *n*, and the coefficient of consistency, *K*, for HPMC/SDS mixtures of different composition

c_{SDS} / mass %	$c/c^* = 3$		$c/c^* = 6$		$c/c^* = 12$	
	n	*K*	*n*	*K*	*n*	*K*
0.00	0.87	0.027	0.70	0.345	0.50	6.531
0.06	0.87	0.027	0.70	0.369	0.51	5.727
0.15	0.87	0.027	0.68	0.439	0.50	6.238
0.35	0.95	0.023	0.64	1.240	0.45	16.32
0.55	0.96	0.010	0.77	0.584	0.45	20.52
0.75	0.96	0.006	0.89	0.208	0.50	17.07
1.00	0.97	0.006	0.90	0.091	0.57	11.03
1.50	0.99	0.005	0.94	0.024	0.66	5.851
2.00	0.98	0.005	0.96	0.016	0.76	2.241
2.50	0.98	0.005	0.96	0.015	0.89	0.294
3.50	0.99	0.005	0.97	0.015	–	–

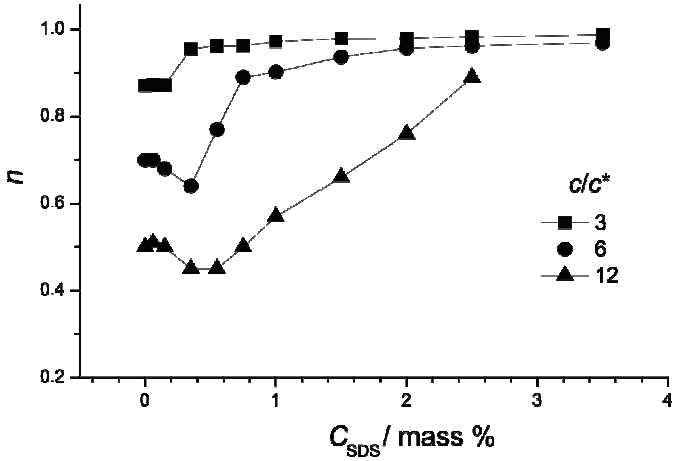

Fig. 2. The influence of the SDS concentration, c_{SDS}, on the degree of shear-thinning, *n*, of HPMC/SDS mixtures with the overlap parameter for HPMC of 3, 6 and 12.

As shown in Table I, the degree of shear-thinning decreased from 0.87 to 0.70 and 0.50, while coefficient of consistency increased from 0.027 to 0.345 and 6.531 as c/c^* was increased from 3 to 6 and 12, respectively. A decrease in *n* corresponds to a more pronounced shear-thinning flow (*i.e.*, more non-Newtonian flow), while an increase in *K* reflects an increase in the solution viscosity, and *vice versa*.[21] Such behavior is typical for polymer solutions with an increasing number of chain entanglements.[22]

The addition of SDS up to 0.15 mass % did not significantly influence the rheological properties of the HPMC solutions, as evidenced by the fact that viscosity curves of HPMC/SDS mixtures containing 0.00, 0.06 and 0.15 mass % SDS overlapped for a given value of c/c^*, Fig. 1. This indicates that there is no

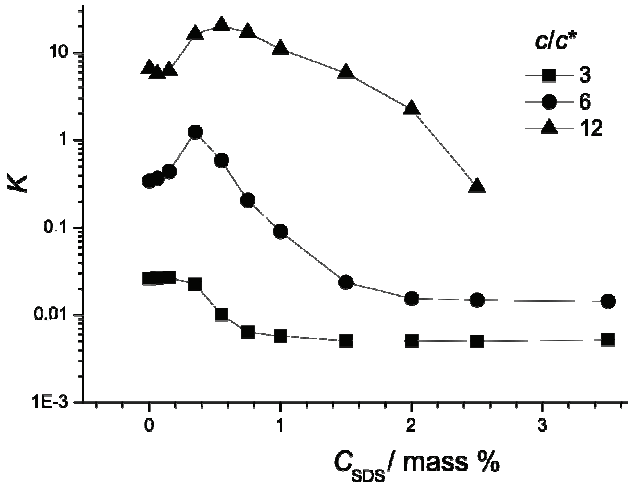

Fig. 3. The influence of the SDS concentration, c_{SDS}, on the coefficient of consistency, *K*, of HPMC/SDS mixtures with the overlap parameter for HPMC of 3, 6 and 12.

interaction between HPMC and SDS in the HPMC/SDS mixtures containing up to 0.15 mass % SDS. An increase in viscosity was observed when c_{SDS} exceeded 0.15 mass % for all the three HPMC/SDS mixtures (c/c^* of 3, 6, or 12), see the 0.35 mass % SDS viscosity curves in Fig. 1. The increase in viscosity was due to the onset of HPMC–SDS interactions and HPMC–SDS complex formation, which occurred when c_{SDS} was higher than the critical association concentration (*CAC*).[12,16] The complex formation occurred *via* hydrophobic interaction in which the SDS molecules bind to the HPMC chains. The SDS formed micelles around the hydrophobic moieties of the neighboring HPMC chains, which strengthens the network of entangled HPMC chains and resulted in an increase in viscosity.[13,17] The fact that the increase in viscosity occurred at c_{SDS} >0.15 mass % regardless of the c/c^* value showed that *CAC* value was independent of the HPMC concentration and was always 0.15 mass %. This is in line with previously reported results.[11,14] Increasing c_{SDS} further resulted in increase in the viscosity until a maximum in the viscosity is reached at a certain concentration (c_M). Maximum in the viscosity attained at c_M of 0.35, 0.35 and 0.55 % SDS for HPMC/SDS mixtures with c/c^* values of 3, 6, and 12, respectively. After reaching the maximum, the viscosity of the mixtures decreased on further increases in c_{SDS}, Figs. 1, 4 and 5.

The decrease in viscosity was due to more and more SDS anions becoming bound to the HPMC chains as c_{SDS} was increased. The binding of SDS caused an increase in the negative net charge on the HPMC chains and thus, electrostatic repulsion between neighboring HPMC chains occurred, which resulted in a gradual disentanglement of the chains, the network loosened and, consequently, the viscosity of the mixtures decreased.[12] Changes in the viscosity of HPMC/

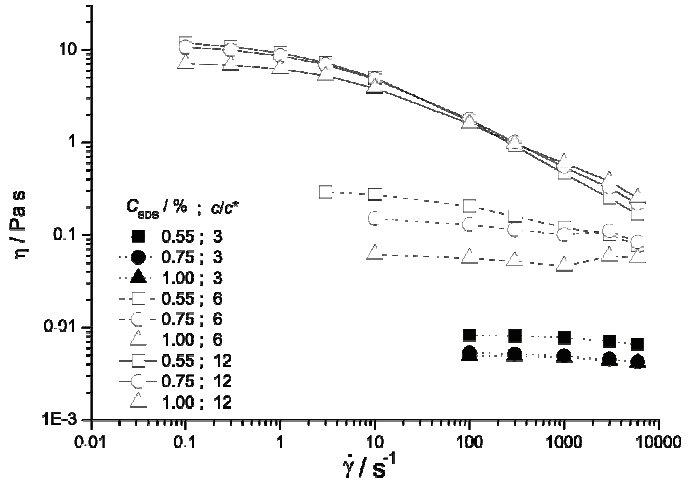

Fig. 4. Viscosity curves of HPMC/SDS mixtures containing 0.55–1.00 mass % SDS and HPMC concentrations that correspond to the overlap parameters of 3, 6 and 12. Viscosity curves of HPMC/SDS mixtures where a significant increase in the first normal stress difference (N_1) was observed are marked with open symbols.

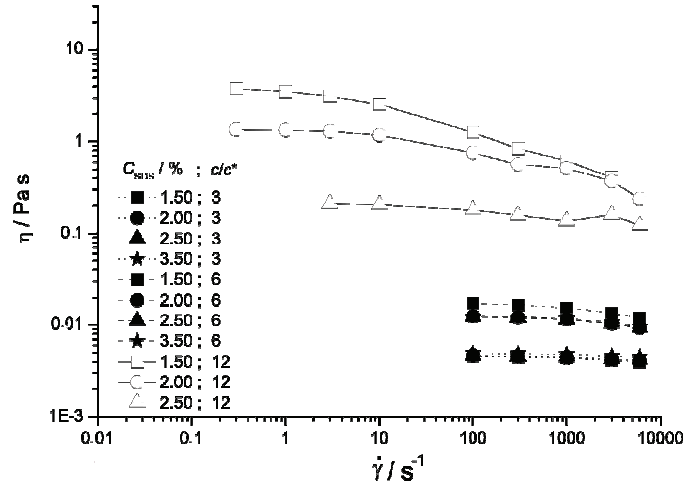

Fig. 5. Viscosity curves of HPMC/SDS mixtures containing 1.50–3.50 mass % SDS and HPMC concentrations that correspond to the overlap parameters of 3, 6 and 12. Viscosity curves of HPMC/SDS mixtures where a significant increase in the first normal stress difference (N_1) was observed are marked with open symbols.

/SDS mixtures no longer occurred when the c_{SDS} reached 0.75 and 2.00 mass % for the mixtures with c/c^* values of 3 and 6, respectively, Figs. 4 and 5. This indicates that the HPMC–SDS interaction was finished and that the c_{SDS} had reached the polymer saturation point (*PSP*). At the *PSP*, all the hydrophobic

moieties of HPMC chains were fully solubilized with SDS micelles, the intermolecular links between neighboring HPMC chains were broken and the 3D network structure was lost.[15,17] Increasing the c_{SDS} above the polymer saturation point (*PSP*) brought about no significant changes in viscosity of the mixtures. The *PSP* increased with increasing c/c^* value (*i.e.*, increasing HPMC concentration) because more SDS is required to solubilize the greater amount of HPMC present in solution. The HPMC/SDS mixture with highest investigated HPMC concentration (*i.e.*, c_{HPMC} = 1.49 mass % and c/c^* = 12) would required the highest concentrations of SDS to fully solubilize the HPMC molecules and to reach the *PSP*. For this HPMC/SDS mixture, the *PSP* was not reached in the investigated range of c_{SDS} (0.00–2.50 mass %). In this case, the viscosity of the mixture changed on addition of SDS when $c_{SDS} > CAC$, and it continued to change up to the highest investigated c_{SDS}, Fig. 5. The described changes in the viscosity of the HPMC/SDS mixtures nicely correlate with the changes in the coefficients of consistency, *K*, as a function of c_{SDS} in the mixtures, Fig. 3.

Apart from being influenced by the concentration of SDS and HPMC, the viscosities of the HPMC/SDS mixtures were also influenced by the applied shear. All of the examined HPMC/SDS mixtures were shear-thinning when examined at the low-end to mid-range of the applied shear rates, and their viscosities decreased on increasing the shear rate, Figs. 1, 4 and 5. The decrease in viscosity could be suitably described by the degree of shear-thinning *n*, Fig. 2. It could be seen, Fig. 2, that increasing c_{SDS} brings about characteristic changes in *n*, irrespective of the c/c^* value. For the lowest c_{SDS} value, below *CAC*, *n* does not change with increasing c_{SDS}, since there is no HPMC-SDS interaction. On further increase in c_{SDS}, the SDS binds to HPMC and supports a network of entangled HPMC chains, which results in more pronounced shear-thinning flow properties and thus a decrease in *n* occurred. The minimum value of *n* was attained at c_M, where the network was the stiffest. Further addition of SDS leads to an increase in *n* due to a gradual disentanglement of the HPMC chains because of the electrostatic repulsion. The network structure loosened and *n* increased until the PSP was reached. At the PSP, the network is completely broken and *n* reaches values close to 1, indicating almost perfect Newtonian flow and the absence of any structural rearrangements in the flow field.

The described changes in *n* with changing c_{SDS} were more pronounced in HPMC/SDS mixtures containing more entanglements of the HPMC chains, *i.e.*, in mixtures with a higher value of the c/c^* parameter. As c/c^* increases from 3 to 6 and 12, the difference between the lowest and the highest value of *n* determined for an HPMC/SDS mixture of a particular c/c^* increased, Fig. 2. Figure 2 shows rather small differences in flow profile over the whole range of c_{SDS} for HPMC/SDS mixtures with c/c^* = 3, and a flow profile ranging from highly shear-thinning to almost Newtonian for mixtures with c/c^* = 12. In addition, the changes in

n spanned over a broader range of c_{SDS} with increasing c/c^*, due to the fact that HPMC–SDS interaction occurred over a broader range of c_{SDS}.

Mid- to high-shear rate range rheology of HPMC/SDS mixtures

The HPMC–SDS interaction is determined by the molecular properties of HPMC and the composition of the HPMC/SDS mixtures. In addition, the shear rate can also influence the interaction, and this becomes especially true with increasing c/c^* parameter.

The HPMC/SDS mixtures with $c/c^* = 3$ were all shear-thinning throughout the employed shear rates (0.1–6000 s^{-1}), Figs. 1, 4 and 5. In addition, in these mixtures, no stresses perpendicular to the shear flow direction were detected (*i.e.*, $N_1 = 0$), irrespective of the composition of the HPMC/SDS mixture or the applied shear rate. However, this was not always the case in HPMC/SDS mixtures when c/c^* was increased from 3 to 6 and to 12. In the HPMC/SDS mixtures with $c/c^* = 6$ and 12 and c_{SDS} 0.55–1.00 and 0.55–2.50 mass %, respectively, a significant increase in N_1 was observed when a critical shear rate, $\dot{\gamma}_{crit}$, was exceeded, Figs. 6 and 7.

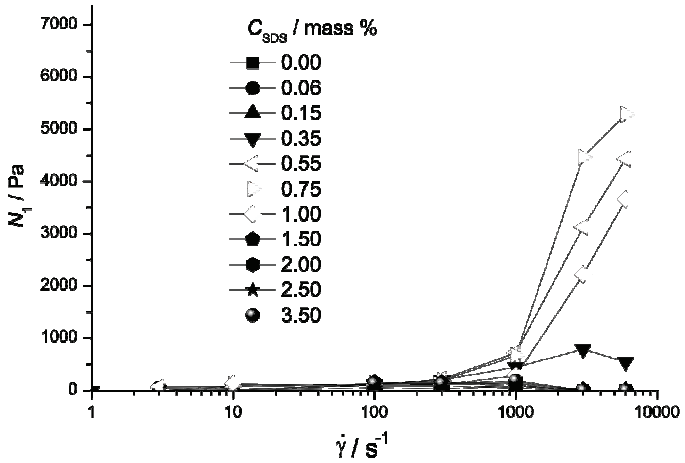

Fig. 6. Influence of the shear rate on the first normal stress difference (N_1) of HPMC/SDS mixtures with $c/c^* = 6$ and c_{SDS} = 0.00–3.50 mass %. HPMC/SDS mixtures where a significant increase in N_1 was observed are marked with open symbols.

A slight increase in N_1 was also observed in the $c/c^* = 6$ and 12 HPMC/SDS mixtures when c_{SDS} = 0.35 mass %. Below $\dot{\gamma}_{crit}$, N_1 was effectively zero. N_1 was also zero for the $c/c^* = 6$ and 12 HPMC/SDS mixtures when c_{SDS} was out of the above range for any of the employed shear rates (0.1–6000 s^{-1}). The observed N_1 values in the $c/c^* = 12$ mixtures were several times larger when compared to those for the $c/c^* = 6$ mixtures, Figs. 6 and 7. The development of a stress normal to the shear direction, N_1, is a typical manifestation of non-linear

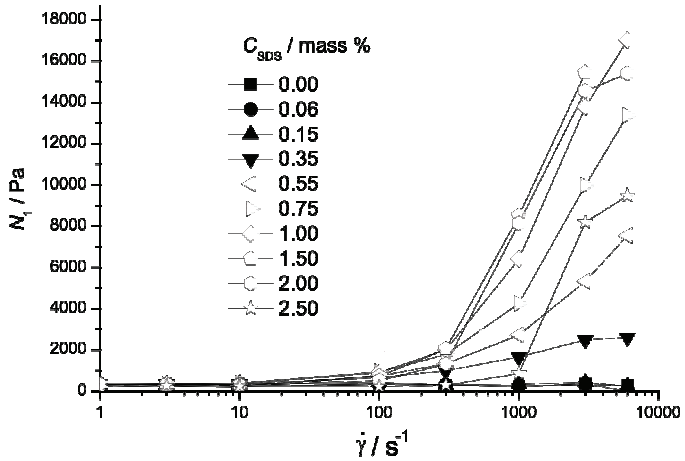

Fig. 7. Influence of shear rate on the first normal stress difference (N_1) of HPMC/SDS mixtures with $c/c^* = 12$ and $c_{SDS} = 0.00–2.50$ mass %. HPMC/SDS mixtures where a significant increase in N_1 was observed are marked with open symbols.

viscoelastic flow, and is indicative of an elastic response of a microstructure subjected to large-amplitude deformations.[22] In the HPMC/SDS mixtures in which an N_1 increase was observed, a change in flow profile of the viscosity curves also occurred when $\dot{\gamma}_{crit}$ was reached, Figs. 4 and 5 (viscosity curves marked with the open symbols). Namely, the decrease in viscosity with increasing shear rate became less steep than expected or even an increase in viscosity (*i.e.*, shear-thickening flow) occurred when $\dot{\gamma}_{crit}$ was reached. A break in a shear-thinning flow followed by a shear-thickening region in HPMC/SDS mixtures was previously reported for highly substituted HPMC macromolecules (degree of substitution for methoxyl group, DS_{Me}, and a molar substitution for hydroxylpropyl group MS_{HP},in ranges 2.2–3.0 and 0.48–1.88, respectively) of high molar mass, $\bar{M}_w$, between 2,200,000 and 3,800,000 g mol^{-1}, and was attributed to a shear-induced formation of HPMC–SDS complex.[19,24] The authors also reported on an increase in the first normal stress difference, and supported their findings on shear-induced structure formation with flow birefringence measurements. Similar results on shear-induced structure formation were also reported for mixtures of SDS and hydrophobically modified hydroxyl ethyl cellulose (hmHEC).[23] The results presented in this work (*i.e.*, an increase in N_1 and the change in the flow profile) thus suggest that a shear-induced structure formation may also occur in HPMC/SDS mixtures containing HPMC macromolecules of significantly lower molar mass ($\bar{M}_v$ = 91,500 g mol^{-1}) that contain less substituents (DS_{Me} = = 1.4 and MS_{HP} = 0.21) provided that the overlap parameter is sufficiently high.

CONCLUSIONS

Rheological investigation of HPMC/SDS mixtures containing different concentrations of SDS (c_{SDS}, 0.00–3.50 mass %) and HPMC concentrations, which corresponded to the overlap parameter, c/c^*, of 3, 6 and 12 were realized by viscosity measurements performed at different shear rates (0.1–6000 s^{-1}). All mixtures proved to be shear-thinning when examined in the low-end to mid--range of the applied shear rates. The degree of shear-thinning, n, and viscosity depended on the composition of the HPMC/SDS mixtures and were influenced by HPMC–SDS complex formation. Change in the c_{SDS} brings about characteristic changes in n, which were more pronounced as c/c^* was increased from 3 to 6 and to 12. A change in flow profile and a buildup of the first normal stress difference was observed in HPMC/SDS mixtures with c/c^* of 6 and 12 and c_{SDS} in ranges 0.55–1.00 and 0.55–2.50 mass %, respectively, when a critical shear rate, $\dot{\gamma}_{crit}$, was exceeded, suggesting that a shear-induced structure formation in the mixtures occurred.

Acknowledgements. This work was financed by Ministry of Education, Science and Technological Development of Republic of Serbia, Grant III 46010. It is realized within COST CM1101 and MP1106 action frameworks.

И З В О Д

РЕОЛОШКА СВОЈСТВА СМЕША ХИДРОКСИПРОПИЛМЕТИЛ-ЦЕЛУЛОЗЕ И НАТРИЈУМ-ДОДЕЦИЛСУЛФАТА

ЈАРОСЛАВ М. КАТОНА, САНДРА Ђ. ЊАРАДИ, ВЕРИЦА Ј. СОВИЉ, ЛИДИЈА Б. ПЕТРОВИЋ, БРАНКИЦА Б. МАРЧЕТА и ЈАДРАНКА Л. МИЛАНОВИЋ

Универзитет у Новом Саду, Технолошки факултет Нови Сад, Бул. цара Лазара 1, 21000 Нови Сад

Испитивана су реолошка својства смеша хидроксипропилметил-целулозе (HPMC), нејонског асоцијативног целулозног етра, и натријум додецилсулфата (SDS), анјонског сурфактанта, мерењем вискозитета при различитим брзинама смицања (0,1–6000 s^{-1}). Припремљене су HPMC/SDS смеше са различитим концентрацијама SDS (c_{SDS}, 0,00–3,50 мас. %) при чему је концентрација HPMC у смешама одговарала вредностима параметра преклапања c/c^* = 3, 6, и 12. Утврђено је да у опсегу нижих и средњих брзина смицања све HPMC/SDS смеше показују псеудопластичан тип протицања. Састав HPMC/SDS смеша и формирање HPMC/SDS комплекса утичу на вредност степена псеудопластичности, n. Вредности параметра n у смешама се крећу у опсегу вредности карактеристичних за изразито псеудопластичне флуиде до скоро потпуно Њутновских флуида, и више су изражене како се c/c^* повећава од 3 до 6 и 12. Код HPMC/SDS смеша са c/c^* вредношћу од 6 и 12 долази до промене у типу протицања као и до пораста прве разлике нормалних напона N_1 ($N_1 > 0$) уколико је c_{SDS} у опсезима 0,55–1,00 и 0,55–2,50 мас. %, редом, и уколико брзина смицања пређе критичну вредност, указујући на формирање смицањем индукованих структура у HPMC/SDS смешама.

(Примљено 7. августа, ревидирано 30. октобра 2013)

REFERENCES

1. B. Lindman, in *Handbook of Applied Surface and Colloid Chemistry*, K. Holmberg, Ed., Wiley, Chichester, 2002, p. 445
2. E. D. Goddard, *J. Colloid Interface Sci.* **256** (2002) 228
3. F. E. Antunes, E. F. Marques, M. G. Miguel, B. Lindman, *Adv. Colloid Interface Sci.* **147**–**148** (2009) 18
4. K. Kogej, *Adv. Colloid Interface Sci.* **158** (2010) 68
5. D. J. F. Taylor, R. K. Thomas, J. Penfold, *Adv. Colloid Interface Sci.* **132** (2007) 69
6. N. A. Camino, O. E. Perez, C. C. Sanchez, J. M. R. Patino, A. M. R. Pilosof, *Food Hydrocolloids* **23** (2009) 2359
7. N. A. Camino, C. C. Sánchez, J. M. R. Patino, A. M. R. Pilosof, *Food Hydrocolloids* **25** (2011) 1
8. T. Futamura, M. Kawaguchi, *J. Colloid Interface Sci.* **367** (2012) 55
9. A. Avranas, P. Iliou, *J. Colloid Interface Sci.* **258** (2003) 102
10. F. M. Winnik, S. T. A. Regismond, *Colloids Surfaces, A* **118** (1996) 118
11. S. Nilsson, *Macromolecules* **28** (1995) 7837
12. S. M. C. Silva, F. E. Antunesa, J. J. S. Sousab, A. J. M. Valentea, A. A. C. C. Pais, *Carbohydr. Polym.* **86** (2011) 35
13. J. C. Su, S. Q. Liu, S. C. Joshi, Y. C. Lam, *J. Therm. Anal. Calorim.* **93** (2008) 495
14. V. Sovilj, L. Petrović, *Carbohydr. Polym.* **64** (2006) 41
15. J. Katona, V. Sovilj, L. Petrović, *Carbohydr. Polym.* **74** (2008) 193
16. L. Picullel, M. Egermayer, J. Sjostrom, *Langmuir* **19** (2003) 3643
17. S. Nilsson, K. Thuresson, P. Hansson, B. Lindman, *J. Phys. Chem., B* **102** (1998) 7099
18. M. Tirrell, in *Interactions of Surfactants with Polymers and Proteins*, E. D. Goddard, K. P. Ananthapadmanabhan, Eds., CRC Press, Boca Raton, FL, 1993, p. 67
19. C. Clasen, W. M. Kulicke, *Prog. Polym. Sci.* **26** (2001) 1839
20. G. Schramm, *A Practical Approach to Rheology and Rheometry*, Gebrüder HAAKE GmbH, Karlsruhe, 2000, p. 31
21. M. J. Lucero, C. Claro, M. Casas, M. R. Jiménez-Castellanos, *Carbohydr. Polym.* **86** (2011) 891
22. H. A. Barnes, *A Handbook of Elementary Rheology*, University of Wales, Aberyswyth, 2000, p. 107
23. V. Tirtaatmadja, J. Cooper-White, S. Gason, *Korea–Aust. Rheol. J.* **14** (2002) 189
24. W. M. Kulicke, O. Arendt, M. Berger, *Colloid Polym. Sci.* **276** (1998) 617.

Journal of the Serbian Chemical Society
JSCS-info@shd.org.rs • www.shd.org.rs/JSCS
J. Serb. Chem. Soc. 79 (4) 469–480 (2014) UDC 536.2:536.7+66.021.3:537.5–962:542.9
JSCS–4600 *Original scientific paper*

Mixed convective–magnetohydrodynamic flow of a micropolar fluid with ohmic heating, radiation and viscous dissipation over a chemically reacting porous plate subjected to a constant heat flux and concentration gradient

HITESH KUMAR*

Department of Information Technology, IBRI College of Technology, Ibri, P. O. Box 466, Oman

(Received 12 June 2012, revised 11 October 2013)

Abstract: In the present paper, chemically reacting mixed convective–magneto-hydrodynamic (MHD) micropolar flow, heat and mass transfer in a porous medium with the effects of ohmic heating, radiation and viscous dissipation past an infinite vertical plate, which was subjected to a constant heat flux and concentration gradient, were analyzed. The non-linear coupled partial differential equations were solved numerically using an implicit finite difference scheme known as the Keller-box Method. The results for concentration, transverse velocity, angular velocity and temperature were obtained and illustrated graphically to observe the effects of various parameters, and a numerical discussion is presented with physical interpretations.

Keywords: mixed convection; heat and mass transfer; heat flux; heat generation; ohmic heating; micropolar fluid; chemical reaction.

INTRODUCTION

Flows arising from temperature difference have great significance not only theoretically, but also for applications in geophysics and engineering. There are many interesting aspects of such flows, so analytical solutions of such problems have been presented by many authors, *e.g.*, Gebhart and Pera,[1] Sparrow *et al.*,[2] Soundalgekar,[3] Acharya *et al.*,[4] Singh and Chand,[5] *etc*. Investigations of flow streaming into a porous and permeable medium assuming a high velocity of the flow (the Reynolds Number is moderately high) were obtained by Yamamoto and Iwamura,[6] Yamamoto and Yoshida,[7] Brinkman[8] and Raptis *et al.*[9–10] All the above-mentioned authors used the generalized Darcy Law, and the generalized Darcy Law was derived without taking into account the angular velocity of the fluid particles. Rapti[11] in his research paper on a horizontal plate used flow

* Correspondence by E-mail: hiteshrsharma@gmail.com
doi: 10.2298/JSC130612121K

equations with angular velocity. Raptis[12] in another research paper discussed magnetopolar fluid through a porous medium.

Combined heat and mass transfer problems with chemical reaction are of importance in many processes, In processes such as drying, evaporation at the surface of a water body, energy transfer in a wet cooling tower and the flow in a desert cooler, heat and mass transfer occur simultaneously. Diffusion rates could be altered tremendously by chemical reactions. The effect of a chemical reaction depends whether the reaction is homogeneous or heterogeneous. Kandasamy *et al.*[13] studied thermophoresis and variable viscosity effects on magnetohydrodynamic (MHD) mixed convective heat and mass transfer past a porous wedge in the presence of a chemical reaction. Kandasamy and Devi[14] studied the effects of chemical reaction, and heat and mass transfer on non-linear laminar boundary--layer flow over a wedge with suction or injection. In addition, studies of heat generation or absorption in moving fluids for problems involving chemical reactions and those concerned with dissociating fluids are equally important. Specifically, the effects of heat generation may alter the temperature distribution, consequently affecting the particle deposition rate in nuclear reactors, electronic chips and semiconductor wafers. The problem of heat transfer in MHD boundary-layer flow through a porous medium, due to a non-isothermal stretching sheet, with suction, radiation, and heat annihilation was considered by Kumar.[15]

Moreover, when the temperature of surrounding fluid is high, radiation effects play an important role and that cannot be ignored,[16,17] Nuclear power plants, gas turbines and various propulsion devices for aircraft, missiles, satellites and space vehicles are examples of such areas of engineering, where high temperature heat transfer occurs. In such cases, the effects of radiation have to be taken into account. Ganesan *et al.*[18] studied the effects of radiation and free convection for an impulsively started infinite vertical isothermal plate using the Rosseland Approximation.[19] The problem of radiative heat transfer with hydromagnetic flow and viscous dissipation over a stretching surface in the presence of a variable heat flux was solved analytically by Kumar.[20] Hossain and Takhar,[21] Raptis and Massals,[22] and Hossain *et al.*[23] studied the radiation effect on free and forced convection flows past a vertical plate, including various physical aspects. Aboeldhab[24] studied the radiation effect in heat transfer in an electrically conducting fluid at a stretching surface. At high operating temperature, the radiation effect can be quite significant.[25] Heat and mass transfer effects on a moving plate in the presence of thermal radiation were studied by Muthukumarswamy and Kumar[26] using the Laplace technique. For the problem of coupled heat and mass transfer in MHD free convection, the effects of both viscous dissipation and ohmic heating were not studied in the above investigations. However, it is more realistic to include these two effects to explore the impact of the magnetic field on the thermal transport in the boundary layer. With this awareness, the effect of

ohmic heating on the MHD free convection heat transfer was examined by Hossain[27] for a Newtonian fluid. Chen[28] studied the problem of combined heat and mass transfer of an electrically conducting fluid in MHD natural convection, adjacent to a vertical surface with ohmic heating.

In the present work, a study of steady mixed convection flow of a laminar, incompressible, MHD micropolar fluid, with thermal and mass diffusion effects in porous media was performed. The object of the study was to analyze the effects of a magnetic field, the heat source and radiation on the thermal transport in the boundary layer, when the wall was at the prescribed heat flux.

MATHEMATICAL ANALYSIS

Herein, a mixed convection flow of an incompressible and electrically conducting viscous thermo-micropolar fluid past an infinite porous vertical plate is considered. The vertical plate was assumed to be at a constant heat flux and a constant concentration gradient. A magnetic field (B_0) of uniform strength was applied transversely to the direction of the flow, that is the y-axis, and the induced magnetic field was neglected. The x-axis was along the vertical porous plate in the upward direction and the y-axis was normal to it. Since the length of the plate is large and fluid flow extends to infinity, all the physical variables are independent of x and hence functions of y only. The governing equations of continuity, momentum, concentration, angular velocity and energy for the flow in the presence of ohmic heating, radiation, heat generation, chemical reaction and viscous dissipation are:

$$\frac{\partial v^*}{\partial y^*} = 0 \tag{1}$$

$$v^* = -V_0 \text{ (Constant)} \tag{2}$$

$$\frac{\mathrm{d}p}{\partial y^*} = 0 \;\Rightarrow\; p \text{ is independent of } y^* \tag{3}$$

$$\rho v^* \frac{\partial u^*}{\partial y^*} = (\kappa + \mu)\frac{\partial^2 u^*}{\partial y^{*2}} + \rho g \beta_T (T - T_\infty) + \rho g \beta_c (c - c_\infty) + \\ + \kappa \frac{\partial \omega_a}{\partial y^*} - \frac{\mu}{K^*} u^* - \sigma B_0^2 u^* \tag{4}$$

$$\rho j \left(v \frac{\partial \omega_a}{\partial y^*} \right) = \gamma \frac{\partial^2 \omega_a}{\partial y^{*2}} - 2\kappa \omega_a \tag{5}$$

$$\rho c_p v^* \frac{\partial T}{\partial y^*} = k \frac{\partial^2 T}{\partial y^{*2}} + \mu \left(\frac{\partial u^*}{\partial y^*} \right)^2 - \frac{\partial q_r}{\partial y^*} + Q(T - T_\infty) + \sigma B_0^2 u^{*2} \tag{6}$$

$$v^* \frac{\partial c}{\partial y^*} = D \frac{\partial^2 c}{\partial y^{*2}} - K_l (c - c_\infty) \tag{7}$$

with the boundary conditions:

$$u^* = V_0,\ \frac{\partial \omega_a}{\partial y^*} = -\frac{\partial^2 u^*}{\partial y^{*2}},\ \frac{\partial T}{\partial y} = -\frac{q}{k},\ -D\frac{\partial c}{\partial y^*} = m_w, \text{ at } \ y = 0 \\ u^* \to 0,\ \omega_a \to 0,\ T \to T_\infty,\ c \to c_\infty, \text{ as } \ y \to \infty \tag{8}$$

where $V_0 > 0$, $\gamma = \left(\mu + \frac{\kappa}{2}\right) j = \mu\left(1 + \frac{a}{2}\right) j$ and $j = \frac{\nu^2}{V_0^2}$

The Rosseland Approximation[20] is assumed for radiative heat flux, which leads to:

$$q_r = -\frac{4\sigma'}{3\kappa^*}\frac{\partial T^4}{\partial y^*} \tag{9}$$

If the temperature differences within the flow are sufficiently small such that T^4 may be expressed as a linear function of the temperature, then the Taylor series for T^4 about T_∞, after ignoring higher order terms, is given by:

$$T^4 = 4T_\infty^3 T - 3T_\infty^4 \tag{9a}$$

In order to write the governing equations and the boundary conditions in dimensionless form, the following non-dimensional quantities were introduced:

$$y = \frac{V_0 y^*}{\nu},\ u = \frac{u^*}{V_0},\ M = \frac{\sigma B_0^2 \nu}{\rho V_0^2},\ Pr = \frac{\mu c_p}{k},\ \theta = \frac{T - T_\infty}{q\nu / k V_0},\ C = \frac{c - c_\infty}{m_w \nu / V_0 D},$$

$$Ec = \frac{k V_0^3}{q\nu c_p},\ G_r = \frac{g\beta_T q \nu^2}{k V_0^4},\ G_c = \frac{g\beta_c m_w \nu^2}{V_0^4 D},\ S = \frac{Q\nu}{\rho c_p V_0^2},\ N = \frac{\kappa^* k}{4\sigma' T_\infty^3},$$

$$\omega = \frac{\nu\omega_a}{V_0^2},\ Sc = \frac{\vartheta}{D},\ K_c = \frac{\vartheta K_l}{\nu_w^2},\ K = \frac{K^* V_0^2}{\vartheta^2},\ a = \frac{\kappa}{\mu}$$

Equations (4)–(7) change to:

$$(1+a)\frac{d^2u}{dy^2} + \frac{du}{dy} - \left(M + \frac{1}{K}\right)u + a\frac{d\omega}{dy} + G_r\theta + G_c c = 0 \tag{10}$$

$$\left(1 + \frac{a}{2}\right)\frac{d^2\omega}{dy^2} + \frac{d\omega}{dy} - 2a\omega = 0 \tag{11}$$

$$\left(1 + \frac{4}{3N}\right)\frac{d^2\theta}{dy^2} + Pr\frac{d\theta}{dy} + SPr\,\theta + Pr\,Ec\left(\frac{du}{dy}\right)^2 + PrEc\,M\,u^2 = 0 \tag{12}$$

$$\frac{d^2c}{dy^2} + Sc\frac{dc}{dy} - K_c\,Sc\,c = 0 \tag{13}$$

and the boundary conditions change to:

$$\text{at}\quad y = 0,\ u = 1,\ \frac{d\theta}{dy} = -1,\ \frac{d\omega}{dy} = -\frac{d^2u}{dy^2},\ \frac{dc}{dy} = -1$$
$$\text{as}\quad y \to \infty,\ u \to 0,\ \theta \to 0,\ \omega \to 0,\ c \to 0 \tag{14}$$

RESULTS AND NUMERICAL DISCUSSION

Equations (10)–(13), subjected to the boundary conditions (14), were solved numerically using the Keller-box method as described by Cebeci and Bradshaw.[29,30] The objective of this study was to determine the effects a magnetic field, radiation, viscous dissipation, the Prandtl number and heat source on the fluid

temperature, and the effects of porosity, viscous dissipation and magnetic field on the velocity. The effects of the Schmidt number and chemical reaction on the concentration were determined and the effect of viscous dissipation on the angular velocity was analyzed.

The profiles of concentration for different values of *Sc* and K_c are presented in Figs. 1 and 2, respectively, which show that the concentration decreases with *Sc* or K_c. Physically, an increase in Sc means a decrease in molecular diffusion coefficient (*D*). This results in a decrease in the concentration boundary layer. Hence, the concentration of the species is higher for small values of Sc. Here, the chemical reaction was considered to be homogeneous first-ordered, and as is known, $K_c > 0$ represents a destructive reaction, and $K_c < 0$ a generative reaction. The destructive chemical reaction was taken into account here. Consequently, the concentration decreases for increments of the chemical reaction parameter. In a mixed convection regime, the concentration of the fluid decrease with increasing destructive reaction and thermophoresis particle deposition.

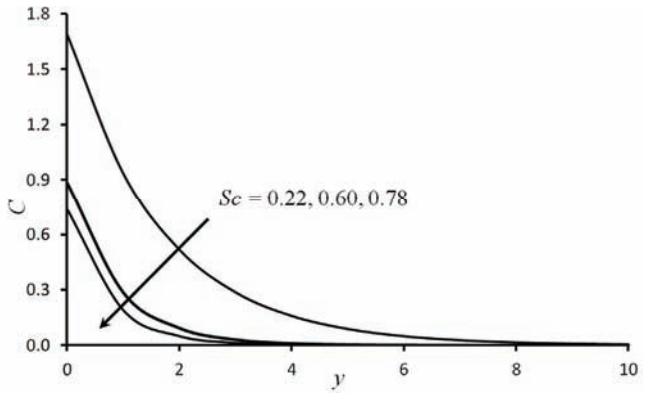

Fig. 1. Concentration for various values of *Sc*, when $K_c = 1.0$.

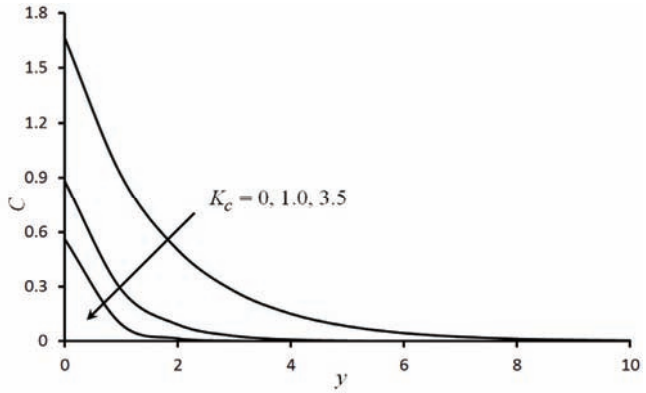

Fig. 2. Concentration for various values of K_c, when *Sc* = 0.6.

The transverse velocity is presented in Figs. 3–6 for different variations in *M*, *K* and *Ec*, respectively. The velocity decreases as *M* increases, whereas it increases with increasing *K* or *Ec*. Physically, the effect of increasing the magnetic field strength is to increase the retarding force and hence reduce the velocity. An increase in the porosity parameter physically means to reduce the drag force and hence causes the flow velocity to increase. An increase in *K* will reduce the resistance of the porous medium, which leads to an increase in the velocity. The effect of *Ec* in the flow field is to increase the energy, yielding a greater buoyancy force; this increase in the buoyancy force due to an increase in the dissipation parameter enhances the convective velocity.

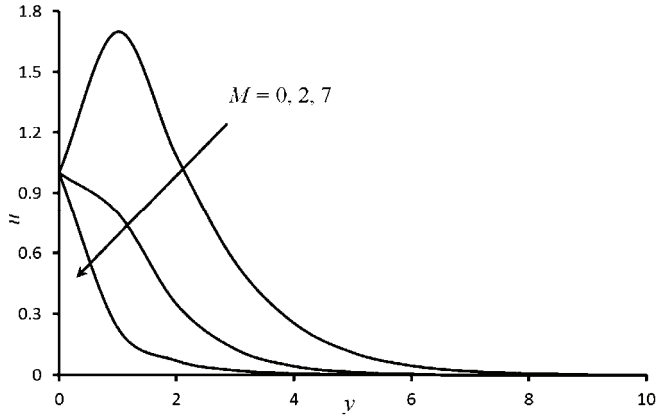

Fig. 3. Velocity for various values of *M*, when *Sc* = 0.6, K_c = 1.0, *a* = 0.5, *Pr* = 2.0, *S* = 0.4, β = 1.13, *K* = 2.0, G_r = 5.0, G_c = 0.5 and *Ec* = 0.03.

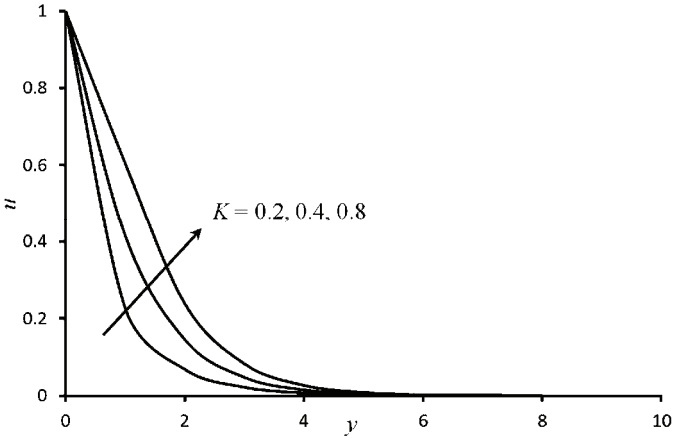

Fig. 4. Velocity for various values of *K*, when *Sc* = 0.6, K_c = 1.0, *a* = 0.5, *Pr* = 2.0, *S* = 0.4, β = 1.13, *M* = 2.0, G_r = 5.0, G_c = 0.5 and *Ec* = 0.03.

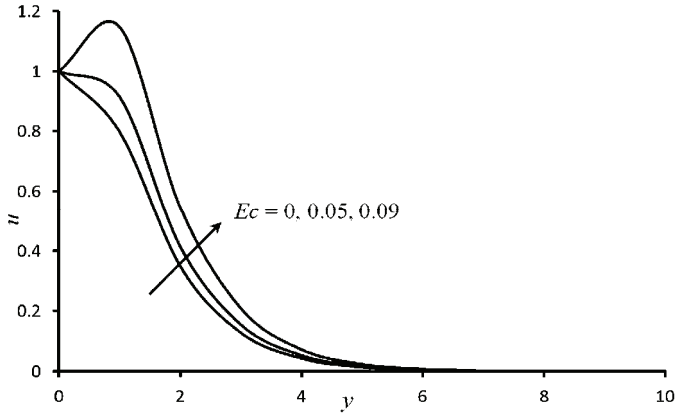

Fig. 5. Velocity for various values of *Ec*, when *Sc* = 0.6, K_c = 1.0, *a* = 0.5, *Pr* = 2.0, *S* = 0.4, β = 1.13, *M* = 2.0, *K* = 2.0, G_r = 5.0 and G_c = 0.5.

The effects of *Ec* on the angular velocity are plotted in Fig. 6. *Ec* increases with ω. With increasing rotational velocity, the shear stress due to the viscosity of the fluid creates a higher dissipation.

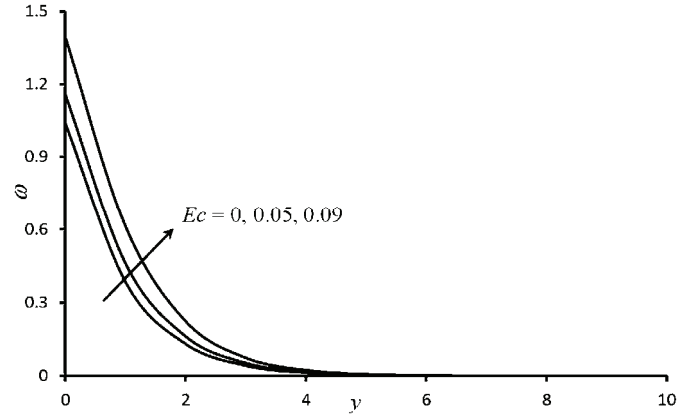

Fig. 6. Angular velocity for various values of *Ec*, when *Sc* = 0.6, K_c = 1.0, *a* = 0.5, *Pr* = 2.0, *S* = 0.4, β = 1.13, *M* = 2.0, *K* = 2.0, G_r = 5.0 and G_c = 0.5.

The fluid temperature for various values of *Pr* and *S* is shown in Figs. 7 and 8, respectively. θ increases with *Pr* and decreases as *S* increases. As the wall is at a prescribed heat flux, the temperature increases with increasing *Pr* due to the heat flux impinging on the surface. Whereas the presence of a heat source with a negative heat flux at the wall is the cause of a reduction in the fluid temperature.

Effects of magnetic field over the temperature are presented in Fig. 9. It was found that θ increases with *M*. This result is evidence for the fact that a magnetic

field increases the temperature of the fluid inside the boundary-layer because of excess heating.

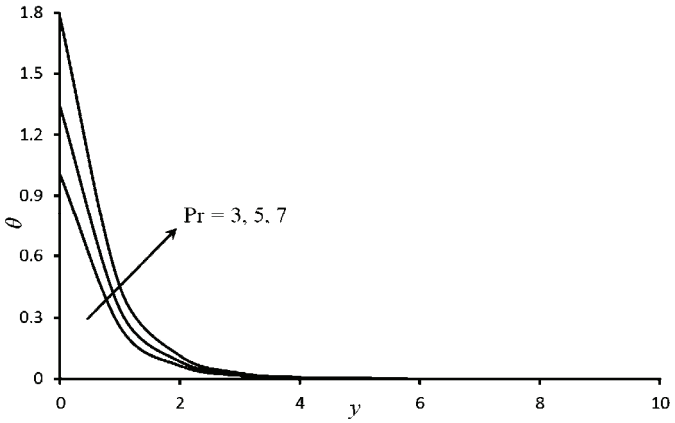

Fig. 7. Temperature for various values of *Pr*, when *Sc* = 0.6, K_c = 1.0, *a* = 0.5, *S* =0.4, β = 1, *M* = 2.0, *K* = 2.0, G_r = 5.0, G_c = 0.5 and *Ec* = 0.03.

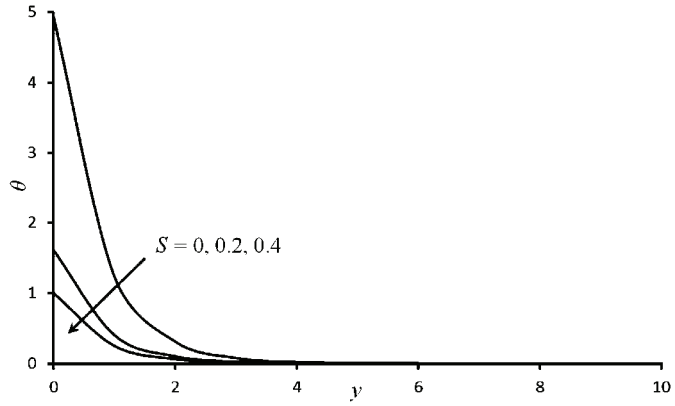

Fig. 8. Temperature for various values of *S*, when *Sc* = 0.6, K_c = 1.0, *a* = 0.5, *Pr* = 3.0, β = 1, *M* = 2.0, *K* = 2.0, G_r = 5.0, G_c = 0.5 and *Ec* = 0.03.

The effects of radiation and viscous dissipation are shown in Figs. 10 and 11. Figure 10 shows that θ decreases as β increases or *N* increases (as β = 1 + + 4/3*N*). It was observed that an increase in the thermal radiation produces significant increases in the thermal condition of the fluid and the thickness of the thermal boundary layer. Moreover, Fig. 11 shows that *Ec* reduces the fluid temperature. An increasing *Ec* implies that dissipation of thermal energy is higher, which reduces the temperature.

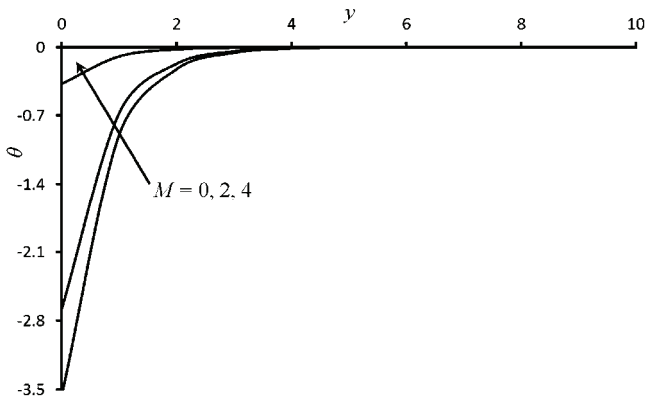

Fig. 9. Temperature for various values of M, when Sc = 0.6, = 1.0, a = 0.5, Pr = 2.0, S = 0.4, β = 1.13, K = 2.0, G_r = 5.0, G_c = 0.5 and Ec = 0.03.

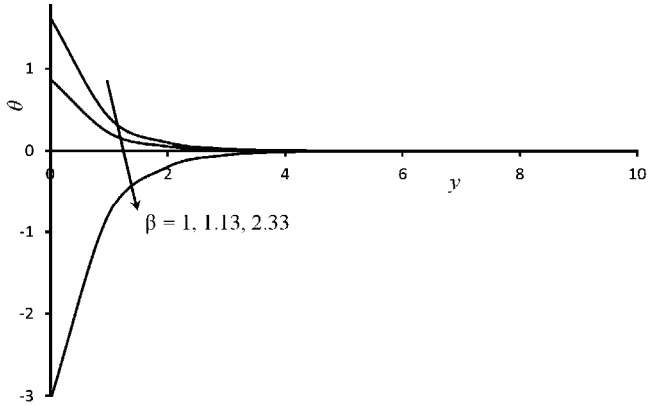

Fig. 10. Temperature for various values of β, when Sc = 0.6, K_c = 1.0, a = 0.5, Pr = 3.0, S = 0.2, M = 2.0, K = 2.0, G_r = 5.0, G_c = 0.5 and Ec = 0.03.

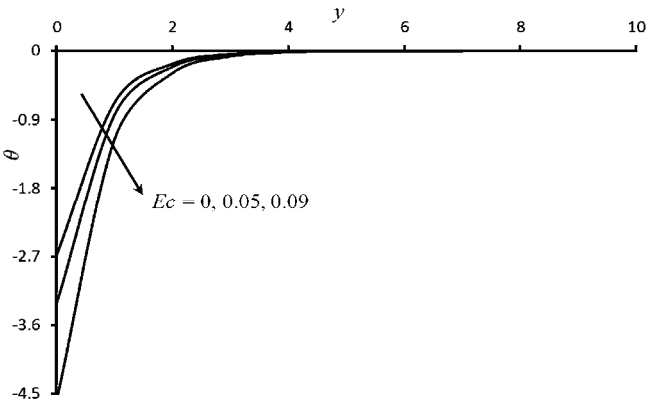

Fig. 11. Temperature for various values of Ec, when Sc = 0.6, K_c = 1.0, a = 0.5, Pr = 2.0, S = 0.4, β = 1.13, M = 2.0, K = 2.0, G_r = 5.0 and G_c =0.5.

CONCLUSIONS

In this paper, the problem of MHD mixed convective flow of a micropolar fluid with the effect of ohmic heating, radiation and viscous dissipation over a chemically reacting porous plate was studied when the plate is at a constant heat flux. The effects of Schmidt number and chemical reaction is to reduce the concentration. The magnetic field reduces the velocity of the boundary layer but enhances the thermal boundary layer. The presence of porosity decreases the transverse velocity. Increasing fluid viscosity increases the fluid temperature. On the other hand, the presence of a heat source or radiation narrows the thermal boundary layer. The effect of viscous dissipation is to increase the transverse velocity and angular velocity, but to reduce the temperature.

NOMENCLATURE

y^* horizontal coordinate (m)
u^* axial velocity (m s^{-1})
v^* transverse velocity (m s^{-1})
ω_a angular velocity vector normal to the *xy*-plane (rad s^{-1})
p^* pressure (Pa)
T^* temperature of the fluid (K)
T_∞ far field temperature (K)
c species concentration (mol m^{-3})
c_∞ far field concentration (mol m^{-3})
ν kinematic viscosity (m^2 s^{-1})
ρ density (kg m^{-3})
κ vortex viscosity (Pa s)
μ dynamic viscosity (Pa s)
g acceleration due to gravity (m s^{-2})
β_T coefficient of thermal expansion (K^{-1})
β_c coefficient of concentration expansion (m^3 mol^{-1})
K^* permeability of porous medium (H m^{-1})
σ electrical conductivity (S m^{-1})
B_0 magnetic field coefficient (T)
J microinertia density (m^2)
γ spin gradient viscosity (kg m s^{-1})
c_p specific heat (J kg^{-1} K^{-1})
k thermal conductivity (W m^{-1} K^{-1})
q_r^* radiative heat flux in the *y*-direction (W m^{-2})
D mass diffusion coefficient (m^2 s^{-1})
K_l rate of chemical reaction (s^{-1})
q rate of heat transfer (W m^{-2})
m_w wall mass flux (mol m^{-2} s^{-1})
σ' Stefan–Boltzmann constant (W m^{-2} K^{-4})
κ^* mean absorption coefficient (m^{-1})
V_0 suction velocity (m s^{-1})
Q heat generation coefficient (W m^{-3} K^{-1})

a material parameter
y dimensionless horizontal coordinate
u dimensionless axial velocity
M magnetic field parameter
Pr Prandtl number
θ dimensionless temperature
C dimensionless species concentration
Ec Eckert number
G_r thermal Grashof number
G_c solutal Grashof number
S heat generation parameter
ω dimensionless angular velocity
Sc Schmidt number
N radiation parameter
K_c chemical reaction parameter
K dimensionless permeability parameter.

Acknowledgment. The author is very much thankful to Prof. (Dr.) S. S. Tak, Jai Narain Vyas University, Jodhpur (India) for offering his valuable suggestions and assistance, and to the learned referee for significant and valuable comments.

ИЗВОД

МЕШОВИТИ КОНВЕКТИВНИ–МАГНЕТОХИДРОДИНАМИЧКИ (MHD) ТОК МИКРОПОЛАРНОГ ФЛУИДА СА ОМСКИМ ГРЕЈАЊЕМ, ЗРАЧЕЊЕМ И ВИСКОЗНОМ ДИСИПАЦИЈОМ, ПРЕКО ХЕМИЈСКИ РЕАКТИВНЕ ПОРОЗНЕ ПЛОЧЕ ИЗЛОЖЕНЕ КОНСТАНТНОМ ТОПЛОТНОМ ФЛУКСУ И КОНЦЕНТРАЦИОНОМ ГРАДИЈЕНТУ

HITESH KUMAR

Department of Information Technology, IBRI College of Technology, Ibri, P. O. Box 466, Oman

У овом раду је приказана анализа мешовите конвекције–магнетохидродинамичког (MHD) микрополарног тока са хемијском реакцијом, преноса топлоте и масе у порозној средини са ефектима омског грејања, зрачења и вискозне дисипације, преко бесконачне вертикалне плоче која је изложена константном топлотном флуксу и концентрационом градијенту. Нелинеарне купловане парцијалне диференцијалне једначине су решаване нумерички коришћењем имплицитне схеме коначних разлика, познате као *Keller box* метод. Резултати за концентрације, трансверзалну и угаону брзину и температуре су добијени и графички илустровани да би се уочили ефекти појединих параметара. Нумеричка дискусија са физичким интерпретацијама је такође приказана.

(Примљено 12. јуна, ревидирано 11. октобра 2013)

REFERENCES

1. B. Ghebhart, L. Pera, *Int. J. Heat Mass Transfer* **14** (1971) 2025
2. E. M. Sparrow, W. J. Minkowycz, E. R. G. Eckert, *ASME J. Heat Transfer* **86** (1964) 508
3. V. M. Soundalgekar, *Proc. Indian Acad. Sci.* **84** (1976) 194
4. M. Acharya, G. C. Dash, L. P. Singh, *Indian J. Pure Appl. Math.* **31** (2000) 1
5. K. D. Singh, K. Chand, *Proc. Nat. Acad. Sci. USA* **70** (2000) 49
6. K. Yamamoto, N. Iwamura, *J. Eng. Math.* **10** (1976) 41

7. K. Yamamoto, Z. Yoshida, *J. Phys. Soc. Jpn.* **37** (1974) 774
8. H. C. Brinkman, *Appl. Sci. Res.* **1** (1947) 27
9. A. Raptis, C. Perdikis, G. Tzivanidis, *J. Phys., D* **14** (1981) 99
10. A. Raptis, N. G. Kafousias, *Rev. Roum. Sci. Techn. – Mec. Appl.* **27** (1982) 37
11. A. Raptis, *Rheol. Acta* **21** (1982) 736
12. A. Raptis, *Bull. de la classe des Sc.* **69** (1983) 530
13. R. Kandasamy, I. Muhaimin, A. B. Khamis, *Heat Mass Transfer* **45** (2009) 703
14. R. Kandasamy, S. P. A. Devi, *J. Comput. Appl. Mech.* **5** (2004) 21
15. H. Kumar, *Chem. Eng. Comm.* **200** (2013) 1
16. M. F. Modest, *Radiative Heat Transfer*, 2nd ed., Academic Press, New York, 2003, p. 281
17. R. Siegel, J. R. Howell, *Thermal Radiation Heat Transfer*, 4th ed., Taylor & Francis, New York, 2002, p. 2
18. P. Ganesan, P. Loganathan, V. M. Soundalgekar, *Int. J. Appl. Mechan. Eng.* **6** (2001) 719
19. M. N. Özisik, *Radiative Transfer and Interaction with Conduction and Convection*, Wiley, New York, 1972, p. 318
20. H. Kumar, *Therm. Sci.* **13** (2009) 163
21. M. A. Hossain, H. S. Takhar, *Heat Mass Transfer* **31** (1996) 243
22. A. Raptis, C. V. Massals, *Heat Mass Transfer* **34** (1998) 107
23. M. A. Hossain, M. A. Alim, D. A. Rees, *Int. J. Heat Mass Transfer* **42** (1999) 181
24. M. Aboeldahab Emad, *J. Phys. D., Appl. Phys.* **33** (2000) 3180
25. A. Y. Ghaly, E. M. E. Elbarbary, *J. Appl. Math.* **2** (2002) 93
26. R. Muthukumarswamy, G. S. Kumar, *Theoret. Appl. Mech.* **31** (2004) 35
27. M. A. Hossain, *Int. J. Heat Mass Transfer* **35** (1992) 3485
28. C. H. Chen, *Int. J. Eng. Sci.* **42** (2004) 699
29. T. Cebeci, P. Bradshaw, *Momentum transfer in boundary layers*, Hemisphere, New York, USA, 1977
30. T. Cebeci, P. Bradshaw, *Physical and computational aspects of convective heat transfer*, Springer-Verlag, New York, 1988.

Journal of the Serbian Chemical Society
JSCS-info@shd.org.rs • www.shd.org.rs/JSCS
J. Serb. Chem. Soc. 79 (4) 481–494 (2014)
JSCS–4601
UDC 632.954:546.26+544.723:628.161.2
Original scientific paper

Study on the efficient removal of clopyralid from water using a resorcinol–formaldehyde carbon cryogel

MILAN Z. MOMČILOVIĆ[1]*, MARJAN S. RANĐELOVIĆ[2#], ANTONIJE E. ONJIA[1], ALEKSANDRA ZARUBICA[2#], BILJANA M. BABIĆ[1] and BRANKO Z. MATOVIĆ[1#]

[1]*University of Belgrade, Vinča Institute of Nuclear Sciences, P. O. Box 522, 11001 Belgrade, Serbia and* [2]*University of Niš, Faculty of Sciences and Mathematics, Department of Chemistry, Višegradska 33, 18000 Niš, Serbia*

(Received 11 June, revised 3 December 2013)

Abstract: A resorcinol–formaldehyde carbon cryogel was prepared, characterized and used for the removal of the commonly used herbicide clopyralid from aqueous solutions under varying experimental conditions. The carbon exhibited a relatively high specific surface area, significant mesoporosity and an amorphous structure. The following isotherm models were used to interpret the equilibrium data: the Langmuir, Freundlich, Temkin, Dubinin–Radushkevich, Jovanović, Hurkins–Jura and the Helsey Model. Several models fitted the data well although the calculated values for q_{max} poorly correlated with the experimentally obtained data. The pseudo-first and pseudo-second-order kinetic models, the models of Elovich, Bangham and the intraparticle diffusion model were employed for fitting the kinetic data. The rate of the process was fast at the beginning, although the adsorption equilibrium was not attained before 24 h. The adsorption was found to be pH dependent and favored in acidic solutions.

Keywords: clopyralid; carbon cryogel; mesoporosity; adsorption mechanism.

INTRODUCTION

Clopyralid (3,6-dichloro-2-pyridinecarboxylic acid) is an auxin-mimic type of herbicide from the chemical class of pyridine compounds that is used extensively to control broadleaf weeds, particularly those of the *Asteraceae*, *Fabaceae*, *Solanaceae*, *Polygonaceae*, and *Violaceae* families. Clopyralid kills the target weed by mimicking the plant growth hormone auxin (indole acetic acid), and when the dose is administered effectively it causes uncontrolled and disorganized growth of the plant, and its eventual death. Its low ability to bind with soils makes it both highly mobile and a long-term contamination threat to water resources.[1]

* Corresponding author. E-mail: milanmomcilovic@yahoo.com
# Serbian Chemical Society member.
doi: 10.2298/JSC130611151M

The presence of clopyralid was reported in the surface drinking-water supplies of the Northern Great Plains.[2] A growing interest in the removal of clopyralid from water has evolved with its increasing usage in agriculture. Recently, several interesting studies reported the degradation of clopyralid by advanced oxidation processes, such as photocatalysis,[3] treatments with UV/H_2O_2 or ozone[4] and electron beam treatment.[5] However, the removal of this undesirable pesticide from water by application of adsorption techniques has been scarcely examined.

Carbon cryogels (CC) are versatile carbon materials with a developed mesoporous structure. They are synthesized mostly by the sol–gel polycondensation process using, for instance, resorcinol and formaldehyde as precursors, followed by drying of the obtained hydrogels and their carbonization in an inert atmosphere.[6,7] Moderately high surface areas (500–1200 m^2 g^{-1}) and large mesoporous volumes (>0.89 ml g^{-1})[8] are specific features of carbon cryogels, which are sufficient to meet application criteria in catalysis,[9] adsorption,[10] gas separations,[11] double layer capacitors,[12] column packings in HPLC,[13] *etc.*

Adsorption is recognized as an efficient and easy to operate technique that is used in the removal of a broad spectrum of chemical species from contaminated industrial and drinking water. Carbonaceous adsorbents, along with some modified clays and various biosorbents, are most frequently used for commercial purposes. Adsorption onto carbon cryogels has gained prominence for the removal of specific classes of compounds, including some inert and hardly binding pesticides that are resistant to photolysis and spontaneous biodegradation.

In the present paper, the batch adsorption properties for clopyralid removal from aqueous solutions using a synthesized resorcinol–formaldehyde (RF) carbon cryogel are presented and discussed. The experimental conditions were varied, *i.e.*, the initial pesticide concentration, the contact time and solution pH. The obtained data were linearly fitted to several adsorption models in order to establish the model that was the most appropriate to describe clopyralid adsorption.

EXPERIMENTAL

Synthesis and characterization of the RF carbon cryogel

The synthesis was based on the polycondensation of resorcinol with formaldehyde in the presence of sodium carbonate as a basic catalyst. The mole ratios of resorcinol to formaldehyde, resorcinol to water, and resorcinol to catalyst were 0.5, 20 and 100, respectively. The obtained homogenous white mixture was decanted into a glass tube of 10 mm inner diameter, sealed and aged for 2 days at 25 °C, 1 day at 50 °C and 4 days at 85 °C. The formation of the hydrogel is given in Fig. 1. Freeze-drying, according to the procedure of Tamon and coworkers, was used.[14-16] RF gel was immersed in a 10-times volume of *t*-butanol for more than one day to displace the liquid contained in the gels with *t*-butanol. Rinsing with *t*-butanol was repeated twice. The gel was freeze-dried using a Modulyo System (Edwards, England). Gel was frozen in a deep-freeze refrigerator at –30 °C for 24 h. After that, the gel was freeze-dried in the acrylic chambers of the freeze dryer with the shelves mounted directly on the top of the con-

denser of the freeze dryer. The pressure during these 24 h of freeze-drying was around 4 mbar. The obtained cryogel was further carbonized in a conventional furnace, in a protective flow of nitrogen at 800 °C. After pyrolysis, the furnace was cooled down to room temperature under a nitrogen atmosphere. The obtained black material was crushed to powder and kept in a closed PVC bottle.

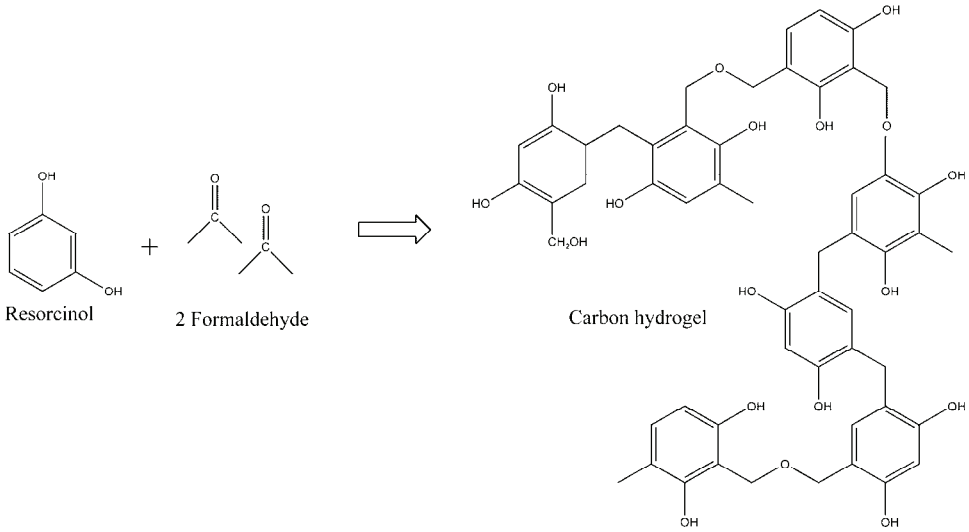

Fig. 1. Synthesis of the carbon cryogel.

The porous properties of the CC were examined by nitrogen adsorption/desorption isotherms obtained at –196 °C, using the gravimetric McBain Method. From the isotherms, the specific surface area (S_{BET}), the pore size distribution, the mesopore area including the external surface area (S_{meso}), and the micropore volume (V_{mic}) were calculated. The pore size distribution was estimated by application of the BJH Method to the desorption branch of the isotherms.[17] The mesopore surface and the micropore volume were estimated using the high resolution α_s-plot method.[18,19] Micropore surface (S_{mic}) was calculated by subtracting S_{meso} from S_{BET}.

The microstructure of the carbon sample was observed using a scanning electron microscope JEOL JSM 5800 LV (Japan). A representative image of micrometric structure of the CC is given in Fig. 2.

The pH_{PZC} of the cryogel suspension, corresponds to the pH value when the carbon surface has zero net charge, was determined using the pH drift method.[20]

Chemicals and solutions

Technical grade clopyralid (99.4 % purity) was purchased from Riedel-de-Haën, resorcinol (99 % purity) from Merck, methanol stabilized formaldehyde (36 % purity) from Fluka Chemie, *t*-butanol (*p.a.* quality) from Centrohem, and sodium carbonate (*p.a.* quality) was purchased from Merck. All the chemicals were used as received without further purification. Deionized water of 18 MΩ cm^{-1} resistivity, obtained from a Milli-Q® Plus Total Water System (Millipore Corporation, Bedford, USA), was used to prepare all the solutions. The chemical structure of clopyralid, including its dimensions, is given in Fig. 3.

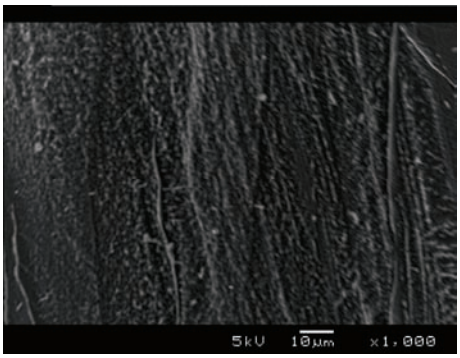

Fig. 2. SEM image of the obtained carbon cryogel.

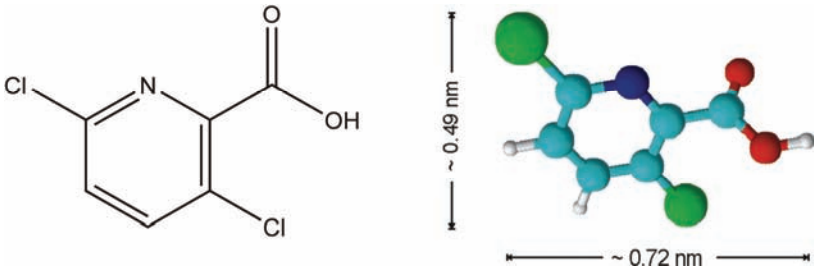

Fig. 3. Structural formula of clopyralid with dimensions.

Clopyralid adsorption

The kinetics of the adsorption were investigated by contacting 30 mg of carbon cryogel with 25 cm^3 of 100 mg dm^{-3} clopyralid solution at 25 °C for different times up to 24 h. The native (unadjusted) pH of the pesticide suspensions were around 3 in all experiments. After contacting, the suspensions were filtered through Macherey-Nagel No. 5 filter paper. The residual concentration of the pesticide in the supernatant was estimated spectrophotometrically by monitoring the absorbance at 280 nm using a Lambda 40 UV/Vis spectrophotometer (Perkin-Elmer Instruments, USA). For the isotherm studies the experiments have been conducted in the same manner by contacting 20 mg of carbon cryogel with clopyralid solutions of different initial concentrations (30–100 mg dm^{-3}) until the equilibrium was attained (24 h). The effect of pH on the adsorption was investigated by contacting 25 mg of carbon with 25 cm^3 of a 100 mg dm^{-3} pesticide solution for 24 h at different initial pH values, from 2 to 12. The pH was measured using a Lutron YK-2001PH LT pH meter (Intelligent Meter, Taiwan). In all the cases, the adsorption capacity, q (mg g^{-1}) was calculated using the equation:

$$q = \frac{(c_0 - c)V}{m} \tag{1}$$

where c_0 (mg dm^{-3}) is the initial clopyralid concentration, V (dm^3) is the volume of the solution, m (g) is the mass of the adsorbent and c (mg dm^{-3}) is the residual pesticide concentration at equilibrium or any time τ (min), which then defines q_e or q_τ (mg g^{-1}), respectively.

RESULTS AND DISCUSSION

Porous properties of CC

The results of the textural analysis of the CC surface are given in Table I. CC exhibited typical type-IV sorption–desorption curves showing a gentle but distinct hysteresis loop. This is characteristic for a material that contains a great deal of mesoporosity, and has a high energy of gas adsorption. The material often contains hysteresis attributed to its mesoporosity. In the present study, the obtained results for S_{BET} are typical and comparable to those reported for mesoporous carbons obtained by similar synthesis approaches.[10] Mesopores are acknowledged to possess an R_p of between 1 and 25 nm, while micropores have an r_p below 1 nm. The pore radius or half the distance across the pore is defined as r_p. Since the pore size distribution gave an r_p value of 2.1 nm, it could be concluded that the dominant number of pores in the CC were within the mesopore size range and this is exactly the reason for considering CCs as suitable mesoporous materials. The determined mesopore surface was 285 m^2 g^{-1}, which is considered large for a carbon material.

TABLE I. Porous properties of the carbon cryogel

Property	Value
S_{BET} / m^2 g^{-1}	517
S_{meso} / m^2 g^{-1}	285
S_{micro} / m^2 g^{-1}	232
r_p / nm	2.1
V_{micro} / m^3 g^{-1}	0.11

Scanning electron microscopy

An SEM image of the CC sample is shown in Fig. 2. Magnifying the figure 1000 times was sufficient to observe the uniform and compact structure of the CC grain. An irregular surface texture could be noticed. In addition, a lamellar structure in the CC grain was assumed present. This would correspond to the parallel network of macropores that leads to pores of smaller dimensions.

Isotherm modeling

The Langmuir Model is defined as:

$$q_e = \frac{K_L c_e}{1 + \alpha_L c_e} \tag{2}$$

which, after linearization, gives:

$$\frac{c_e}{q_e} = \frac{1}{K_L} + \frac{\alpha_L}{K_L} c_e \tag{3}$$

where q_e (mg g^{-1}) and c_e (mg dm^{-3}) are the amount of adsorbate per unit mass of adsorbent and the concentration of unadsorbed adsorbate in solution at equilibrium, respectively. K_L (dm^3 g^{-1}) represents the Langmuir equilibrium constant and K_L/α_L gives the theoretical monolayer saturation capacity, q_0. A plot of c_e/q_e *vs.* c_e gives a straight line of slope α_L/K_L and intercepts $1/K_L$. The essential features of the Langmuir isotherm can be expressed in terms of a dimensionless constant called the separation factor (R_L) which is according to the following equation:

$$R_L = \frac{1}{1 + K_L c_0} \tag{4}$$

where c_0 (mg dm^{-3}) is the initial adsorbate concentration and α_L (dm^3 mg^{-1}) is the Langmuir constant related to the energy of the adsorption. The value of R_L indicates the shape of the isotherms and could be unfavorable ($R_L > 1$), linear ($R_L = 1$), favorable ($0 < R_L < 1$) or irreversible ($R_L = 0$).[21]

The Freundlich Model is used to describe adsorption onto heterogeneous surfaces where the adsorbate species are bound with different binding energies. It is represented by the equation:

$$q_e = K_F c_e^{1/n} \tag{5}$$

which, after linearization, becomes:

$$\log q_e = \log K_F + \frac{1}{n} \log c_e \tag{6}$$

The lower fractional value of $1/n$ ($0 < 1/n < 1$) indicates that some weak adsorptive forces are effective on the surface of the adsorbent.[21]

The Temkin Model is presented as:

$$q_e = \frac{RT}{b} \ln(K_T c_e) \tag{7}$$

After linearization, its form becomes:

$$q_e = \frac{RT}{b} \ln K_T + \frac{RT}{b} \ln c_e \tag{8}$$

where constant K_T (dm^3 mg^{-1}) corresponds to the maximum binding energy, the constant $B = RT/b$ represents the heat of adsorption, while $1/b$ indicates the adsorption potential of the adsorbent. This model generally emphasizes that the adsorption process occurs through indirect adsorbate–adsorbate interactions.[21]

Dubinin–Radushkevich (D–R) isotherm postulates a fixed volume or "sorption space" close to the sorbent surface where sorption occurs. This very often-used model is based on the equation:

$$q_e = q_{ads} \exp(-k_{ad} \varepsilon^2) \tag{9}$$

It is applied in its linearized form as:

$$\ln c_{ads} = \ln q_{ads} - k_{ads}\varepsilon^2 \quad (10)$$

where ε is the Polanyi sorption potential ($\varepsilon = RT \ln(1 + 1/c_e)$) equal to the energy required to pull a sorbed molecule from its sorption site to infinity. β (mol^2 kJ^{-2}) is the activity coefficient related to the mean adsorption free energy E (kJ mol^{-1}), which is defined as the free energy change required to transfer 1 mol of substance from solution to the solid surfaces.[22] This relation is given as:

$$E = \frac{1}{\sqrt{-2\beta}} \quad (11)$$

The value of E of the Dubinin–Radushkevich Equation ranges from 1 to 8 kJ mol^{-1} for physical adsorption and from 8 to 16 kJ mol^{-1} for chemical adsorption and ion exchange.

The Jovanović Model was developed to explain monolayer adsorption.[23] It is given as:

$$q_e = q_{max}(1 - \exp(-K_J c_e)) \quad (12)$$

and in linear form by:

$$\ln q_e = \ln q_{max} - K_J c_e \quad (13)$$

The Hurkins–Jura Model accounts for multilayer adsorption and can be explained by the existence of a heterogeneous pore distribution. It is given by:[23]

$$q_e = \left(\frac{A_H}{B_2 - \log c_e} \right)^{1/2} \quad (14)$$

and in linear form

$$\frac{1}{q_e^2} = \frac{B_2}{A_H} - \frac{1}{A_H} \log c_e \quad (15)$$

Fitting of the experimental data to the equation of the Hasley Model attests to the heteroporous nature of the adsorbent and multilayer adsorption.[23] This model is represented as:

$$q_e = \exp\left(\frac{\ln K_H + \ln c_e}{n} \right) \quad (16)$$

and in linear form:

$$\ln q_e = \frac{\ln K_H}{n} + \frac{1}{n} \ln c_e \quad (17)$$

The Temkin Model showed quite good fitting to the equilibrium data, indicating indirect interactions between the CC surface and the adsorbate. The

Langmuir Model, which is the most indicative proof of monolayer adsorption, also gave a high correlation coefficient. The determined separation factor R_L (0.44) indicates a favorable adsorption process (Table II).

TABLE II. Isotherm parameters for the adsorption of clopyralid onto the carbon cryogel

Parameter	Value	Parameter	Value
Langmuir		Jovanović	
K_L / L g^{-1}	0.013	q_{max} / mg g^{-1}	5.805
q_{max} / mg g^{-1}	32.2	K_j	0.014
R_L	0.44	r^2	0.895
r^2	0.971	Hurkins–Jura	
Freundlich		A_H	–34.542
K_F / (mg g^{-1}) (L mg^{-1})$^{1/n}$	0.975	B_2	–1.962
n	1.52	r^2	0.887
r^2	0.980	Halsey	
Temkin		K_H	0.914
K_T / L mg^{-1}	0.117	n	1.52
B	7.231	r^2	0.981
r^2	0.991		
Dubinin–Radushkevich			
q_{max} / mg g^{-1}	22.6		
E / kJ mol^{-1}	1.47		
r^2	0.991		

The value of adsorption free energy in the Dubinin–Radushkevich Model ranges from 1 to 8 kJ mol^{-1} for physical adsorption and from 8 to 16 kJ mol^{-1} for chemical adsorption and ion exchange.[24] Since in the present study, the calculated energy value was 1.47 kJ mol^{-1}, physisorption interactions are probably most important for the binding of the adsorbate to the CC surface. In this context, van der Waals forces are the most probable. A molecule of clopyralid in acidic solutions, where the uptake is the most expressed, is rarely dissociated. In contact with the CC surface, polarization of the charge in the clopyralid molecule occurs and correlates the attraction to the active site on the CC surface, which is the most probable scenario for the binding and overall removal of this pesticide.

The Langmuir, D–R and Jovanović models indicate certain theoretical values of maximum adsorption capacities. In this work, large disagreement between the calculated and experimentally obtained values was registered. This refers to the inability of the models that were used to interpret the specific adsorption of clopyralid in an adequate manner under the applied conditions.

As can be seen from Fig. 4, an almost linear adsorption isotherm was present in the case of the studied adsorption. Such a shape indicates that the availability of sites remains constant at all the examined concentrations, without reaching a saturation level. This situation could arise when the solute has a higher affinity

for the substrate molecules than the solvent itself. With its molecular dimensions (Fig. 3), clopyralid could penetrate into the structure of the substrate in regions (narrow hydrophobic pores) that had not already been penetrated by the solvent; thus, the linear isotherm indicates that the solute penetrates into the regions that are inaccessible to the solvent.[25]

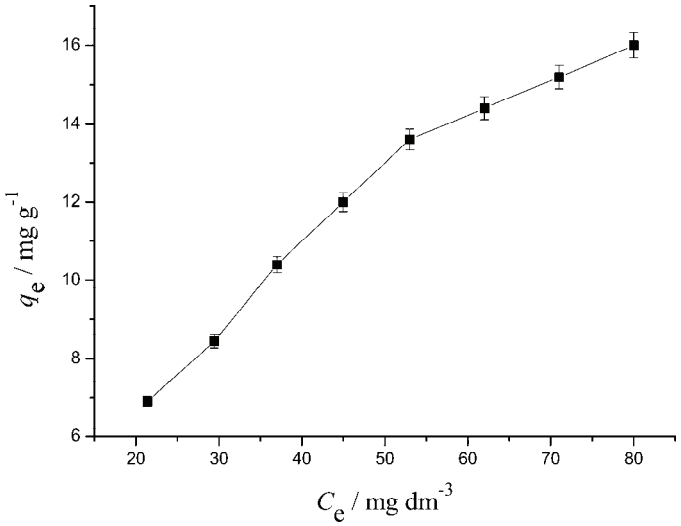

Fig. 4. Adsorption isotherm of clopyralid onto the carbon cryogel.

Adsorption kinetics

To evaluate the kinetic mechanism that controls an adsorption process, it is well-established that several theoretical models should be used. The applicability of the pseudo-first-order, the pseudo-second-order model, the Elovich Model, the Bangham Model and the intraparticle diffusion model were tested for the adsorption of clopyralid onto CC. The best-fit model was selected based on the values of the linear regression correlation coefficients, r^2.

A linear form of the pseudo-first-order model was defined by Lagergren as:

$$\ln(q_e - q_\tau) = \ln q_e - k_1\tau \quad (18)$$

where k_1 (min^{-1}) is the rate constant of pseudo-first-order adsorption.[26] The slope of the linear plots of $\ln(q_e - q_\tau)$ *vs.* τ was used for the determination of q_e and k_1.

The Ho pseudo-second-order kinetics is represented in its linearized form as:

$$\frac{\tau}{q_\tau} = \frac{1}{k_2 q_e^2} + \frac{1}{q_e}\tau \quad (19)$$

This is an indicator of the chemisorption nature of the adsorption process. In Eq. (19), k_2 (g mg^{-1} min^{-1}) is the equilibrium rate constant for pseudo-second order adsorption.[27]

The Elovich Model describes a number of reaction mechanisms, including bulk and surface diffusion and the activation and deactivation of catalytic surfaces.[22] It is represented as:

$$q_\tau = \frac{1}{\beta}\ln(\alpha\beta) + \frac{1}{\beta}\ln\tau \tag{20}$$

where α (mg g^{-1} min^{-1}) and β (g mg^{-1}) are adsorption constants and are determined from a plot q_τ *vs.* ln τ.[21]

The applicability of the Bangham kinetic model was tested using the equation:

$$\log\log\left(\frac{c_0}{c_0 - q_\tau m}\right) = \log\left(\frac{k_0 m}{2.303V}\right) + \alpha\log\tau \tag{21}$$

where V the volume of solution (cm^3), m is the adsorbent dose (g dm^{-3}) and α and k_0 are constants. A plot of log log (c_0/(c_0–$q_\tau m$)) *vs.* log τ confirmed the applicability of the Bangham Equation and indicated that diffusion of clopyralid into the CC pores mainly controled the adsorption process.[28]

The possibility of adsorptive diffusion in the volume of the particles of the adsorbent was explored using the intraparticle diffusion model, which is given as:

$$q_\tau = k_\mathrm{i}\tau^{1/2} + C \tag{22}$$

where k_i (g mg^{-1} min^{-1}) is the intraparticle diffusion rate constant and C is a constant, which reflects the boundary effect.[27]

In the present study, several models fitted the experimental data well with quite high correlation coefficients (Table III). The theoretical maximum saturation capacity calculated under the pseudo-second-order model corresponded to the experimental values the best. Under all the other conditions, high disagreement was observed. The good fitting to the Bangham Model emphasized the importance of diffusion in the adsorption kinetics.

Considering the adsorption mechanism, it might be postulated that certain electrostatic attractions between the solute and the adsorbent occur. CC is considered as a complex carbonaceous matrix composed of regions of hydrophobic microcrystallites scattered in an irregular 3D structure. These are interconnected by various functional groups present at the edges of the graphene layers. Electron-rich regions located in the graphene layers could interact with the π electrons of the aromatic ring of pesticide. The two chlorine atoms in the clopyralid molecule act as electron-acceptor substituents and deplete the electron charge in the graphene rings, forming partially positive charges. Therefore, electostatic inter-

actions between the partially negative benzene rings of clopyralid with the negative charge of the graphene layers are probable. The retained pesticide molecules are most likely adsorbed flat onto carbon surface or within its pores.

TABLE III. Comparison for kinetic parameters for adsorption of clopyralid onto the carbon cryogel

Parameter	Value
Pseudo-first-order	
k_1 / min^{-1}	0.186
q_e / mg g^{-1}	8.8
r^2	0.980
Pseudo-second-order	
k_2 / g mg^{-1} min^{-1}	0.061
q_e / mg g^{-1}	37.0
r^2	0.9997
Elovich	
α / mg g^{-1} min^{-1}	102534.3
β / g mg^{-1}	0.376
r^2	0.975
Bangham	
k_0	35.914
α	0.109
r^2	0.971
Intraparticle diffusion	
k_i / g mg^{-1} min^{-1}	2.222
r^2	0.842

Effect of pH

The solution pH is an important factor that could affect the interactions of the adsorbent surface and the molecules of an adsorbate. The effect of the initial pH on the adsorption of clopyralid onto CC under the given experimental conditions is shown in Fig. 5. At first sight, the strong dependence of the adsorption on the solution pH is obvious. It is evident that at pH values under 6, the adsorption capacity is much higher. As for many carbon materials including CC, the existence of various organic functional groups on their surface has been established. Groups such as carboxylic, phenolic, lactonic, pyrrolic, hydrophilic, *etc*. play the main role in their surface reactivity. All those groups are deprotonated and negatively charged in strongly basic solutions. The pH_{PZC} of the carbon cryogel was determined earlier using the pH drift method and a value of 10.5 was found. This means that under this pH value, surface of this material is dominantly positively charged. This is in accordance with the rule: the more acidic the solution is, the more positive charges on the surface exist.

Acidic characteristics of clopyralid are defined by the acidity constant $pK_a \approx 2.1$ at 25 °C. Having such acidic properties, the clopyralid molecule is

almost completely dissociated in water at pH values above 3, and so bears a negative charge.[29] Hence, certain electrostatic attractions between the positively charged CC surface and the negatively charged clopyralid molecule occur over a wide range of pH values, especially in acidic conditions. With increasing pH, the positive charge at the CC surface decreases, thereby reducing the uptake of clopyralid. Celis and coworkers also reported a higher uptake of clopyralid in acidic solutions under adsorption onto montmorillonite–chitosan bionanocomposites.[30]

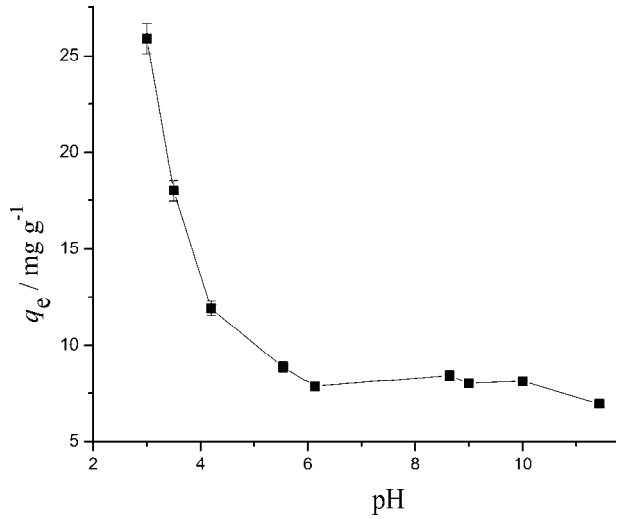

Fig. 5. Effect of pH on the adsorption of clopyralid onto the carbon cryogel.

CONCLUSIONS

A resorcinol–formaldehyde carbon cryogel that was synthesized in this study exhibited a pronounced adsorption affinity towards the commonly used pesticide clopyralid under batch adsorption conditions. Characterization of the synthesized carbon cryogel revealed it a porous carbon material with an amorphous structure, a considerably high specific surface area and developed mesoporosity, which is particularly important for the adsorption of pesticides. Although a set of seven isotherm models fitted the adsorption results well in most cases, the predicted values for the maximum adsorption capacities showed considerable disagreement with the experimental data. The maximum adsorption capacity, experimentally obtained from isotherm studies, was 16 mg g^{-1}. The adsorption process is considered slow since equilibrium was only fully attained after 24 h of contact. However, most of the uptake was related to the first few hours of the process. The effect of solution pH was noticeable and defined, the uptake being favored under acidic conditions. This was attributed to a probable electrostatic attractions between the positively charged cryogel surface and the dissociated clopyralid molecule. Another possibility of electrostatic interactions is based on the inter-

actions between a partial positive charge on the clopyralid molecule and a negative charge on the graphene layers of the CC.

Acknowledgements. This study was conducted under the Interdisciplinary Project III 43009 funded by the Ministry of Education, Science and Technological Development of the Republic of Serbia.

И З В О Д

ЕФИКАСНО УКЛАЊАЊЕ КЛОПИРАЛИДА ИЗ ВОДЕ ПОМОЋУ РЕЗОРЦИНОЛ-ФОРМАЛДЕХИДНОГ УГЉЕНИЧНОГ КРИОГЕЛА

МИЛАН З. МОМЧИЛОВИЋ[1], МАРЈАН С. РАНЂЕЛОВИЋ[2], АНТОНИЈЕ Е. ОЊИА[1], АЛЕКСАНДРА ЗАРУБИЦА[2], БИЉАНА М. БАБИЋ[1] и БРАНКО З. МАТОВИЋ[1]

[1]*Универзитет у Београду, Институт за нуклеарне науке „Винча“, п. пр. 522, 11001 Београд и* [2]*Универзитет у Нишу, Природно–математички факултет, Одсек за хемију, Вишеградска 33, 18000 Ниш*

Резорцинол-формалдехидни угљенични криогел је припремљен, окарактерисан и употребљен за уклањање често коришћеног пестицида под именом клопиралид из водених раствора при различитим експерименталним условима. Добијени угљенични материјал поседује релативно велику специфичну површину, аморфну структуру и има значајан удео мезопорозности. У раду је коришћен низ модела адсорпционих изотерми за интерпретацију равнотежног стања, и то: Ленгмиров, Фројндлихов, Тјомкинов, Дубинин–Радушкевичев, Јовановићев, Хуркинс–Јурин и Хелсијев модел. Иако је неколико модела показало добро поклапање са теоријским моделима уз високе корелационе коефицијенте, предвиђене вредности за q_e се слабо слажу са експериментално измереним вредностима. Кинетички модели псеудо-првог и псеудо-другог реда, Еловичев модел, Бангамов модел и модел унутарчестичне дифузије су коришћени за фитовање кинетике. Брзина процеса је на почетку велика, а до успостављања адсорпционе равнотеже долази после 24 h. Утврђено је да процес адсорпције зависи од и pH, као и да је фаворизован у киселој средини.

(Примљено 11. јуна, ревидирано 3. децембра 2013)

REFERENCES

1. M. Tu, C. Hurd, J. M. Randal, *The Nature Conservancy*, *Weed Control Methods Handbook: Tools and Techniques for Use in Natural Areas*, 2001, All U.S. Government Documents (Utah Regional Depository), Paper 533, http://digitalcommons.usu.edu/ /govdocs/533
2. D. B. Donald, A. J. Cessna, E. Sverko, N. E. Glozier, *Environ Health Perspect*. **115** (2007) 1183
3. D. V. Šojić, V. B. Anderluh, D. Z. Orčić, B. F. Abramović, *J. Hazard. Mater*. **168** (2009) 94
4. C. Tizaoui, K. Mezughi, R. Bickley, *Desalination* **273** (2011) 197
5. G. Xu, T. Bu, M. Wu, J. Zheng, N. Liu, L. Wang, *J. Radioanal Nucl Chem*. **288** (2011) 759
6. K. Kraiwattanawong, S. R. Mukai, H. Tamon, A. W. Lothongkum, *Microporous Mesoporous Mater*. **98** (2007) 258
7. H. Nishihara, S. R. Mukai, H. Tamon, *Carbon* **42** (2004) 885

8. N. Tonanon, W. Tanthapanichakoon, T. Yamamoto, H. Nishihara, S. R. Mukai, H. Tamon, *Carbon* **41** (2003) 2981
9. A. Smirnova, X. Dong, H. Hara, A. Vasiliev, N. Sammes, *Int. J. Hydrogen Energ.* **30** (2005) 149
10. S. Kim, T. Yamamoto, A. Endo, T. Ohmori, M. Nakaiwa, *Microporous Mesoporous Mater*. **96** (2006) 191
11. T. Yamamoto, A. Endo, T. Ohmori, M. Nakaiwa, *Carbon* **42** (2004) 1671
12. B. Babic, B. Kaludjerovic, L. Vracar, N. Krstajic, *Carbon* **42** (2004) 2617
13. T. Yamamoto, T. Sugimoto, T. Suzuki, S. R. Mukai, H. Tamon, *Carbon* **40** (2002) 1345
14. H. Tamon, H. Ishizaka, T. Yamamoto, T. Suzuki, *Carbon* **37** (1999) 2049
15. T. Yamamoto, T. Sugimoto, T. Suzuki, S. R. Mukai, H. Tamon, *Carbon* **40** (2002) 1345
16. H. Tamon, H. Ishizaka, T. Yamamoto, T. Suzuki, *Carbon* **38** (2000) 1099
17. E. P. Barret, L. G. Joyner, P. P. Halenda, *J. Am. Chem. Soc*. **73** (1951) 373
18. K. Kaneko, C. Ishii, M. Ruike, H. Kuwabara, *Carbon* **30** (1992) 1075
19. M. Kruk, M. Jaroniec, K. P. Gadakaree, *J. Colloid Interface Sci*. **192** (1997) 250
20. D. Prahas, Y. Kartika, N. Indraswati, S. Ismadji, *Chem. Eng. J*. **140** (2008) 32
21. M. Momčilović, M. Purenović, A. Bojić, A. Zarubica, M. Ranđelović, *Desalination* **276** (2011) 53
22. M. Akhtar, S. M. Hasany, M. I. Bhanger, S. Iqbal, *Chemosphere* **66** (2007) 1829
23. M. R. Samarghandi, M. Hadi, S. Moayedi, F. Barjasteh Askari, *Iranian J. Environ. Health Sci. Eng.* **6** (2009) 285
24. M. Ranđelović, M. Purenović, A. Zarubica, J. Purenović, B. Matović, M. Momčilović, *J. Hazard. Mater*. **199** (2012) 367
25. C. H. Giles, T. H. MacEwans, N. Nakhwa, D. D. Smith, *J. Chem. Soc*. (1960) 3973
26. B. H. Hameed, A. L. Ahmad, K. N. A. Latiff, *Dyes Pigm.* **75** (2007) 143
27. Y. Bulut, H. Aydın, *Desalination* **194** (2006) 259
28. V. K. Gupta, I. Ali, Suhas, V. K. Saini, *J. Colloid Interface Sci*. **299** (2006) 556
29. B. F. Abramović, V. B. Anderluh, D. V. Šojić, F. F. Gaál, *J. Serb. Chem. Soc.* **72** (2007) 1477
30. R. Celis, M. A. Adelino, M. C. Hermosín, J. Cornejo, *J. Hazard. Mater*. **209** (2012) 67.

Journal of the Serbian Chemical Society
JSCS-info@shd.org.rs • www.shd.org.rs/JSCS
J. Serb. Chem. Soc. *79* (4) 495–508 (2014)
JSCS–4602
UDC **Pseudomonas aeruginosa*:66.081.2.000.57:546.482'817+54–145.2:536.5
Original scientific paper

Bio-adsorption characteristics of *Pseudomonas aeruginosa* PAO1

ANIKÓ KŐNIG-PÉTER[1], BÉLA KOCSIS[2], FERENC KILÁR[1,4] and TÍMEA PERNYESZI[3,4]*

[1]*Institute of Bioanalysis, University of Pécs, Faculty of Medicine, 12 Szigeti, H-7624 Pécs, Hungary,* [2]*Institute of Medical Microbiology and Immunology, University of Pécs, Faculty of Medicine, Szigeti út. 12, H-7624, Pécs, Hungary,* [3]*Department of Analytical and Environmental Chemistry, Faculty of Science, Ifjúság u. 6, H-7624 Pécs, Hungary and* [4]*Analytical Chemistry and Geoanalytical Research Group, Szentágothai Research Center, University of Pécs, H-7624 Pécs, Ifjúság útja 20, Hungary*

(Received 14 March 2012, revised 21 June 2013)

Abstract: Biosorption of Cd(II) and Pb(II) ions from aqueous solution using lyophilized *Pseudomonas aeruginosa* PAO1 cells were observed under various experimental conditions. The effect of pH, initial metal concentration, equilibration time and temperature on bio-adsorption was investigated. The optimum pH value for Pb(II) adsorption was found to be 5.0, and for Cd(II) 5.0–6.0. The Pb(II) and Cd(II) bio-adsorption equilibrium were analyzed employing the Freundlich and Langmuir Models using nonlinear least-squares estimations. The experimental maximum uptake capacity of Pb(II) and Cd(II) was estimated to be 164 and 113 mg g^{-1}, respectively. For a kinetic study of the biosorptions, the pseudo second-order kinetic model was applied at various temperatures. The temperature had no significant effect on Pb(II) bio-adsorption. In case of Cd(II) bio-adsorption, the adsorbed amount decreased with increasing temperature.

Keywords: heavy metals, kinetics, isotherm, temperature, atomic absorption spectrometer.

INTRODUCTION

Heavy metal pollution is one of the most important environmental problems today. In recent years, the biotechnology applied to control and remove metal pollution has received much attention, and gradually, becomes a hot topic in the field of metal pollution control because of its potential application. For heavy metal removal, an alternative process is biosorption, which utilizes various certain natural materials of biological origin, including bacteria, fungi, yeast and algae. These biosorbents possess metal-sequestering properties and can be used

* Corresponding author. E-mail: ptimea@gamma.ttk.pte.hu
doi: 10.2298/JSC130314070K

to remove rapidly heavy metal ions from dilute complex solutions with high efficiency; therefore, they are ideal candidates for the treatment of high volume and low concentration of complex wastewaters. In general, removal of chemical pollutants from aqueous solution is difficult at low pollutant concentrations. Most of the industrial techniques are ineffective and excessively expensive at the metal concentration less than 100 mg mL^{-1}.[1] Therefore, studies on biosorption have become an active field for the removal of metal ions or organic compounds.[2,3]

The capability of some living microorganisms to accumulate metallic elements was observed at first from a toxicological point of view. However, inactive/dead microbial biomass can also passively bind metal ions *via* various physicochemical mechanisms. The mechanisms responsible for biosorption may be one or combination of ion exchange, complexation, coordination, adsorption, electrostatic interaction, chelation and microprecipitation.[2,4] The uptake of heavy metals by biomass is usually classified into three categories: 1) cell surface binding, 2) intracellular accumulation and 3) extra-cellular accumulation.[2,5,6] Being metabolism-independent, the cell surface binding can occur in either living or in inactivated microorganisms, whereas the intracellular and extra-cellular accumulation of metals are usually energy-driven processes, and thus can occur in living cells. [7]

Several investigations have reported that *Pseudomonas aeruginosa* displays efficiency for metal uptake.[8–10] Chang and Chen studied the biosorption of copper(II), lead(II) and cadmium(II) ions on *P. aeruginosa* and the multi-metal adsorption results showed that lead(II) and copper(II) significantly inhibited the adsorption of cadmium(II), while the effects of cadmium(II) on the adsorption of copper(II) and lead(II) was limited.[11] They also reported the combined effects of two or more metal ions on inactivated *P. aeruginosa*, which depended on the number of the metals competing for binding sites, metal combination, levels of metal ion concentration, order of metal addition, and residence time.[11,12] Leung *et al*. selected *Pseudomonas* as a biosorbent for lead(II), copper(II) and nickel(II), among 12 bacteria isolated from activated sludge. They reported the maximum sorption capacities of 271.7 and 46.8 mg g^{-1} for lead(II) and copper(II) ions, respectively.[13] The order of affinity of the three metals toward *P. pseudoalcaligenes* was Ni < Cu < Pb. Gialamouidis *et al.* compared *Pseudomonas* sp. (Gram-negative) and *Staphylococcus xylosus* (Gram-positive) isolated from contaminated soil for the removal of Ni(II) in aqueous solution. Desorption experiments by treating biomass with 0.1 M HNO_3 solution resulted in more than 87 % recovery of the adsorbed Ni(II) ions from *Pseudomonas* sp. and almost 98 % from *S. xylosus*, indicating that Ni(II) could be easily and quantitatively recovered from biomass, as well.[14] Kang *et al.* studied Cr(III) and Cr(VI) biosorption onto the cell surface of *P. aeruginosa.* Batch experiments were conducted with various initial concentrations of chromium ions to obtain the sorption capacity and iso-

therm. It was found that the sorption isotherms of Cr(III) were described well by the Langmuir isotherm model, while Cr(VI) appeared to fit the Freundlich model. The results of FT-IR analysis suggested that the chromium binding sites on the bacterial cell surface were most likely carboxyl and amino groups. The bacterial surface of *P. aeruginosa* seemed to engage in reductive and adsorptive reactions with respect to Cr(VI) biosorption.[15] *Pseudomonas* genus plays an important role in bio-adsorption studies, a genus including members with well-characterized biochemical and genetic characteristics, and for which a considerable range of genetic tools are available. In addition, the resistance against antibiotics by many strains was well described.[16] *Pseudomonas* strains can protect plant roots from an excess of heavy metal ions in the soil.[17] However, many studies use *Pseudomonas* strains isolated from contaminated soil and water,[18–21] and in the case of living cells, the risk of multiplication of multi-resistant cultures is high.[22,23]

In this study, the biosorption characteristics of lyophilized *P. aeruginosa* PAO1 laboratorial bacterial strain for cadmium(II) and lead(II) ions in aqueous suspension is presented. The effect of pH, contact time and initial heavy metal concentrations on the biosorption were investigated for both cations. This microbiologically well-characterized *P. aeruginosa* PAO1 laboratorial bacterial strain as biosorbent has not hitherto been studied for the sorption of lead(II) and cadmium(II). The effect of temperature is less studied field in the field of biosorption of metal cations.

EXPERIMENTAL

Bacterial strain and cultivation

The microorganism used in this study was *P. aeruginosa* PAO1. The strain was cultivated in Mueller–Hinton broth (Difco, Germany) using shaken flasks. They were incubated at 37 °C and the liquid cultures were agitated at 220 rpm. The reproduction curve was determined by spectrophotometry (Spectronic, Genesys 5, Milton Roy Company, USA) using the OD_{600} value (optical density at λ = 600 nm). The optical density of the bacterial cell suspension is presented against the incubation time in Fig. 1. The aim of broth dilution methods is to determine the lowest concentration of the assayed metal cations (minimal inhibitory concentration, *MIC*) that, under defined test conditions, inhibits the visible growth after overnight incubation of the bacterium under investigation. MIC values are used to determine the susceptibilities of bacteria to metal cations. For broth dilution, bacteria are inoculated into a liquid growth medium in the presence of different concentrations of metal cations.[24] The *MIC* values were determined by the broth dilution method using 96 mmol L^{-1} initial heavy metal concentrations. The concentrations were 96, 48, 24, 12, 6, 3 and 1.5 mmol L^{-1}. The *MIC* values were determined after solid plate cultivation and the colony formation was compared with that of a control culture.

Preparation of biosorbents

The cells were harvested by centrifugation (10000 rpm, 30 min) at the early-stationary phase of growth, after 38 h incubation. The cells were rinsed twice with physiological saline solution, centrifuged and then lyophilized at –40°C in a freeze drier (HETO, Dry Winner, Denmark).

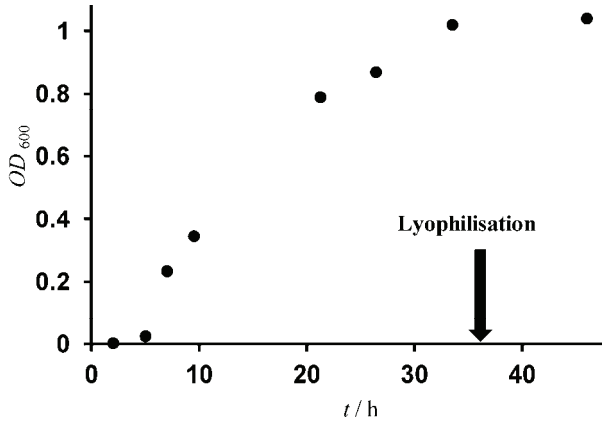

Fig. 1. Time-course profiles of the growth of *P. aeruginosa* PAO1 cells.

Preparation of heavy metal solutions

The heavy metal test solutions containing Pb(II) and Cd(II) ions were prepared from $Pb(NO_3)_2$ (Fluka, Germany) and $Cd(NO_3)_2 \cdot H_2O$ (Fluka, Germany) in the concentration range 5–250 mg L^{-1}. All employed chemicals were of analytical grade. The pH values of the adsorption systems were adjusted using 0.1 M NaOH and 0.1 M HCl solutions.

Analysis of heavy metals

The concentration of heavy metals in the solutions was measured by atomic absorption spectrometry (AAS, Perkin-Elmer 2380) at 217 nm for Pb(II) and 228 nm for Cd(II). Before measurement, the heavy metal solutions were diluted with deionized water to ensure that the heavy metal concentration in the sample was linearly dependent on the absorbance detected. The calibration of Cd(II) and Pb(II) was made with standard cadmium(II) and lead(II) solution (Scharlau, Germany) in the concentration range of 0–2.5 mg L^{-1} for Cd(II) and for Pb(II) 0–20 mg L^{-1}.

Effect of pH on biosorption

The effect of pH on the adsorption Cd(II) and Pb(II) by *P. aeruginosa* PAO1 biomass in aqueous suspension was investigated. To determine the optimum pH range of bio-adsorption, adsorption measurements with 25 and 50 mg L^{-1} solutions were performed for both Cd(II) and Pb(II) ions in the pH range of 3.0–8.0. The suspension concentration was 1 g L^{-1}. The expected pH was regulated with 0.1 M NaOH and 0.1 M HCl solutions, then the adsorption systems were agitated at 250 rpm. After 24 h, samples were taken from the adsorption systems and were spin-dried at 10,000 rpm for 10 min and diluted for analysis by atomic absorption spectrometry.

Kinetics study of biosorption

In the kinetics study of Cd(II) and Pb(II) biosorption by *P. aeruginosa*, the concentration of Cd(II) and Pb(II) ions were 50 mg L^{-1} at a suspension concentration of 1 g L^{-1}. Samples were taken from the solutions at desired time intervals and the metal concentrations of the supernatants were measured after centrifugation. The supernatants were spin-dried at 10,000 rpm for 10 min and diluted for analysis by flame atomic absorption spectrometry.

Determination of bio-adsorption isotherms

The biomasses (1 g L^{-1}) were suspended in heavy metal solutions in glass containers that were gently agitated at room temperature. Solutions in the concentration range 5–250 mg L^{-1} were used for the determination of adsorption isotherms for Pb(II) and Cd(II). After 24 h incubation, samples were taken from the suspensions, the biomass was separated from the heavy metal solution at 10,000 rpm for 5 min, and then the heavy metal content of the supernatant was measured by AAS. The metal uptake was calculated using the following equation:

$$q = \frac{(c_0 - c_e)V}{m} \quad (1)$$

where q is the adsorbed amount of heavy metals (mg g^{-1}), c_0 is the initial heavy metal concentration (mg L^{-1}), c_e is the heavy metal concentration at adsorption equilibrium (mg L^{-1}), V is the volume of the solution (L) and m is the mass of biosorbent (g).

All experiments were performed in triplicate.

For equilibrium modeling, the following isotherm equations were used:

Langmuir isotherm. The Langmuir isotherm is valid for monolayer adsorption onto a surface with a finite number of identical sites. It is given as Eq. (2):

$$q_e = \frac{q_{max} b c_e}{1 + b c_e} \quad (2)$$

where b is the adsorption equilibrium constant including the affinity of the binding sites (L mg^{-1}), c_e and q_e are the non-adsorbed metal ions in solution and adsorbed metal ions on the biosorbent at equilibrium, respectively, q_{max} is the maximum amount of metal ion per unit weight of adsorbent required to form a complex monolayer on the surface (mg g^{-1}).[2,3,7,12,25]

Freundlich isotherm. The Freundlich Equation, based on sorption on a heterogeneous surface, is given as Eq. (3):

$$q_e = k_F c_e^{1/n} \quad (3)$$

where k_F and n are the Freundlich constants, which are indicators of the adsorption capacity and adsorption intensity of the sorbents, respectively. The Freundlich isotherm provides no information on the monolayer adsorption capacity, whereas the Langmuir model does.[26,27]

RESULTS AND DISCUSSION

Determination of the lowest inhibitory concentration for cadmium(II) and lead(II) ions

Free cells of *Pseudomonas aeruginosa* were cultivated in aqueous solutions containing heavy metals at various concentrations. The determined *MIC* values for cadmium(II) and Pb(II) were 20 and 12 mmol L^{-1}, respectively. These values are similar to that previously reported for *P. aeruginosa* (15 mmol L^{-1}) for Pb(II).[28] A growth medium having a complex rich composition (Mueller–Hinton broth) was used, which resulted in a high level of complexation between the metal cations and components of the growth medium. The residual concentrations of supernatant in the heavy metal stock solutions were determined after centrifugation. Due to precipitation, the *MIC* value was found to be 6 mmol L^{-1} for

cadmium(II) and 1.8 mmol L^{-1} for lead(II). The concentrations of metal cations employed in this study do not inhibit bacterial proliferation.

The effect of pH on cadmium(II) and lead(II) bio-adsorption

It has been shown that the affinity of cationic species towards functional groups present in the cellular surface is strongly dependent on the pH.[29] The results of Cd(II) and Pb(II) adsorption by *P. aeruginosa* bacterial cells as a function of pH at initial concentrations of 25 and 50 mg L^{-1} are summarized in Fig. 2a and b. In all cases, metal uptake by the biomass increased with increasing pH until a maximum was reached, after which the metal uptake decreased for Pb(II). For Pb(II), the results could be influenced by precipitation above pH 7. For Cd(II), the adsorbed amount did not decrease in the pH range 6−8. The bacterial cell wall contains negatively charged functional groups, such as carboxyl, phosphate, imidazole and amino groups. They are primarily responsible for the

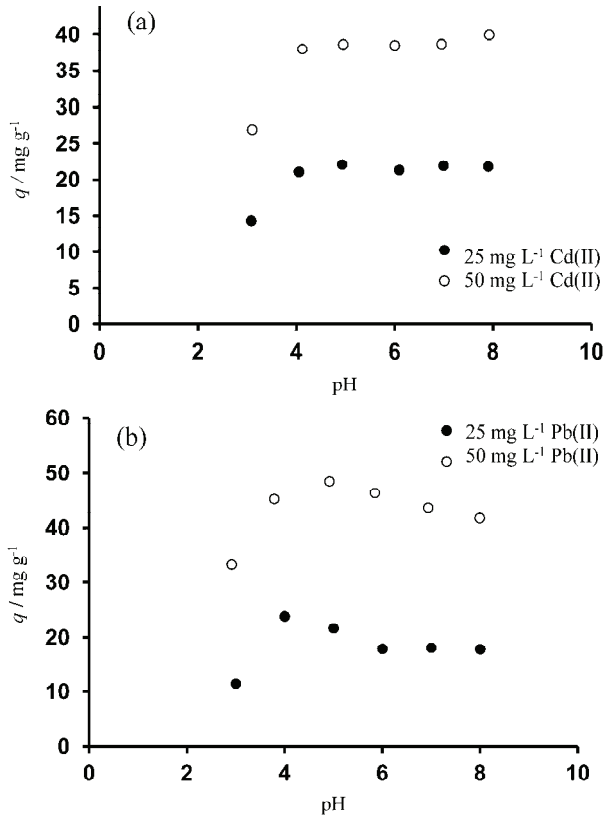

Fig. 2. Effect of pH on (a) Cd(II) and (b) Pb(II) biosorption by *P. aeruginosa* PAO1 bacterial biomass. Initial metal ion concentrations, 25 and 50 mg L^{-1}; contact time, 24 h; biomass concentration, 1 g L^{-1}; temperature, 285 K.

anionic character and metal binding capacity of the cell wall by Gram-negative bacteria.[30] With increasing pH, the negative charge on the cell surface increases, which favors the adsorption of the heavy metal cations. Strong acidic pH range (pH < 3) is not appropriate for adsorption due to protonation. In addition, metal ions undergo hydrolysis as the pH increases and highly alkaline pH values (pH > > 8) results in metal precipitation. Hence, the effect of pH was determined in the pH range 3.0–8.0. Optimum pH values were found to be 5.0–6.0 for cadmium(II) and about 5.0 for lead(II) biosorption. Other researchers, such as Chang *et al.* reported that the optimal pH values for inactivated and resting cells of *P. aeruginosa* PU21 were 5.5 for lead(II) and 6.0 for cadmium(II).[7,25] For *P. pudita*, the value was pH 6.0.[31] Gabr *et al.* found that the optimal pH value for Pb(II) bio-adsorption was 6 using *P. aeruginosa* ASU 6a.[25] There is no available information in the literature on the effect of pH in case of *P. aeruginosa* PAO1.

Effect of time on the bio-adsorption

The time-course profiles for the adsorption of Pb(II) and Cd(II) by lyophilized bacterial cells are shown in Figs. 3 and 4 at 285, 290 and 295 K. Figures 3 and 4 represent the adsorbed amounts of Cd(II) and Pb(II) by the biomass, res-

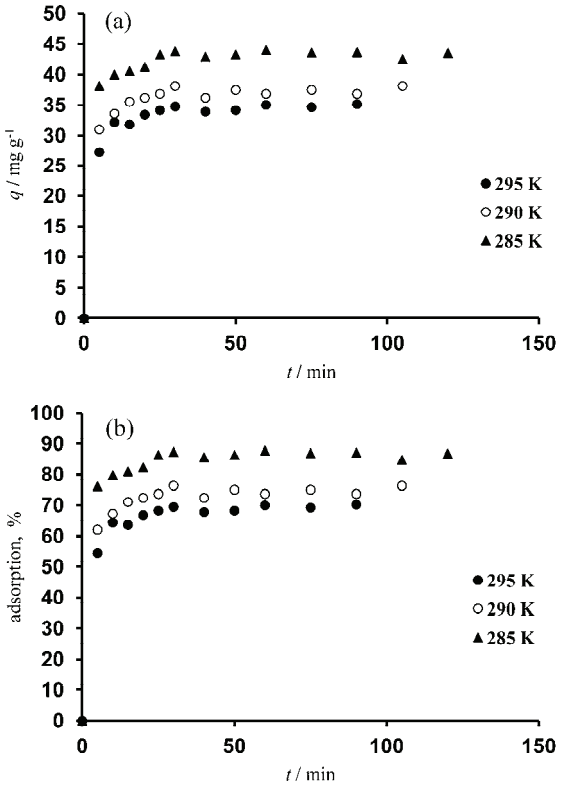

Fig. 3. Biosorption of Cd(II) by lyophilized cells of *P. aeruginosa* PAO1 (pH 6) as a function of time. Initial Cd(II) concentration, 50 mg L^{-1}; biomass concentration, 1 g L^{-1}; T = 285, 290 or 295 K.

pectively, a function of contact time. It was observed from figures that the uptake of heavy metals by biomass increased with increasing contact time. No significant increase in the sorption was found after 20 min, and the adsorption was rapid. The rapid adsorption was in agreement with the results of Gabr *et al*., in which the time required for equilibrium was 30 min.[25] According to Chang *et al*., metal concentration decreased rapidly during the first 30 min and remained nearly constant after 2 h of adsorption, suggesting that the bio-adsorption is fast and reaches saturation within 2 h.[7] The amount of bio-adsorbed Cd(II) decreased by increasing temperature and the adsorption efficiency decreased from 87 to 70 %. For Pb(II) bio-adsorption, the temperature had no significant effect; the adsorption efficiency decreased from 89 to 83 %.

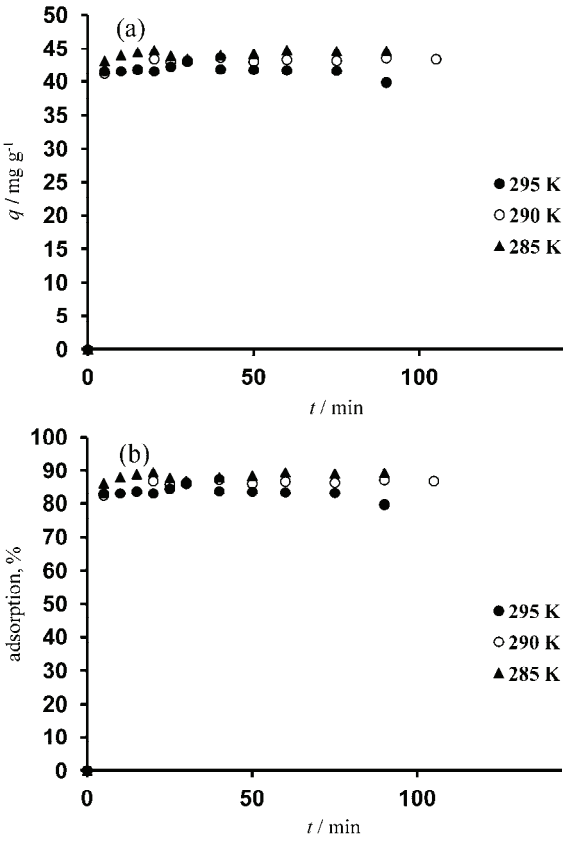

Fig. 4. Biosorption of Pb(II) by lyophilized cells of *P. aeruginosa* PAO1 (pH 5) as a function of time. Initial Pb(II) concentration, 50 mg L^{-1}, biomass concentration, 1 g L^{-1}; T = 285, 290 and 295 K.

This finding is in agreement with earlier studies.[7,25] The cells can accumulate metal ions on their surface and intracellular binding sites. The metal adsorption capacities of the lyophilized cells for Cd(II) and Pb(II) were 47.6 (95 %) and

46.6 mg g^{-1} (92 %), for an initial metal concentration of 50 mg L^{-1}, *i.e.*, the values for the two metal ions were not significantly different. There is no available information in the literature for the effect of temperature on the bio-adsorption of Cd(II) and Pb(II) by *P. aeruginosa* PAO1.

Modeling of the adsorption kinetics

Several kinetic models exist for the adsorption of heavy metals.[4] For the evaluation of the kinetics bio-adsorption of the heavy metals by lyophilized bacterial cells at 285, 290 and 295 K, the pseudo second-order model was used to fit the determined experimental data. The pseudo first-order model could not be used for modeling the biosorption kinetics.

The pseudo second-order kinetic rate equation can be written as follows:

$$\frac{dq}{dt} = k_{2,ad}\left(q_{eq} - q\right)^2 \quad (4)$$

where, $k_{2,ad}$ is the rate constant of the second order bio-adsorption (g mg^{-1} min^{-1}), q is the adsorbed amount (mg g^{-1}) and q_{eq} is the adsorption capacity (mg g^{-1}) at equilibrium.

For the utilization of this model, it is not necessary pre-estimated the experimental value of q_{eq}. Straight lines were obtained by plotting t/q against t (Fig. 5a and b). The second-order rate constants $k_{2,ad}$ and the theoretical adsorption capacities q_{eq} were calculated from the slope and intercept of the plots (Fig. 5a and b) and are summarized in Table I together with the corresponding correlation coefficients. The Cd(II) sorption rate constant $k_{2,ad}$ varied in the range of 2.1×10^{-2}–-2.4×10^{-2} g mg^{-1} min^{-1}, while the Pb(II) sorption rate constant $k_{2,ad}$ varied in the range of 6.5×10^{-2}–7×10^{-2} g mg^{-1} min^{-1}. The temperature had no effect on the biosorption rate in the studied temperature range. The theoretical adsorption capacities $q_{eq,calcd.}$ were 44.25 mg g^{-1} at 285 K, 37.45 mg g^{-1} at 290 K, and 35.46 mg g^{-1} at 295 K for Cd(II) and 44.84 mg g^{-1} at 285 K, 43.67 mg g^{-1} at 290 K and 40.48 mg g^{-1} at 295 K for Pb(II). The adsorbed amount of metal ions decreased with increasing temperature in the interval 285−295 K. The calculated adsorption capacities agreed well with the experimental data. The correlation coefficients for the second-order kinetic model were close to 1.0 in all cases. This suggests that the sorption of heavy metals by the bacterial biomass follow second-order kinetics.

Kong *et al*. performed kinetic and equilibrium studies for the adsorption process of Cd(II) and Cu(II) onto *P. aeruginosa* using the wave anodic stripping voltammetry method.[32] The kinetic characteristics of the adsorption process were studied and all the corresponding regression parameters were obtained by fitting the electrochemical experimental data to the pseudo second-order kinetic model. Lin *et al*. immobilized *P. aeruginosa* PU21 in chitosan and alginate. The Pb(II) bio-adsorption was studied by immobilized bacterial biomass in the temperature

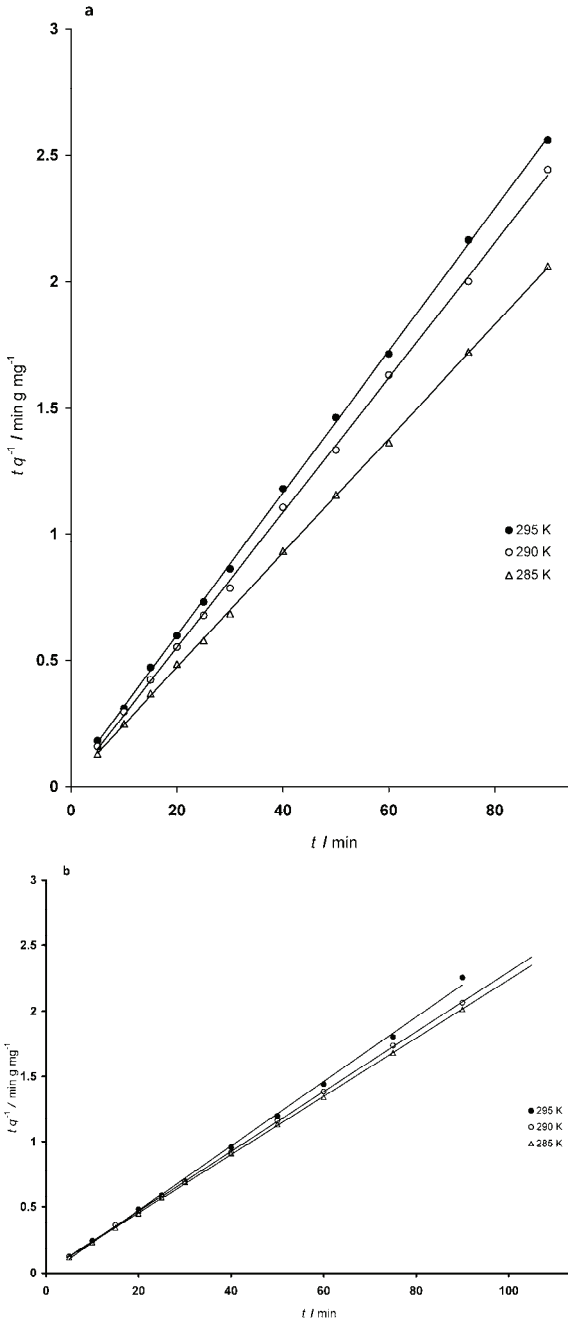

Fig. 5. Linearized pseudo second-order kinetic model for a) Cd(II) and b) Pb(II) adsorption by lyophilized cells of *P. aeruginosa* PAO1. Initial metal ion concentration, 50 mg L^{-1}; biomass concentration, 1 g L^{-1}; T = 285, 290 and 295 K.

range of 293–323 K. They found that the adsorption of Pb(II) onto optimized beads was consistent with a first-order/spontaneous reaction.[33] It is difficult to model

the kinetic experimental data in the studied temperature range, because the adsorption process is very fast. On the other hand, the pseudo second-order kinetic model using linearized presentation fitted the experimental data determined under these environmental conditions.

TABLE I. The pseudo second-order rate constants and the calculated equilibrium adsorption capacities for *P. aeruginosa* PAO1. Biomass concentration, 1 g L^{-1}; initial metal ion concentration, 50 mg L^{-1}; T = 285, 290 and 295 K

T / K	$k_{2,ad}$ / 10^{-2} g mg^{-1} min^{-1}	$q_{eq,cal}$ / mg g^{-1}	R^2	$q_{eq,exp}$ / mg g^{-1}
	Cd(II)			
285	2.4	44.25	0.999	43.90
290	4.0	37.45	0.999	38.13
295	2.1	35.46	0.999	35.16
	Pb(II)			
285	6.5	44.84	0.999	44.57
290	6.7	43.67	0.999	43.37
295	7.0	40.48	0.998	41.34

Bio-adsorption isotherms

Cadmium(II) and lead(II) sorption uptakes by the lyophilized bacterial cells of *P. aeruginosa* were determined by biosorption equilibrium measurements at initial concentrations of 5–250 mg L^{-1} for Cd(II) at pH 6.0 and for Pb(II) at pH 5.0. The biomass concentration was 1 g L^{-1}. The bio-adsorption isotherms determined for both heavy metals using batch technique showed the metal uptake by the bacterial biomass (Fig. 6). Thus, there was an increase in metal uptake as long as binding sites were free. A different adsorption mechanism could be observed for Pb(II) adsorption in comparison with the Cd(II) adsorption process. Experimental data were applied to adsorption models given by Langmuir and Freundlich and the adsorption constants were estimated using the nonlinear least-squares mathematical method.

Previous work[7] showed that resting cells of *P. aeruginosa* PU21 (harvested by centrifugation from early-stationary cultures and twice rinsed with deionized water) were able to adsorb 110 mg Pb(II) g^{-1} dry cell at pH 5.5 and 58 mg Cd(II) g^{-1} dry cell at pH 6.0. The Langmuir isotherm was used to describe the adsorption equilibrium of the heavy metals.[7] The results of Gabr *et al*.[27] demonstrated that for Ni(II) and Pb(II) biosorption by living and lyophilized *P. aeruginosa* ASU 6a cells, the adsorption equilibrium data fitted well the Langmuir and Freundlich models for metal ions in the 0−160 mg L^{-1} concentration range.

The nonlinearly fitted Langmuir and Freundlich adsorption isotherms of the heavy metals obtained using *P. aeruginosa* PAO1 biomass are shown in Fig. 6.

The estimated values of q_{max} and b are given in Table II. The maximum adsorption capacity q_{max} was 158.25 mg g^{-1} and Langmuir constant b was $2.7 \cdot 10^{-2}$ L mg^{-1} for Cd(II) biosorption, and q_{max} was 182.10 mg g^{-1} and b was $2.8 \cdot 10^{-1}$ L mg^{-1} for Pb(II) biosorption. The estimated q_{max} value obtained for Pb(II) was higher than that for Cd(II). The experimental q_{max} value for Pb(II) was 164 mg g^{-1}, while it was 113 mg g^{-1} for Cd(II). The values of the4 equilibrium constant b for Pb(II) and Cd(II) were calculated to be $2.8 \cdot 10^{-1}$ L mg^{-1} and $2.7 \cdot 10^{-2}$ L mg^{-1}, respectively, which indicates that the lyophilized cells of *P. aeruginosa* PAO1 possessed a higher adsorption affinity for Pb(II) ions than for Cd(II) ions. Such a fact led to the conclusion that the energy of adsorption was more favorable for Pb(II) than for Cd(II). The regression correlation coefficients of the Langmuir Model were 0.938 and 0.915 for Pb(II) and Cd(II) biosorption, respectively.

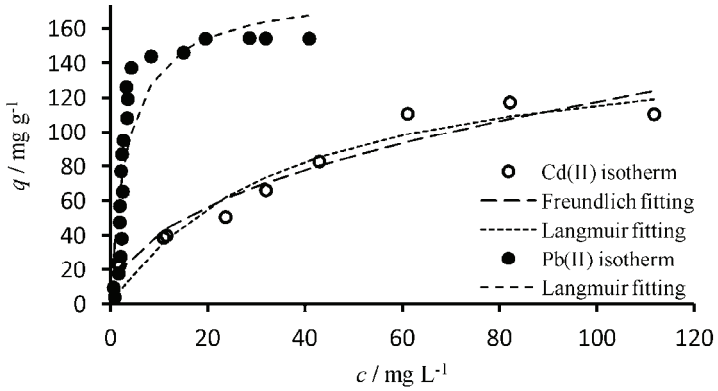

Fig. 6. Bio-adsorption isotherms of lyophilized *P. aeruginosa* PAO1 bacterial cells for Cd(II) and Pb(II) ions. The initial concentration of the metal ions varied between 5 and 250 mg L^{-1}. Biomass concentration, 1 g L^{-1}. $pH_{Cd(II)}$ 6; $pH_{Pb(II)}$ 5; T = 285 K.

TABLE II. The Langmuir and Freundlich isotherm constants for Cd(II) and Pb(II) adsorption by *P. aeruginosa* PAO1 lyophilized cells at 285 K

Metal	Freundlich isotherm model			Langmuir isotherm model		
	k_F / (mg g^{-1})(mg L^{-1})^n	n / L mg^{-1}	R^2	q_{max} / mg g^{-1}	b / L mg^{-1}	R^2
Cd(II)	14.60	2.20	0.936	158.25	0.027	0.915
Pb(II)	54.17	3.05	0.659	182.10	0.28	0.938

The estimated values of k_F and n are also given in Table II, together with the regression correlation coefficients. The parameter k_F related to the sorption capacity was 14.6 (mg g^{-1})(mg L^{-1})n for Cd(II) biosorption. The exponent n of cadmium(II) biosorption was greater than unity, indicating that the heavy metal was favorably adsorbed by the bacterial cells. The regression correlation coefficient of Freundlich model was 0.936 for Cd(II) biosorption, suggesting that the Freundlich model was able to describe the adsorption equilibrium well. In the

case of Pb(II) biosorption, the Freundlich model could not be used to evaluate the adsorption equilibrium.

CONCLUSIONS

In this study, the high potential of lyophilized bacterial cells of *P. aeruginosa* PAO1 to adsorb Cd(II) and Pb(II) ions from aqueous solution was demonstrated. The optimum pH values were 5.0–6.0 for Cd(II) and about 5.0 for Pb(II) biosorption. A different adsorption mechanism could be observed for Pb(II) in comparison with that for Cd(II) adsorption. The Freundlich (Cd(II)) and Langmuir (Cd(II), Pb(II)) models exhibited good fits to the biosorption data. The heavy metal biosorption by bacterial biomass followed pseudo second-order adsorption kinetics. The second-order kinetic constants did not vary with increasing temperature, while the adsorbed amounts of heavy metals decreased in the case of Cd(II).

Acknowledgements. This work was supported by grants of TÁMOP-4.2.2/B-10/1-2010-0029, TÁMOP-4.2.2.A-11/1/KONV-2012-0065 and TIOP 1.3.1-07/1.

ИЗВОД

БИО-АДСОРПЦИОНЕ КАРАКТЕРИСТИКЕ *Pseudomonas aeruginosa* PAO1

ANIKÓ KŐNIG-PÉTER[1], BÉLA KOCSIS[2], FERENC KILÁR[1,4] и TÍMEA PERNYESZI[3,4]

[1]*Institute of Bioanalysis, University of Pécs, Faculty of Medicine, 12 Szigeti, H-7624 Pécs, Hungary,* [2]*Institute of Medical Microbiology and Immunology, University of Pécs, Faculty of Medicine, Szigeti út. 12, H-7624, Pécs, Hungary,* [3]*Department of Analytical and Environmental Chemistry, Faculty of Science, Ifjúság u. 6, H-7624 Pécs, Hungary и* [4]*Analytical Chemistry and Geoanalytical Research Group, Szentágothai Research Center, University of Pécs, H-7624 Pécs, Ifjúság útja 20, Hungary*

Биосорпција јона Cd(II) и Pb(II) из водених раствора коришћењем ћелија *Pseudomonas aeruginosa* (PAO1) посматрана је под различитим експерименталним условима. Испитани су утицај pH, почетне концентрације метала, времена уравнотежавања и температуре на биоадсорпцију. Нађено је да је оптимална pH вредност за адсорпцију Pb(II) једнака 5,0, а за Cd(II) износи 5 до 6. Равнотежне адсорпције Pb(II) и Cd(II) су анализиране Фројндлиховим и Лангмировим моделима, уз коришћење процене помоћу нелинеарне методе најмањих квадрата. Експериментално добијен максимум сорпционог капацитета за Pb(II) и Cd(II) је 164, односно 113 mg g^{-1}. За проучавање кинетике биосорпције примењен је модел псеудо-другог реда на више температура. Температура није показала значајан утицај на биоадсорпцију Pb(II). У случају биоадсорпције Cd(II), адсорбована количина се смањивала са растом температуре.

(Примљено 14. марта, ревидирано 21. јуна 2013)

REFERENCES

1. S. S. Ahluwalia, D. Goyal, *Bioresour. Technol.* **98** (2007) 2243
2. J. L. Wang, C. Chen, *Biotechnol. Adv.* **24** (2006) 427
3. J. L. Wang, C. Chen, *Biotechnol. Adv.* **27** (2009) 195
4. K. Vijayaraghavan, Y. S. Yun, *Biotechnol. Adv.* **26** (2008) 266

5. G. M. Gadd, in *Biotechnology, Vol. 6b, Special Microbial Processes*, H.-J. Rehm, Ed., VCH, Weinheim, Germany, 1988, p. 401
6. F. Veglio, F. Beolchini, *Hydrometallurgy* **44** (1997) 301
7. J.-S. Chang, R. Law, C. Chung-Cheng, *Water Res.* **31** (1997) 1651
8. G. M. Strandberg, S. E. Shumate, J. R. Parott, *Appl. Environ. Microbiol.* **41** (1981) 237
9. A. C. Texier, Y. Andrès, P. Le Cloirec, *Environ. Sci. Technol.* **33** (1999) 489
10. A. C. Texier, Y. Andrès, P. Le Cloirec, *Environ. Sci. Technol.* **34** (2000) 610
11. J.-S. Chang, C.-C. Chen, *Sep. Sci. Technol.* **33** (1998) 611
12. G. Uslu, M. Tanyol, *J. Hazard. Mater., B* **135** (2006) 87
13. W. C. Leung, H. Chua, W. Lo, *Appl. Biochem. Biotech.* **91**–**93** (2001) 171
14. D. Gialamouidis, M. Mitrakas, M. Liakopoulou-Kyriakides, *Desalination* **248** (2009) 907
15. S.-Y. Kang, J.-U. Lee, K.-W. Kim, *Biochem. Eng. J.* **36** (2007) 54
16. J. L. Ramos, E. Díaz, D. Dowling, V. de Lorenzo, S. Molin, O'Gara Fergal, C. Ramos, K. N. Timmis, *Nat. Biotechnol.* **12** (1994) 1349
17. M. Valls, V. de Lorenzo, R. González-Duarte, S. Atrian, *J. Inorg. Biochem.* **79** (2000) 219
18. R. M. P. Silva, A. Á. Rodríguez, J. M .G. M. De Oca, D. C. Moreno, *Bioresour. Technol.* **100** (2009) 1533
19. R. Nadeem, M. A. Hanif, A. Mahmood, M. S. Jamil, M. Ashraf, *J. Hazard. Mater.* **168** (2009) 1622
20. A. A. Juwakar, A. Nair, K. V. Dubey, S. K. Singh, S. Devotta, *Chemosphere* **68** (2007) 1996
21. D. L. Vullo, H. M. Ceretti, M. A. Daniel, S. A. M. Ramírez, A. Zalts, *Bioresour Technol.* **99** (2008) 5574
22. E. Kaszab, J. R. Bedros, S. Szoboszlay, B. Atzél, I. Szabó, M. Cserháti, B. Kriszt, *Acad. Appl. Res. Military Sci. – AARMS* **5** (2006) 383
23. E. Kaszab, B. Kriszt, B. Atzél, G. Szabó, P. Harkai, S. Szoboszlay, *Microbial Ecol.* **59** (2010) 37
24. I. Wiegand, K. Hilpert, R. E. Hancock, *Nat. Protoc.* **3** (2008) 163
25. R. M. Gabr, S. H. A. Hassan, A. A. M. Shoreit, *Int. Biodeter. Biodegr.* **61** (2008) 195
26. K. Vjayaraghavan, T. V. N. Padmesh, K. Palanivelu, M. Velan, *J. Hazard. Mater., B* **133** (2006) 304
27. J.-H. Joo, H. A. Hassan, S.-E. Oh, *Int. Biodeter. Biodegr.* **64** (2010) 734
28. A. de Vincente, M. Avilés, J. C. Codina, J. J. Borrego, P. Romero, *J. Appl. Bacteriol.* **68** (1990) 625
29. B. Volesky, Z. R. Holan, *Biotechnol. Progr.* **11** (1995) 235
30. G. V. Sherbert, *The biophysical characterization of the cell surface*, Academic Press, London, 1978, p. 31
31. R. Pardo, M. Herguedas, E. Barrado, M. Vega, *Anal. Bioanal. Chem.* **376** (2003) 26
32. B. Kong, B. Tang, X. Liu, X. Zeng, H. Duan, S. Luo, W. Wie, *J. Hazard. Mater.* **167** (2009) 455
33. C.-C. Lin, Y.-T. Lai, *J. Hazard. Mater.* **137** (2006) 99.

Journal of the Serbian Chemical Society
JSCS@tmf.bg.ac.rs • www.shd.org.rs/JSCS
J. Serb. Chem. Soc. 79 (4) 509–516 (2014)
UDC 543+061.3(4)
EuCheMS news

DIVISION OF ANALYTICAL CHEMISTRY
EUROPEAN ASSOCIATION FOR CHEMICAL AND MOLECULAR SCIENCES

EUCHEMS NEWS

European Analytical Column No. 42

ROMÀ TAULER[1], FEDERICO MARINI[2], BEATA WALCZAK[3], LUTGARDE BUYDENS[4], RICHARD G BRERETON[5], WOLFGANG BUCHBERGER[6] and PAUL WORSFOLD[7]*

[1]IDAEA-CSIC, Barcelona, Spain (Roma.Tauler@idaea.csic.es), [2]Department of Chemistry, University of Rome "La Sapienza", Rome, Italy (federico.marini@uniroma1.it), [3]Institute of Chemistry, University of Silesia, Katowice, Poland (beata.walczak@us.edu.pl), [4]Radboud University, Nijmegen, The Netherlands (l.buydens@science.ru.nl), [5]University of Bristol, United Kingdom (r.g.brereton@bristol.ac.uk), [6]Analytische Chemie, Universität Linz, Altenbergerstrasse 69, A-4040 Linz, Austria (Wolfgang.Buchberger@jku.au) and [7]School of Geography, Earth and Environmental Sciences, Plymouth University, Plymouth PL48AA, United Kingdom

INFORMATION FROM THE EUCHEMS DIVISION OF ANALYTICAL CHEMISTRY (DAC)

Euroanalysis XVII, held in Warsaw, Poland, August 25–29, was the prime event within the DAC portfolio of activities for 2013. It attracted more than 700 participants from 64 countries. Maciej Jarosz as chair and Ewa Bulska as co-chair, together with their team of local organizers, provided an excellent environment for scientific discussions and networking. One of the highlights of this conference was the Robert Kellner Lecture given by Jürgen Popp from Jena, Germany.

Further events organized in co-operation with DAC included the In Vino Analytica Scientia Conference 2013 held in Reims, France, July 2–5, 2013, and the 4th Danish Metabolomics Seminar in Copenhagen, November 15, 2013.

The 44th Annual Meeting of DAC took place within the Euroanalysis conference in Warsaw on August 25, 2013. Delegates and Observers from 22 countries attended the meeting. They had the privilege to witness the DAC Tribute to Bo Karlberg and Adam Hulanicki for their achievements for DAC and the Euroanalysis series (a report about the DAC Tributes was published in the EuCheMS Newsletter November 2013).

* Corresponding author. E-mail: pworsfold@plymouth.ac.uk

The delegates of the Annual Meeting unanimously elected Paul Worsfold (UK) as Chair of DAC for a second term (2014–2016). The current Secretary (2013–2015) is Wolfgang Buchberger (Austria). The delegates also approved the other members of the Steering Committee for 2014, namely Jiri Barek (Czech Republic), Slavica Razic (Serbia), Christian Rolando (France) and Charlotta Turner (Sweden). In 2013, the Steering Committee held a meeting in Nicosia (Cyprus) on April 7, which was followed by a Mini-symposium, with lectures given by the members of the Steering Committee at the University of Cyprus. Everyone enjoyed the great hospitality of Constantina Kapnissi-Christodoulou who acted as the local coordinator. Another meeting of the Steering Committee took place prior to the DAC Annual Meeting in Warsaw.

Recently, an Open Call for the Robert Kellner Lecture 2015 and the DAC--EuCheMS Award 2015 has been made. The Robert Kellner Lecture is intended for a mid-career person with significant achievements in analytical sciences during the last five years, whereas the DAC-EuCheMS Award is for lifetime achievements of a senior person. Both awards are sponsored by Springer. Nominations should be sent to the Secretary of DAC by October 31, 2014.

The next Annual Meeting of DAC will be held on Sunday, August 31, 2014, at the 5th EuCheMS Chemistry Congress (August 31–September 4, 2014) in Istanbul. Various sections of the EuCheMS conference are closely related with analytical topics, and analytical chemists are encouraged to attend and to submit contributions.

Please make a note now of the date for the next Euroanalysis conference, Euroanalysis XVIII, which will be held in Bordeaux, France, September 6–10, 2015, under the auspices of the Societé Chimique de France. It is also important to note that in 2017 Euroanalysis XIX will be organized in Stockholm by the Swedish Chemical Society.

Further information about ongoing DAC activities can be found on its website, which has recently been moved from the old web address to the EuCheMS website and is available at www.euchems.eu/divisions/analytical-chemistry. Thanks go to Slavica Ražić (a member of the DAC Steering Committee) who has spent a lot of time and effort setting up this webpage, which contains a wide range of historical information and topical news of relevance to DAC members and the wider Analytical Chemistry community.

Currently, DAC operates five Study Groups devoted to major topics of particular importance, namely “Education in Analytical Chemistry“, “Bioanalytics“, “History”, “Quality Assurance and Accreditation”, and “Chemometrics” (see http://www.euchems.eu/divisions/analytical-chemistry/news-current-activities-conferences-and-events/study-groups-and-task-forces.html). These Study Groups are evaluated after a period of three years and may be renewed. Besides, DAC has set up a Task Force on “Archaeometry and Cultural Heritage in Anal-

ytical Chemistry" which will run for another year. In this European Analytical Column, Roma Tauler, Federico Marini, Beata Walczak, Lutgarde Buydens and Richard G. Brereton provide the Chemometrics Study Group's view on the role of chemometrics in Analytical Chemistry.

CHEMOMETRICS AND ANALYTICAL CHEMISTRY

Definition of chemometrics

Chemometrics can be defined as the science of extracting information from chemical systems using data analysis methods. It is characterized by the application of mathematical, statistical and computer methods to solve problems in different chemical disciplines and related fields, such as chemical engineering, biochemistry, medicine, environmental sciences and biology, and is related to other "-metrics" fields, such as psychometrics, biometrics and econometrics. Chemometrics is an application driven discipline that is widely used in industry and in academic and research institutions. Chemometric techniques are widely used in Analytical Chemistry and are acquiring increasing acceptance in emerging "omics" fields and Biological Sciences.

The discipline of chemometrics is distinguished from other computational branches of chemistry designed for theoretical studies (Computational Chemistry) or for the curve fitting determination of parameters using pre-established physical, chemical or empirical models (hard modeling approaches). Historically, when measured data were scarce (and often only univariate measurements were available) and computational resources limited, science progressed slowly in the description of natural systems. Advances were consequently strongly influenced by the theoretical postulation of appropriate models, based on experimental data obtained in the laboratory and under very controlled conditions, to describe the behavior of the system under study. The investigation of natural systems and of real life problems and situations was beyond the scope of these rather limited data analysis approaches. Theoretical Computational Chemistry, on the other hand, investigates the intimate nature of chemical systems at the atomic level and has developed in an independent way. In this area, the amount of available experimental data was also scarce due to the difficulty in acquisition, at least until very recently. In contrast to these two "hard" modeling approaches, the concept of "soft-modeling" can be widely applied in chemometrics. In this case, instead of the *a priori* postulation of a physical (chemical) model in which parameters are tuned (adjusted) according to an optimal fit to measured experimental data, no underlying physical model is initially proposed. Soft modeling approaches propose a simple empirical model describing the behavior of the data. A typical example is the bilinear extension of the Beer Law in UV–Visible absorption spectrometry for multi-wavelength, multi-component and multi-sample data analysis. In contrast to traditional hard modeling curve fitting

approaches, soft modeling approaches imply that one has lots of multivariate data measured over many samples that have common sources of variation (see below). Knowledge of the laws governing the system being studied (*e.g.*, the theory behind the separation mechanism in chromatography) is not required in soft modeling chemometric approaches, which are, therefore, more widely applicable than the traditional hard or "parametric" methods, since the assumptions made are less restrictive. On the other hand, these characteristics can sometimes be considered a limitation (*e.g.*, because the lack of a hard model may hamper the interpretation). To overcome this drawback, mixed "hard-soft" or hybrid approaches are being developed for different applications, *e.g.*, studying the kinetics or thermodynamics of chemical reaction systems. In these cases, the wealth of information contained in multivariate measurements (such as spectroscopic data) is combined with a knowledge of reaction orders, mass balances, rate laws and mass action thermodynamic laws to optimally describe the behavior of the experimental data. The variability of these data is not only associated with a systematic component that can be described by physical and chemical laws, but also with measurement uncertainties and interfering, unknown sources of variance. An example of this situation is the description of complex chemical reaction systems in industrial environments.

Chemometrics in analytical science

Although there may be common aspects and similarities among different computational approaches and with "-metrics"-based soft modeling disciplines in other scientific disciplines (*e.g.*, biometrics, econometrics and psychometrics), the unique feature of chemometrics is the model free analysis of experimental measurements and data to extract information about systems. The current widespread applicability of chemometric methods is precisely because of the rapidly expanding availability of experimental measurements from new analytical instruments and from the widespread use of computer systems to analyze the data. This focus of chemometrics on the analysis of experimentally measured data is the reason why it is intimately related to Analytical Science. Since Analytical Science in general, and Analytical Chemistry in particular, can be described as measurement sciences applied to materials systems (including chemical systems as well as biological, earth, physical, environmental and all other natural systems), chemometrics should be considered a cornerstone and a powerful reinforcement of the theoretical foundations of these systems. Chemometrics uses computational, mathematical, statistical and logical tools to achieve similar goals in Analytical Chemistry and should be considered an important and integral part of the subject. Analytical chemists have devoted considerable effort into the development of new instrumental methods of analysis and new methods of sample preparation, pretreatment and separation but data analysis (including the acquis-

ition, treatment and interpretation steps) should also be considered as a key step in the analytical process. Due to the limited availability of appropriate data handling and data analysis methods, most effort in analytical problem solving has been directed towards the development and improvement of physical (instrumental) and chemical (separation) solutions to the ubiquitous twin challenges of selectivity and sensitivity. In the past, simple numerical calculations and traditional univariate statistical analysis were considered sufficient to address these challenges but, even with more sophisticated analytical methods and instrumentation (*e.g.*, mass spectrometry), new challenges continually arise, especially in the analysis of natural samples. This is particularly the case with the explosion of massive and megavariate analytical data from the "-omics" platforms, which cannot be processed using these traditional data analysis tools.

Chemical concepts

Chemometrics has been applied to solve both descriptive and predictive problems in the experimental sciences, especially in chemistry. In descriptive applications, the properties of chemical systems are modeled with the objective of understanding the underlying relationships and structure of the system (*i.e.*, model understanding and identification). In predictive applications, quantitative numerical values (*e.g.*, concentrations of the analytes) and properties of chemical systems are modeled with the intent of estimating new values and properties. Many early applications involved multivariate classification, multivariate calibration and numerous quantitative predictive applications.

Compared with data analysis disciplines in other fields, chemometrics depends on certain highly characteristic steps. From the beginning, finding techniques for optimal data preprocessing and pretreatment have been extraordinarily important and they are still at the core of the best strategies to extract reliable information from instrumental data. From the well-known Savitzky–Golay differentiation and smoothing filters, to the more recently developed wavelet transforms, asymmetric least squares baseline correction and optimized warping techniques for signal alignment and correction, together with the more traditional preprocessing methods of data centering, normalization and scaling, at present a plethora of possibilities exist for handling many of the problems currently encountered in real life experimental measurements.

Another very important concept in chemometrics is that of "latent variables" (originally developed 80 years ago in the psychometric and factor analysis literature), *i.e.*, variables which are not directly measured (they are hidden, not explicit), which need to be uncovered for a proper interpretation of what is observed and for future predictions. This concept is in the core of many of the more widely used methods in chemometrics, such as Principal Component Analysis and Partial Least Squares, and of Factor Analysis and Pattern Recognition methods in

general. This also implies recognition of the fact that, in most cases, the ultimate object of investigations can only be measured indirectly.

Another core concept related to latent variables is that of Mixture Analysis, which recognizes that existing analytical methods are imperfect, in the sense that they are not (and that they probably cannot be) totally selective, and therefore that the measured signal is usually a mixed signal which needs to be "unmixed" into its component parts before one can use and interpret its content.

An additional concept that is not unique to Chemometrics but which, in this context, has become highly important if not fundamental is the concept of validation. For predictive modeling, the results and method performance should be validated properly and no new approach should be accepted until this is clearly shown. Validation, as the name suggests, is the step in which the reliability of the analytical approach to the data is established. In its most commonly adopted meaning, it involves taking out samples that are not part of the training set and then checking how well the model performs when applied to these external samples. However, the concept of validation is broader and includes an evaluation of the appropriateness of the model in describing the data, the identification and treatment of outlying observations, the chemical interpretability of the results, as well as more technical issues, such as whether the solutions are stable or whether the algorithm has truly converged to the global optimum. Accordingly, it follows that the number of possible strategies for validation is very large.

The number of instrumental data sources that are now available significantly increases the possibility of having the same system simultaneously investigated by multiple methods and instruments. The concept of data fusion and the design of novel chemometric techniques for this purpose are opening up new possibilities to correlate and interpret more deeply the nature of complex systems. Data sources can now be massive and, in addition, natural systems (such as environmental or biological systems) are intrinsically complex. Their investigation and analysis are very challenging and require the development and adaptation of new methods and strategies for data analysis.

Emerging trends

Since the historical development of chemometrics, new situations are constantly emerging. Although one may think that many of the initial goals of chemometrics have already been reached and that chemometrics can now be absorbed by other disciplines, such as "-omics" or bioinformatics, there should be a clear scientific recognition of the extraordinary efforts and successes achieved by this discipline. More and more, the worldwide spread of chemometrics solving new problems and providing new solutions to both new and old analytical challenges can be observed. The development of new chemometric methods and solutions is still required to address emerging challenges in the measurement sciences.

Nowadays chemometrics has reached a mature state and is accepted in many universities, research institutions and research departments of large chemical industries throughout the world. For instance, it is routinely applied as a fundamental part of Process Analytical Technologies (PAT) in the oil, food and pharmaceutical industries. New application areas have appeared in different domains, such as molecular modeling, QSAR, and chemoinformatics. It has a strong impact on the development of new tools in hyperspectral image analysis, environmental analysis and especially in the "-omics" (genomics, proteomics and metabolomics) branch of analytical science. "-Omic" disciplines are changing the face of analytical science, and will continue to do so over the next few years, and chemometrics has an important role to play in this development. It is only with this intimate relationship between chemometrics and "-omic" analytical methodologies that the challenges posed in the analysis of overwhelmingly large instrumental data sets can be overcome and extraction of the required information be enabled. This will then allow the differentiation of natural sources of variation from the effects caused by, *e.g.*, stressors and treatments.

Publications

Apart from scientific journals uniquely devoted to chemometrics such as the *Journal of Chemometrics* (Wiley) and *Chemometrics and Intelligent Laboratory Systems* (Elsevier), most routine applications of existing chemometric methods are published in broad analytical journals (*e.g.*, *Analytical Chemistry*, *Analytica Chimica Acta* (which was the first journal with a separate chemometrics section), *Analytical and Bioanalytical Chemistry*, *Analyst*, *Talanta* and *Applied Spectroscopy*). Moreover, several important books/monographs on chemometrics have been published over the last 30 years, either dealing with specific or more general aspects of the discipline. These include: Malinowski's "Factor Analysis in Chemistry" (Wiley, 1989, 2002), the two milestone chemometrics textbooks from Sharaf, Illman and Kowalski (Wiley, 1986) and Massart *et al.* (Elsevier 1988, 1998), "Multivariate Calibration" by Martens and Naes (Wiley, 1989), and more recent publications such as "Comprehensive Chemometrics", a multi-authored chemometrics "encyclopedia" in four volumes (Elsevier, 2009), the "Practical Guide to Chemometrics" edited by Paul Gemperline (CRC Press, 2006), the monographs by Richard Brereton ("Chemometrics Data Analysis for the Laboratory and Chemical Plant" (Wiley, 2003) and "Chemometrics for Pattern Recognition" (Wiley, 2009) and the "Multi-way Analysis with Applications in the Chemical Sciences" by Smilde, Bro and Geladi (Wiley, 2004).

In addition, the interest in using chemometrics in different fields is witnessed by application-oriented monographs such as "Chemometrics in Environmental Chemistry" by Einax (Springer, 1995), "Multi- and Mega-Variate Data Analysis"

by Eriksson *et al.* for omics data analysis (Umetrics Academy, ISBN-13: 978-91--973730-2-9) and Marini's "Chemometrics in Food Chemistry" (Elsevier, 2013).

Since chemometrics involves the use of mathematical, statistical and computer methods, a very important aspect of this discipline from its very beginning has been the attention placed on software development and dissemination. The forefathers of chemometrics took particular care in writing computer routines to perform essential chemometric computations and to organize them in packages that could be easily used by less expert researchers: Kowalski's ARTHUR, Pirouette (Infometrix, WA, USA), Wold's SIMCA (UMETRICS, Umeä, Sweden), Forina's PARVUS and Martens' Unscrambler (CAMO, Oslo, Norway) have played an important role in the dissemination of the discipline and most still exist, even if now developed by software companies, flanked by new contributions such as Eigenvector's PLS-Toolbox (Eigenvector Research, WA, USA).

CONCLUSIONS

In conclusion, although applications of chemometrics are not restricted to Analytical Chemistry, its "home" within this discipline is well justified, and in many situations the goals of both coincide. In addition, in the same way that Analytical Chemistry has expanded to encompass all branches of Analytical Science, the same is true of Chemometrics, which can easily be extended from chemically related measurements to most other types of measurements performed throughout science and engineering, including chemical engineering.